Baryons and baryonic matter in four-fermion interaction models

$$(\bar{\psi}\psi)^2$$

Den Naturwissenschaftlichen Fakultäten
der Friedrich-Alexander-Universität Erlangen Nürnberg
zur Erlangung des Doktorgrades

vorgelegt von
Konrad Urlichs
aus Erlangen

Als Dissertation genehmigt von den Naturwissenschaftlichen Fakultäten
der Universität Erlangen-Nürnberg

Tag der mündlichen Prüfung:	23. Februar 2007
Vorsitzender der Promotionskommission:	Prof. Dr. E. Bänsch
Erstberichterstatter:	Prof. Dr. M. Thies
Zweitberichterstatter:	Prof. Dr. U.-J. Wiese

Zusammenfassung

In dieser Arbeit werden Baryonen und baryonische Materie in einfachen Theorien mit Vier-Fermion-Wechselwirkung behandelt, dem Gross-Neveu Modell und dem Nambu-Jona-Lasinio Modell in 1+1 und 2+1 Raumzeitdimensionen. Diese Modelle sind als Spielzeugmodelle für dynamische Symmetriebrechung in der Physik der starken Wechselwirkung konzipiert. Die volle, durch Gluonaustausch vermittelte Wechselwirkung der Quantenchromodynamik wird dabei durch eine punktartige ("Vier-Fermion") Wechselwirkung ersetzt. Die Theorie wird im Limes einer großen Zahl an Fermionflavors betrachtet. Hier ist die mittlere Feldnäherung exakt, die äquivalent zu der aus der relativistischen Vielteilchentheorie bekannten Hartree-Fock Näherung ist.

In 1+1 Dimensionen werden bekannte Resultate für den Grundzustand auf Modelle erweitert, in denen die chirale Symmetrie durch einen Massenterm explizit gebrochen ist. Für das Gross-Neveu Modell ergibt sich eine exakte selbstkonsistente Lösung für den Grundzustand bei endlicher Dichte, der aus einer eindimensionalen Kette von Potentialmulden besteht, dem Baryonenkristall. Für das Nambu-Jona-Lasinio Modell führt die Gradientenentwicklung auf eine Näherung für die Gesamtenergie in Potenzen des mittleren Feldes. Das Baryon ergibt sich als ein topologisches Soliton, ähnlich wie im Skyrme Modell der Kernphysik. Die Lösung für das einzelne Baryon und baryonische Materie kann in einer systematischen Entwicklung in Potenzen der Pionmasse angegeben werden.

In 2+1 Dimensionen ist die Lösung der Hartree-Fock Gleichungen schwieriger. Im masselosen Gross-Neveu Modell kann eine exakt selbst-konsistente Lösung hergeleitet werden, die den Baryonenkristall des 1+1 dimensionalen Modells so erweitert, dass die Translationssymmetrie in einer Raumrichtung beibehalten wird. Diese eindimensionale Feldkonfiguration ist zur translationssymmetrischen Lösung energetisch entartet, was als Hinweis auf die Möglichkeit der Brechung der Translationssymmetrie durch allgemeinere geometrische Strukturen gewertet werden kann. Im Nambu-Jona-Lasinio Modell indudziert ein topologisches Soliton eine endliche Baryonzahl. Im Gegensatz zum 1+1 dimensionalen Modell ist das einzelne Baryon aber nicht masselos, sondern ein Zustand mit verschwindender Bindungsenergie.

Abstract

In this work we discuss baryons and baryonic matter in simple four-fermion interaction theories, the Gross-Neveu model and the Nambu-Jona-Lasinio model in 1+1 and 2+1 space-time dimensions. These models are designed as toy models for dynamical symmetry breaking in strong interaction physics. Pointlike interactions ("four-fermion" interactions) between quarks replace the full gluon mediated interaction of quantum chromodynamics. We consider the limit of a large number of fermion flavors, where a mean field approach becomes exact. This method is formulated in the language of relativistic many particle theory and is equivalent to the Hartree-Fock approximation.

In 1+1 dimensions, we generalize known results on the ground state to the case where chiral symmetry is broken explicitly by a bare mass term. For the Gross-Neveu model, we derive an exact self-consistent solution for the finite density ground state, consisting of a one-dimensional array of equally spaced potential wells, a baryon crystal. For the Nambu-Jona-Lasinio model we apply the derivative expansion technique to calculate the total energy in powers of derivatives of the mean field. In a picture akin to the Skyrme model of nuclear physics, the baryon emerges as a topological soliton. The solution for both the single baryon and dense baryonic matter is given in a systematic expansion in powers of the pion mass.

The solution of the Hartree-Fock problem is more complicated in 2+1 dimensions. In the massless Gross-Neveu model we derive an exact self-consistent solution by extending the baryon crystal of the 1+1 dimensional model, maintaining translational invariance in one spatial direction. This one-dimensional configuration is energetically degenerate to the translationally invariant solution, a hint in favor of a possible translational symmetry breakdown by more general geometrical structures. In the Nambu-Jona-Lasinio model, topological soliton configurations induce a finite baryon number. In contrast to the 1+1 dimensional model we do not find a massless baryon, but a state with zero binding energy.

Contents

1. Introduction

The description of dense relativistic matter is a major field of current research in quantum field theory. An important question in this area is: What are the properties of strongly interacting matter under extreme conditions, for instance in the center of a neutron star? For a theoretical treatment of this question from first principles one has to consider a region occupied by quarks described by Quantum Chromodynamics (QCD). The basic task is to determine the ground state at zero temperature. When the density of quarks is increased, one expects phase transitions from a gas of hadrons to nuclear matter and eventually to quark matter. Apart from this basic picture, there is a very rich spectrum of possibilities for the ground state, e.g. color superconducting phases, where quark pairing occurs via the BCS mechanism of superconductivity [1].

The most important framework for a numerical description of QCD is lattice gauge theory. With this method it is possible to determine numerically the properties of single baryons as bound states of quarks, whereas the treatment of dense baryonic matter is not accessible with the standard Monte Carlo techniques. The results for the ground state of QCD in this regime thus rely mostly on effective models. The most commonly used model is the Nambu-Jona-Lasinio (NJL) model [2, 3] in which pointlike interactions ("four-fermion" interactions) between quarks replace the full gluon mediated quark interaction. This model reproduces the spontaneous breakdown of chiral symmetry observed in QCD: The ground state consists of a homogeneous condensate of quark-antiquark pairs which acts as an effective mass of the "constituent quarks".

In this work, we will discuss the properties of dense matter in four-fermion models in 1+1 and 2+1 dimensions. In contrast to the 3+1 dimensional case, these toy models are renormalizable, which is an important property of QCD. In order to implement the breakdown of chiral symmetry in the vacuum, we will take the limit of a large number of fermion flavors, the 't Hooft limit. This circumvents no-go theorems which forbid spontaneous symmetry breakdown in low dimensions. In addition, mean field methods become exact in this limit, which makes it possible to find an analytical solution in some cases.

The restriction to low dimensions is interesting from a theoretical point of view: In the 1+1 dimensional models we can find an analytical, non-perturbative description of the finite density ground state including baryons as bound states of fermions. This is very rare in quantum field theory. Since it is more desirable to study the physically relevant case of 3+1 dimensions, the transition from 1+1 to 2+1 dimensions is particularly interesting. Naturally, the complexity added by the extra spatial dimension will require further approximations and numerical calculations.

The best known 1+1 dimensional four-fermion model is the Gross-Neveu (GN) model [4], which was designed as a toy model for chiral symmetry breakdown. It is perhaps the most simple interacting field theory of fermions one can write down. The four-fermion interaction term $\sim (\bar{\psi}\psi)^2$ is the fermionic analog of the ϕ^4 model often used to introduce the basic

concepts of field theory. In the 't Hooft limit the GN model uncovers a surprising number of phenomena of interest to strong interaction physics. These are asymptotic freedom, dimensional transmutation, the existence of mesons and spontaneous breakdown of chiral symmetry. In addition, shortly after the initial work by Gross and Neveu, localized bound states of fermions were found [5]. They are interpreted as the "baryons" of the model and have a kink-antikink like structure: The baryon carves out a spatial region around itself, wherein the fermion condensate is suppressed, thus reducing its effective mass at the expense of volume and gradient energy associated with the deviation of the condensate from its vacuum value.

The properties of the GN model at finite density where first investigated in 1985 [6]. At zero temperature, a first order phase transition from a massive Fermi gas to a chirally symmetric state was found. This description did not take into account the existence of baryons, which form a one-dimensional crystal at finite density. Following a variational calculation to approximate the correct ground state for dense matter [7], the exact solution was found in 2003 [8]. The emergence of such an inhomogeneous state of cold, dense matter is also discussed in QCD, where it is analogous to the "LOFF" state of superconductivity, first explored by Larkin, Ovchinnikov, Fulde and Ferrell (see Ref. [9]).

The mechanism which drives spontaneous breakdown of translational invariance in the GN model is closely related to the Peierls effect known from condensed matter physics. In fact, apart from its use as a toy model in particle physics, the GN model describes a variety of quasi-one-dimensional condensed matter systems such as the Peierls-Fröhlich model, conducting polymers like polyacetylene, or inhomogeneous superconductors. Of course, the Dirac description of fermions has a different origin in these systems than in high energy physics. It is derived from a linearized dispersion relation of the electrons at the Fermi surface in a (nearly) half-filled band, where the Fermi velocity plays the role of the velocity of light and the band width the role of the ultra-violet (UV) cutoff (see Ref. [10] for a review).

The second 1+1 dimensional toy model we will discuss in this work is the 1+1 dimensional version of the NJL model with a continuous rather than a discrete chiral symmetry, also discussed in the work by Gross and Neveu [4]. The higher symmetry is motivated by the approximate continuous chiral symmetry of QCD and has important consequences for the properties of the ground state. The baryons in this model emerge as topologically non-trivial excitations of the Goldstone boson field. This leads to a picture similar to the Skyrme model of nuclear physics, which describes nucleons as chiral solitons [11]: A finite winding number of the meson field induces baryon number through the interaction with the fermions. At finite density, the baryons in the 1+1 dimensional NJL model form a crystal with a helical shape, the "chiral spiral" [12].

Since quarks are massive in nature, it is worthwhile to discuss these toy models including a bare mass of the fermions, breaking chiral symmetry explicitly. In view of the fact that a lot of effort is presently devoted to computing chiral corrections, the 1+1 dimensional four-fermion models could be used as testing ground for new theoretical approaches. As described above, the massless models have been studied comprehensively by now. In contrast, the massive versions have not yet been solved in any systematic manner. In Part I of this work we will be able to give a consistent picture of the properties of dense matter in both the massive GN model and the massive NJL model. As compared to the chirally symmetric limit, the calculations become significantly more complex.

In Part II of this work we will discuss the 2+1 dimensional versions of the massless GN and the NJL model. As in the 1+1 dimensional case, the models have been studied extensively assuming a translationally symmetric ground state [13, 14, 15]. However, baryons as localized multi-fermion bound states are not known so far, so that the initial situation for a description of dense matter is rather different. Hence, in the case of the NJL model, this work concentrates on the question whether the four-fermion interaction in 2+1 dimensions is strong enough to support baryonic bound states. The extra spatial dimension induces additional complexity, so that an analytical treatment like in the 1+1 dimensional model does not seem to be possible. One has to rely on approximation techniques and numerical calculations to get information on the ground state. For the GN model, we choose a different approach. We extend the baryon crystal solution of the 1+1 dimensional model assuming translational invariance in one spatial direction. This "stripe" ansatz is not motivated by physics arguments, but should be viewed as a preliminary calculation to explore the possibility of a spontaneous breakdown of translational symmetry.

This work is organized as follows. Chapter 2 gives the basic definitions for the four-fermion models discussed in this work and describes the techniques needed to calculate the ground state. This includes the mean field, or Hartree-Fock method, the renormalization procedure, the definition of the baryon number and the derivative expansion. The subject of Chapter 3 is the massive GN model in 1+1 dimensions. We first give the self-consistent solution for the single baryon and then investigate the properties of the baryon crystal which emerges at finite density. In Chapter 4, the massive NJL model is discussed using the derivative expansion technique. In contrast to the GN model, here we aim at an expansion of ground state properties for small bare mass parameters and low densities.

In Chapter 5 of Part II, we derive a self-consistent solution of the 2+1 dimensional GN model with a stripe structure based on the baryon crystal in 1+1 dimensions. In Chapter 6 we describe the search for stable baryon solutions of the NJL model in 2+1 dimensions. In order to calculate the total energy for a given configuration, we use the derivative expansion for slowly varying fields and a numerical technique for small sized solitons. In Chapter 7 we summarize our results and give a brief outlook. Appendix A discusses some subtleties of the description of Dirac fermions in 1+1 and 2+1 space-time dimensions. The known results with a translationally invariant mean field are reviewed in Appendix B and C for the 1+1 and 2+1 dimensional models, respectively. Appendices D-H contain further technical details.

2. Basic definitions and methods

Four-fermion interaction models are relativistic, fermionic quantum field theories with a self-interaction term consisting of four fermion fields. In the literature a large variety of such models can be found, designed for applications in high energy, nuclear and condensed matter physics. The theories differ in the number of space-time dimensions, the number of different fermion field species and in the symmetries of the underlying Lagrangian. The best known four-fermion models are the Gross-Neveu (GN) model and the Nambu-Jona-Lasinio (NJL) model. In this work, we work out the properties of these basic models in 1+1 and 2+1 space-time dimensions. The following chapter gives an overview of the vacuum properties of the models and introduces the methods used to describe the ground state.

2.1. Lagrangians and symmetries

In its original form, the GN model [4] is a renormalizable quantum field theory of N species of fermions in 1+1 dimension with the Lagrangian

$$\mathcal{L}_{\mathrm{GN}_2} = \sum_{n=1}^{N} \bar{\psi}^{(n)}(\mathrm{i}\gamma^\mu\partial_\mu - m_0)\psi^{(n)} + \frac{1}{2}g^2\left(\sum_{n=1}^{N}\bar{\psi}^{(n)}\psi^{(n)}\right)^2 . \tag{2.1}$$

The bare mass term $\sim m_0$ explicitly breaks the discrete chiral symmetry $\psi \to \gamma^5\psi$ of the massless model. Gross and Neveu also introduced the corresponding model with continuous chiral symmetry $\psi \to \mathrm{e}^{\mathrm{i}\alpha\gamma^5}\psi$, which is nothing but the Nambu-Jona-Lasinio (NJL) [2, 3] model in 1+1 dimensions. It is defined by the Lagrangian

$$\mathcal{L}_{\mathrm{NJL}_2} = \bar{\psi}\left(\mathrm{i}\gamma^\mu\partial_\mu - m_0\right)\psi + \frac{1}{2}g^2\left[(\bar{\psi}\psi)^2 + (\bar{\psi}\mathrm{i}\gamma^5\psi)^2\right], \tag{2.2}$$

where the sum over fermion species is suppressed. In 1+1 dimensions, ψ is a two-component spinor. The two gamma matrices γ^μ can be chosen proportional to two Pauli matrices. The chiral gamma matrix $\gamma^5 = \gamma^0\gamma^1$ is then proportional to the third Pauli matrix (see Appendix A for details).

In 2+1 dimensions, the GN model is defined by the same Lagrangian (2.1), with the index μ summed over 3 space-time directions [15]. Due to the additional spatial dimension the fermion fields are defined in a different representation of the Lorentz group in 2+1 dimensions. With a two-dimensional representation of the Dirac algebra $\{\gamma^\mu, \gamma^\nu\} = 2g^{\mu\nu}$, e.g.

$$\gamma^0 = \sigma_3 \quad \gamma^1 = \mathrm{i}\sigma_1 \quad \gamma^2 = \mathrm{i}\sigma_2,$$

there does not exist a matrix γ^5 which anticommutes with all these γ^μ. This shows that chiral symmetry cannot be defined in the usual sense. Moreover, the standard mass term $\sim \bar{\psi}\psi$ violates parity, which in 2+1 dimensions can be defined by inversion of one spatial coordinate

$$(t, x^1, x^2) \to (t, -x^1, x^2) \qquad \psi_P = -\mathrm{i}\gamma^1\psi.$$

A common way around this problem is to introduce an additional "isospin" degree of freedom for the fermion fields [16, 17, 15]. The fields ψ become 4-component spinors with a spin and an isospin index. A mass term is then defined with an additional matrix acting in isospin space (see Appendix A for details). In terms of isospin matrices $\tau_i = \sigma_i$, the Lagrangian of the massless GN model in 2+1 dimension reads

$$\mathcal{L}_{\mathrm{GN}_3} = \mathrm{i}\bar{\psi}\gamma^\mu\partial_\mu\psi + \frac{g^2}{2}(\bar{\psi}\tau_3\psi)^2.$$

The theory is invariant under the discrete "chiral" symmetry transformations

$$\psi \mapsto \tau_1\psi, \qquad \psi \mapsto \tau_2\psi.$$

The symmetry is dynamically broken if $\bar{\psi}\tau_3\psi$ acquires a non-zero ground state expectation value, because this scalar is odd under discrete chiral transformations. In the literature one also finds the same model with an interaction term proportional to $(\bar{\psi}\psi)^2$ [18]. In such a model, the vacuum breaks parity spontaneously.

The 2+1 dimensional analog of a continuous "chiral" symmetry is the set of global $U(2)$ transformations generated by the isospin matrices τ_a and the unit matrix. The four-fermion model which respects this continuous symmetry will be referred to as the NJL model in 2+1 dimensions. Its Lagrangian reads

$$\mathcal{L}_{\mathrm{NJL}_3} = \bar{\psi}\mathrm{i}\gamma^\mu\partial_\mu\psi + \frac{g^2}{2}\left[(\bar{\psi}\tau_1\psi)^2 + (\bar{\psi}\tau_2\psi)^2 + (\bar{\psi}\tau_3\psi)^2\right].$$

If $\bar{\psi}\tau_3\psi$ acquires a ground state expectation value, the symmetry group $U(2)$ is broken down to $U(1)\times U(1)$. This corresponds to conservation of fermion number and the 3-component of the isospin with the Noether currents

$$j^\mu = \bar{\psi}\gamma^\mu\psi, \qquad j_3^\mu = \bar{\psi}\gamma^\mu\tau_3\psi.$$

Like in 1+1 dimensions one can also consider a mass term $\sim m_0\bar{\psi}\tau_3\psi$, explicitly breaking chiral symmetry. In this work we only consider the chirally symmetric 2+1 dimensional models.

2.2. Hartree-Fock method

The four-fermion models described above will be discussed in the 't Hooft limit $N \to \infty$, $g^2 \sim 1/N$. In the models discussed in this work, this limit is taken for different reasons. In the 1+1 dimensional models the large N limit is used to circumvent the Mermin-Wagner theorem [19, 20] which rules out spontaneous breakdown of a continuous symmetry at zero temperature or of a discrete symmetry at finite temperature. In the 2+1 dimensional models this theorem does not apply for zero temperature. Here the large N limit is needed to define a non-perturbative renormalization procedure in a similar way as in 1+1 dimensions (see Ref. [13]). For the finite temperature case Hohenberg showed that a continuous symmetry cannot be broken spontaneously in 2+1 dimensions [21]. This restriction is again circumvented by the 't Hooft limit.

Apart from that, semiclassical methods become exact in the large N limit, which is crucial for the solvability of the models. In order to determine the properties of the ground state, we can

use a mean field method. This is a common approach also for more elaborate four-fermion models in 3+1 dimensions aiming to describe quark matter. In the language of many particle physics, we apply the Hartree-Fock (HF) approximation. This method will be described in the following.

The large N limit implies that interaction terms like $\bar{\psi}\psi$ in GN_2 are equal to their expectation value up to terms of order $1/N$ [22]. The Euler-Lagrange equation for GN_2

$$\left[\mathrm{i}\gamma^\mu\partial_\mu - m_0 + g^2(\bar{\psi}\psi)\right]\psi = 0$$

can be interpreted as a theory of independent particles in the mean field potential $\langle\bar{\psi}\psi\rangle$. For stationary states the mean field is time-independent. The field is then expressed in terms of the solutions of the single particle Dirac-Hartree-Fock equation

$$\left[-\mathrm{i}\gamma^5\partial_1 + \gamma^0\sigma(x)\right]\psi_\alpha(x) = E_\alpha\psi_\alpha(x). \tag{2.3}$$

The mean field σ is subject to the self-consistency condition

$$\sigma = -g^2\langle\bar{\psi}\psi\rangle + m_0. \tag{2.4}$$

This relativistic HF approach can also be formulated in the functional integral formalism. Here, it is equivalent to the saddle-point condition for the generating functional (see Refs. [5, 23]).

We apply the HF method also to the large N limit of NJL_2 and to both models in 2+1 dimensions. The HF Hamiltonians for the models with continuous chiral symmetry are

$$H_{\mathrm{NJL}_2} = -\mathrm{i}\gamma^5\partial_1 + \gamma^0\sigma + \mathrm{i}\gamma^1\pi \tag{2.5}$$

$$H_{\mathrm{NJL}_3} = -\mathrm{i}\gamma^0\gamma^k\partial_k + \gamma^0\sum_{a=1}^{3}\phi_a\tau_a, \tag{2.6}$$

where the index k runs over the two spatial directions. The self-consistency conditions read

$$\sigma = -g^2\langle\bar{\psi}\psi\rangle + m_0, \quad \pi = -g^2\langle\bar{\psi}\mathrm{i}\gamma^5\psi\rangle \tag{2.7}$$

$$\phi_a = -g^2\langle\bar{\psi}\tau_a\psi\rangle \quad (a = 1, 2, 3). \tag{2.8}$$

The Hamiltonians for the models with discrete chiral symmetry in 1+1 and 2+1 dimensions are obtained by setting $\pi = 0$ and $\phi_1 = \phi_2 = 0$, respectively. In the following we will use vector notation for the 3 mean fields in 2+1 dimensions,

$$\boldsymbol{\phi}\cdot\boldsymbol{\tau} \equiv \sum_{a=1}^{3}\phi_a\tau_a.$$

The fields σ, π and $\boldsymbol{\phi}$ serve as order parameters for the corresponding chiral symmetries. If they are spatially varying, the ground state breaks translational symmetry.

For finite N and finite temperature, quantum fluctuations of the mean field potentials destroy any long range order. This is the essence of the no-go theorems mentioned in the beginning of this section. The large N limit suppresses quantum fluctuations of σ, π and $\boldsymbol{\phi}$ and thus lifts this restriction.

In the HF approach, the ground state energy is calculated by summing over single particle energies of all occupied states and adding a term correcting the double counting of the interaction energy. The occupation is determined by the fermion number of the system. With the HF energies from Eq. (2.3) this is

$$E_{\mathrm{gs}} = \sum_{\alpha}^{\text{occupied}} E_\alpha + E_{\mathrm{dcc}}, \tag{2.9}$$

with the double counting correction (dcc) terms (set $\pi = 0$ and $\phi_1 = \phi_2 = 0$ for GN_2 and GN_3)

$$E_{\mathrm{dcc}}^{\mathrm{NJL}_2} = \int \mathrm{d}x \frac{(\sigma - m_0)^2 + \pi^2}{2Ng^2}, \qquad E_{\mathrm{dcc}}^{\mathrm{NJL}_3} = \int \mathrm{d}^2x \frac{\boldsymbol{\phi}^2}{2Ng^2}. \tag{2.10}$$

Due to the Dirac sea, the sum in Eq. (2.9) diverges. The next section introduces the standard regularization and renormalization procedure for the HF method.

2.3. Vacuum and renormalization

In 1+1 dimensions, the coupling constant g is dimensionless and four-fermion models are therefore perturbatively renormalizable. This is different in 2+1 dimensions, where the models are renormalizable in every order of an expansion in $1/N$ [13]. Using the HF method, a consistent renormalization scheme can be defined for both cases in which the bare coupling constant is traded for the physical fermion mass.

In all models considered here, chiral symmetry is broken in the vacuum if the mean fields are non-vanishing. Homogeneous self-consistent fields act as a dynamical fermion mass generated by the four-fermion interaction. In the chiral limit ($m_0 = 0$), the possible ground states for NJL_2 lie on the chiral circle $\sigma^2 + \pi^2 = m^2$, for NJL_3 on the chiral sphere $\boldsymbol{\phi}^2 = m^2$. For the 1+1 dimensional models with a bare mass term $m_0 > 0$, the vacuum is unique with $\sigma = m$, $\pi = 0$. In order to find the self-consistent fermion mass m, we calculate the total HF vacuum energy density regulated with the momentum cutoff Λ,

$$\text{(1+1)} \qquad E_{(0)} = -\int_{-\Lambda/2}^{\Lambda/2} \frac{\mathrm{d}p}{2\pi} \sqrt{p^2 + m^2} + \frac{(m - m_0)^2}{2Ng^2} \tag{2.11}$$

$$\text{(2+1)} \qquad E_{(0)} = -2\int_{|\mathbf{p}|<\Lambda} \frac{\mathrm{d}^2p}{(2\pi)^2} \sqrt{\mathbf{p}^2 + m^2} + \frac{m^2}{2Ng^2}. \tag{2.12}$$

The energy is now minimized with respect to m,

$$\frac{\partial E_{(0)}}{\partial m} = 0. \tag{2.13}$$

As is well-known from HF theory, the minimum condition is equivalent to the self-consistency conditions (2.7) and (2.8). It leads to the gap equations

$$\text{(1+1)} \qquad \frac{(m - m_0)}{Ng^2} = \frac{m}{\pi} \ln \frac{\Lambda}{m} \tag{2.14}$$

$$\text{(2+1)} \qquad \frac{1}{Ng^2} = \frac{1}{\pi}(\Lambda - m). \tag{2.15}$$

In the 1+1 dimensional case, Eq. (2.14) determines a global minimum for all values of the dimensionless coupling constant. In 2+1 dimensions however, the gap equation leads to the minimum of $E_{(0)}$ only if the coupling constant is tuned to be above a critical value, i.e., $Ng^2 > Ng_c^2 = \pi/\Lambda$. In this work, we will only consider this case where chiral symmetry is broken by the vacuum and the dynamical fermion mass is determined by Eq. (2.15).

The gap equations are now used to eliminate the coupling constant g in favor of m in physically meaningful quantities like the fermion density or the chiral condensate. Renormalizability of the model then leads to the cancellation of all divergent terms involving the cutoff Λ. The remaining finite part is expressed in terms of the vacuum fermion mass m as the only mass scale. Hence, the gap equations (2.14) summarize the renormalization scheme for four-fermion models in the large N limit.

In the massive case in 1+1 dimensions, a second physically meaningful, renormalization group invariant parameter appears, m_0/Ng^2. It enters the renormalized vacuum energy (2.11) and observables like the fermion-antifermion scattering amplitude or the mass of the "pion" in the NJL_2 model [24]. The σ-meson is unbound and disappears from the spectrum for any $m_0 \neq 0$, the π-meson becomes massive in the familiar way (Gell-Mann, Oakes, Renner relation). We introduce the physical parameter[1]

$$\gamma = \frac{\pi}{Ng^2}\frac{m_0}{m} = \frac{m_0}{m}\ln\frac{\Lambda}{m}.$$

Notice that it can also be expressed in terms of the physical fermion masses at bare mass m_0 and in the chiral limit

$$\gamma = \ln\frac{m[m_0]}{m[0]}. \tag{2.16}$$

Whereas the gap equation (2.14) introduces the vacuum fermion mass m as the overall mass scale, the parameter $\gamma \geq 0$ labels different physical theories. It measures the amount of chiral symmetry breaking and vanishes in the massless ($m_0 = 0$) case. The gap equation (2.14) can now be written as

$$\frac{\pi}{Ng^2} = \gamma + \ln\frac{\Lambda}{m}. \tag{2.17}$$

Using the gap equation, the renormalized vacuum energy density (2.11) and (2.12) becomes

$$\text{(1+1)} \qquad E_{(0)}^{\mathrm{ren}} = -\frac{m^2}{4\pi} - \frac{\gamma m^2}{2\pi} \tag{2.18}$$

$$\text{(2+1)} \qquad E_{(0)}^{\mathrm{ren}} = -\frac{m^3}{6\pi}. \tag{2.19}$$

Divergent terms independent of m have been dropped ($-\Lambda^2/8\pi$ and $\Lambda^3/3\pi$).

2.4. Baryon number

In order to study fermionic matter or antimatter, the number of filled levels in the single particle spectrum as compared to the vacuum case has to be increased or reduced. In GN_2 and GN_3 this can only be achieved by filling positive energy levels or leaving holes in the

[1] Note the different definition without the factor of π in [25] and [23]

Dirac sea, since the spectrum of the HF Hamiltonian of these models is symmetric, i.e., every eigenstate with energy E has a corresponding eigenstate with energy $-E$. This is due to the fact that there exists a matrix in spin/isospin space which anticommutes with H, such as γ^1 in 1+1 dimensions, and for example $\gamma^0\tau_2$ in 2+1 dimensions (cp. (2.5) and (2.6)). The fermion number of a single bound state is now determined by the occupation fraction of the valence state $\nu = n/N$.

In the models with continuous chiral symmetry, NJL_2 and NJL_3, topologically nontrivial configurations of the mean field (σ, π in 1+1 dimensions and $\boldsymbol{\phi}$ in 2+1 dimensions) can lead to additional negative/positive energy levels in the single particle spectrum as compared to the topologically trivial vacuum. This spectral asymmetry induces a finite fermion number in the system. If all negative energy states are filled completely, this number is an integer multiple of N. We can define the baryon number by

$$B = -\frac{1}{2}(\#\text{ positive eigenvalues} - \#\text{ negative eigenvalues}). \tag{2.20}$$

Each additional positive energy level is interpreted as a bound state of N fermions, i.e., a baryon. Note that it is also possible to describe partially filled bound states, where the valence state is filled with $n < N$ fermions [26].

For mean field configurations restricted to a sphere of degenerate ground states, $\boldsymbol{\phi}^2 = m^2$ and $\sigma^2 + \pi^2 = m^2$, it can be shown that B is determined by a topological invariant of these fields (see Refs. [27, 28, 29, 30, 31]).

In 1+1 dimensions we define the chiral angle $\chi(x)$ by

$$\sigma = m\cos 2\chi \qquad \pi = -m\sin 2\chi. \tag{2.21}$$

The topological invariant is the winding number, which counts the number of times the mean field wraps around the circle of ground states. It labels the elements of the homotopy group $\pi_1(S^1) = \mathbb{Z}$ and can be written as

$$B_{\mathrm{top}} = \frac{1}{\pi}\int \mathrm{d}x\, \chi'. \tag{2.22}$$

In 2+1 dimensions the topological invariant is the wrapping number (related to the homotopy group $\pi_2(S^2) = \mathbb{Z}$)

$$B_{\mathrm{top}} = \frac{1}{4\pi}\int \mathrm{d}^2x\, \boldsymbol{\phi}\cdot\left[(\partial_1\boldsymbol{\phi})\times(\partial_2\boldsymbol{\phi})\right]. \tag{2.23}$$

These two results will be derived in Sections 4.1 and 6.1, where the derivative expansion method is applied to calculate the baryon number. It will be shown that Eqs. (2.22), (2.23) hold in every order of an expansion for slowly varying mean fields.

2.5. Derivative expansion method

The principle of the relativistic HF method described above is quite simple. In order to calculate baryon number and ground state energy, the HF equations have to be solved. This is done by minimization of the HF energy in a space of trial functions for the mean fields. However, the eigenvalue problem for the Hamiltonians in (2.5) and (2.6) can in general not be

treated analytically and a numerical solution is quite involved due to the Dirac sea. In specific cases, one may be able to circumvent the HF procedure. One important example is the case of slowly varying fields, where energy and baryon number can be calculated in an expansion in powers of derivatives of the mean field. This derivative expansion will be introduced in the following, based on Refs. [32],[31]. Basic formulae and the notation are taken over from the latter reference.

The central quantity for the calculation of total energy and baryon number is the spectral density, for which we write down the formal expression

$$\sigma(E) = \mathrm{Tr}\,\delta(H-E) = \frac{1}{\pi}\mathrm{Im}\,R(E+\mathrm{i}\epsilon),$$

where we have introduced the resolvent

$$R(z) = \mathrm{Tr}\,\frac{1}{H-z} = \mathrm{Tr}\,\frac{H+z}{H^2-z^2}.$$

The induced baryon number (2.20) is

$$B = -\frac{1}{2}\int_{-\infty}^{\infty}\mathrm{d}E\,\sigma(E)\,\mathrm{sgn}(E) = -\frac{1}{2\pi}\mathrm{Im}\int_0^{\infty}\mathrm{d}E\,[R(E+\mathrm{i}\epsilon)+R(-E-\mathrm{i}\epsilon)]\,, \tag{2.24}$$

whereas the ground state energy can be written as an integral over the HF energies plus the double counting correction (cp. (2.9))

$$E_{\mathrm{gs}} - E_{\mathrm{dcc}} = \int_{-\infty}^{0}\mathrm{d}E\,E\,\sigma(E) = \frac{1}{\pi}\mathrm{Im}\int_{-\infty}^{0}\mathrm{d}E\,E\,R(E+\mathrm{i}\epsilon). \tag{2.25}$$

The derivative expansion involves a systematic expansion of the resolvent in powers of derivatives of the mean fields. In a notation similar to Ref. [31] we decompose H and H^2 formally into a kinetic part and an interaction part which contains the mean field,

$$H = K + I\ , \qquad H^2 = H_0^2 + V \tag{2.26}$$

and expand the resolvent in powers of V,

$$R(z) = \mathrm{Tr}(K+I+z)\frac{1}{H_0^2-z^2+V} = \mathrm{Tr}(K+I+z)\left(G\sum_{n=0}^{\infty}(-VG)^n\right) \tag{2.27}$$

with the "free Green's function"

$$G = \frac{1}{H_0^2-z^2}.$$

If one commutes the V's through the G's by repeatedly applying the identity

$$GV = VG + G\left[V, H_0^2\right]G,$$

one generates the derivative expansion, because the commutator $[V, H_0^2]$ involves derivatives of V. As is well known, this method quickly becomes tedious due to the proliferation of higher order terms. Therefore we shall use another technique, which can be more easily realized using computer algebra programs such as Maple. The trace in the basic building blocks of the expansion (2.27)

$$\mathrm{Tr}(K+I+z)G(VG)^n \tag{2.28}$$

is evaluated in momentum space. We first consider the 1+1 dimensional case, which can be easily generalized to higher dimensions. In momentum space the term proportional to z is

$$\begin{aligned}\mathrm{Tr}G(VG)^n = \int \frac{\mathrm{d}p}{2\pi}\frac{\mathrm{d}q_1}{2\pi}\ldots\frac{\mathrm{d}q_{n-1}}{2\pi}G(p)^2G(p+q_1)\ldots \\ G(p+q_{n-1})\,\mathrm{tr}\,V(q_1)V(q_2-q_1)\ldots V(-q_{n-1}),\end{aligned}$$

where now tr is only the Dirac trace. In p-space, the potentials vary rapidly as compared to the Green's functions. We can therefore expand the product of G's in a power series in the q_i's. Once this is done, we transform the potentials back to coordinate space and carry out most of the integrations. The q_i's are replaced by derivatives acting on the V's,

$$\begin{aligned}\mathrm{Tr}G(VG)^n = \int \mathrm{d}x \int \frac{\mathrm{d}p}{2\pi}G(p)^2G(p+q_1)\ldots G(p+q_{n-1})|_{q_k=i(\partial_1+\ldots+\partial_k)} \\ \cdot\ \mathrm{tr}\ V(x_1)V(x_2)\ldots V(x_n)|_{x_k=x}\,.\end{aligned} \tag{2.29}$$

We have suppressed the Taylor expansion in Eq. (2.29) in order to keep the structure of the formula transparent. The other two terms in Eq. (2.28) can be handled similarly with the result

$$\begin{aligned}\mathrm{Tr}IG(VG)^n &= \int \mathrm{d}x \int \frac{\mathrm{d}p}{2\pi}G(p)G(p+q_1)\ldots G(p+q_n)|_{q_k=i(\partial_1+\ldots+\partial_k)} \\ &\quad\cdot\ \mathrm{tr}\ I(x_1)V(x_2)V(x_3)\ldots V(x_{n+1})|_{x_k=x} \\ \mathrm{Tr}KG(VG)^n &= \int \mathrm{d}x \int \frac{\mathrm{d}p}{2\pi}p\,G(p)^2G(p+q_1)\ldots G(p+q_{n-1})|_{q_k=i(\partial_1+\ldots+\partial_k)} \\ &\quad\cdot\ \mathrm{tr}\ \sigma_3V(x_1)V(x_2)\ldots V(x_n)|_{x_k=x}\,.\end{aligned} \tag{2.30}$$

In 2+1 dimensions, the same formulas apply if we replace the one-dimensional integrals over x and p in the results Eqs. (2.29,2.30) by two-dimensional integrals, $\mathrm{d}x \to \mathrm{d}^2x$, $\mathrm{d}p/(2\pi) \to \mathrm{d}^2p/(2\pi)^2$.

Note, that this procedure is not expected to give a good approximation of the spectral density but only of integrals over $\sigma(E)$. This is sufficient for our purpose.

Part I.

1+1 dimensional models

3. Model with discrete chiral symmetry

The bound states of fermions in the massless 1+1 dimensional GN model have been found by Dashen, Hasslacher and Neveu (DHN) [5] shortly after the model was proposed. These bound states ("baryons") were derived by DHN with functional and inverse scattering methods. A different approach using methods from relativistic many particle physics [22] (introduced in Chapter 2) prepared the ground for the description of dense baryonic matter in the massless model [8].

Since the GN model is used as a toy model for dense relativistic quark matter, and since quarks in nature are massive, it is worthwhile to study the extension of the GN model to massive fermions. It turns out that with this additional complication, it is still possible to apply the same methods as in the chiral limit to get an analytical solution of the ground state of the theory. The baryons and the behavior of dense baryonic matter of the massive 1+1 dimensional GN model are the subject of this chapter (published in [25] and [33]).

The starting point of the discussion is the HF equation (2.3). We choose a representation of the γ-matrices where γ^1 is diagonal,

$$\gamma^0 = -\sigma_1, \qquad \gamma^1 = \mathrm{i}\sigma_3, \qquad \gamma^5 = \gamma^0\gamma^1 = -\sigma_2. \tag{3.1}$$

In this representation, the equations for the upper and lower components $\phi_\pm$ of the Dirac spinor ψ can be decoupled by squaring the Hamiltonian,

$$\left(-\partial_x^2 \mp \sigma' + \sigma^2\right)\phi_\pm = E^2\phi_\pm. \tag{3.2}$$

Eq. (3.2) states that the Schrödinger-type Hamiltonians with potentials $U_\pm = \sigma^2 \pm \sigma'$ have the same spectrum, a textbook example of supersymmetric quantum mechanics with superpotential σ [34].

The Schrödinger potentials of static localized solutions of the GN_2 model have to be reflectionless. A proof of this fact is given in Refs. [5] and [35]. In these references the energy density is written in terms of "scattering data", i.e., the reflection amplitude and parameters specifying the bound states. The minimization of the energy as a function of the scattering data then leads to reflectionless Schrödinger potentials. This fact will guide our choice of the ansatz for the mean field potential $\sigma(x)$.

3.1. Baryons

In the search for bound states in the massive GN model, Feinberg and Zee [23] have performed a variational calculation, based on the scalar potential of the DHN kink-antikink baryon. They compute the energy of the baryon and discuss the limiting cases of small and large bare quark masses. They conclude that their ansatz does not satisfy the self-consistency condition.

Claims made in this paper about the non-existence of static bags in the massive GN model have later been retracted by the authors [36]. In this section, we will revise the result of Ref. [23] by proving that the ansatz for the baryon potential is a self-consistent solution to the HF equation.

Our trial scalar potential for baryons is the same as in the $m_0 = 0$ case [22],

$$\sigma(x) = m\left[1 + y\left(\tanh\xi_- - \tanh\xi_+\right)\right] \tag{3.3}$$

with

$$\xi_\pm = ymx \pm \frac{1}{2}\operatorname{arctanh} y,$$

where m is the physical fermion mass in the vacuum and $y \in [0,1]$ the only variational parameter. The mean field leads to the Schrödinger potentials in Eq. (3.2)

$$\sigma^2 \pm \sigma' = m^2\left[1 - \frac{2y^2}{\cosh^2\xi_\pm}\right], \tag{3.4}$$

which differ only by a translation in space (they are "self-isospectral" in the terminology of supersymmetric quantum mechanics). Since these are the unique reflectionless potentials with a single bound state, the ansatz (3.3) is a good candidate for the self-consistent single baryon potential. As compared to the massless case we will get a different relation between the variational parameter y and the occupation fraction $\nu = n/N$ of the valence state.

We first evaluate the baryon mass which is the ground state energy (2.9) of the baryon configuration minus the vacuum energy. In order to calculate the difference between the two spectra, the system is enclosed in a box with periodic boundary conditions. The divergent sum over the energy differences is regulated with a momentum cutoff Λ. This calculation is identical to the massless case from where we take over the result for the mass contribution from the continuum states (see Eqs. (3.42) and (3.44) in [22])

$$\begin{aligned}\Delta E_{\text{cont}} &= \frac{2Nym}{\pi} + 2Nym\int_{-\Lambda/2}^{\Lambda/2}\frac{\mathrm{d}k}{2\pi}\frac{1}{\sqrt{k^2+m^2}} + \frac{2Nm}{\pi}\sqrt{1-y^2}\arctan\frac{\sqrt{1-y^2}}{y} \\ &= \frac{2Nym}{\pi}\left[1 + \ln\frac{\Lambda}{m} + \frac{\sqrt{1-y^2}}{y}\arctan\frac{\sqrt{1-y^2}}{y}\right],\end{aligned} \tag{3.5}$$

and the discrete states

$$\Delta E_{\text{discr}} = -N(1-\nu)m\sqrt{1-y^2}. \tag{3.6}$$

The only difference to the chiral limit stems from the double counting correction Eq. (2.10)

$$\Delta E_{\text{dcc}} = \int \mathrm{d}x\,\frac{(\sigma - m_0)^2 - (m - m_0)^2}{2g^2}.$$

Using the gap equation (2.17), this becomes

$$\Delta E_{\text{dcc}} = \frac{N}{2\pi}\ln\frac{\Lambda}{m}\int \mathrm{d}x\,(\sigma^2 - m^2) + \frac{N}{2\pi}\gamma\int \mathrm{d}x\,(\sigma - m)^2.$$

Carrying out the integrations then yields

$$\Delta E_{\text{dcc}} = -\frac{2Nym}{\pi}\ln\frac{\Lambda}{m} - \frac{2Nm\gamma}{\pi}(y - \operatorname{arctanh} y). \tag{3.7}$$

Collecting the results (3.5), (3.6) and (3.7), the logarithmically divergent terms cancel and we get the baryon mass for our variational ansatz

$$\frac{M_B}{Nm} = \frac{2y}{\pi} + \frac{2}{\pi}\sqrt{1-y^2}\arctan\frac{\sqrt{1-y^2}}{y} - (1-\nu)\sqrt{1-y^2} - \frac{2\gamma}{\pi}(y - \operatorname{arctanh} y). \tag{3.8}$$

We now choose ν (i.e., the fermion number $N\nu$) and vary M_B with respect to y

$$\frac{\partial M_B}{\partial y} = 0,$$

or (discarding the trivial solution $y = 0$)

$$\sqrt{1-y^2}\left[\frac{1}{\pi}\arctan\frac{\sqrt{1-y^2}}{y} - \frac{1-\nu}{2}\right] = \frac{\gamma y}{\pi}. \tag{3.9}$$

Introducing the angle θ via $y = \sin\theta$ $(0 \le \theta \le \pi/2)$, we obtain

$$\frac{\pi\nu}{2} = \theta + \gamma\tan\theta. \tag{3.10}$$

If we eliminate ν from Eq. (3.8) with the help of Eq. (3.10), the baryon mass at the minimum finally becomes

$$\frac{M_B}{N} = \frac{2m}{\pi}\sin\theta + \frac{2m\gamma}{\pi}\operatorname{arctanh}(\sin\theta). \tag{3.11}$$

The last two equations agree with Ref. [36].

Now consider the self-consistency condition (2.4) for the condensate and scalar potential

$$-\frac{(\sigma - m_0)}{Ng^2} = \sum^{\text{occ}} \bar\psi\psi. \tag{3.12}$$

The r.h.s. of Eq. (3.12) gets contributions from the discrete states

$$\begin{aligned}\sum_{\text{discr}}^{\text{occ}} \bar\psi\psi &= (1-\nu)\frac{m}{2}\sqrt{1-y^2}\,(\tanh\xi_- - \tanh\xi_+)\\ &= (1-\nu)\frac{\sqrt{1-y^2}}{2y}(\sigma - m)\end{aligned} \tag{3.13}$$

and from the negative energy continuum,

$$\begin{aligned}\sum_{\text{cont}}^{\text{occ}} \bar\psi\psi &= -\sigma\int_{-\Lambda/2}^{\Lambda/2}\frac{\mathrm{d}k}{2\pi}\frac{1}{E(k)} - m^3 y(1-y^2)(\tanh\xi_- - \tanh\xi_+)\int\frac{\mathrm{d}k}{2\pi}\frac{1}{E(k)(k^2+m^2y^2)}\\ &= -\frac{\sigma}{\pi}\ln\frac{\Lambda}{m} - \frac{(\sigma-m)}{\pi}\frac{\sqrt{1-y^2}}{y}\arctan\frac{\sqrt{1-y^2}}{y},\end{aligned} \tag{3.14}$$

where we have again taken over results from Ref. [22]. The l.h.s. of Eq. (3.12) can be rewritten with the help of the gap equation (2.17),

$$-\frac{(\sigma - m_0)}{Ng^2} = -\frac{\sigma}{\pi}\ln\frac{\Lambda}{m} - \frac{\sigma - m}{\pi}\gamma. \tag{3.15}$$

Combining Eqs. (3.13), (3.14) and (3.15), the self-consistency condition assumes the form

$$\frac{1-\nu}{2}\frac{\sqrt{1-y^2}}{y} - \frac{1}{\pi}\frac{\sqrt{1-y^2}}{y}\arctan\frac{\sqrt{1-y^2}}{y} + \frac{\gamma}{\pi} = 0$$

which coincides with the variational equation (3.9). Therefore the variational potential turns out to be self-consistent and hence provides us with the exact baryon of the massive GN model in the large N limit. Although our variational calculation agrees with Ref. [36], we have come to a different conclusion concerning the self-consistency of this ansatz.

3.2. Dense matter

Due to the existence of baryons as localized bound states of fermions, we expect the ground state of the massive GN_2 model at finite density to break translational symmetry. In the massless limit $\gamma = 0$, a self-consistent solution of the HF equation consisting of a one-dimensional array of baryons, also referred to as baryon "crystal", was found analytically in Ref. [8]. In this section we will show that this analysis can be generalized to the massive case with an ansatz for the scalar potential taken from condensed matter physics literature. We will proceed as follows. After the periodic ansatz for the mean field is introduced, the ground state energy of such a configuration will be calculated with the HF method of Section 2.2. The self-consistency conditions (2.7) for this ansatz are derived in Subsection 3.2.3. Then it remains to prove that the self-consistent baryon crystal is energetically favored over the HF solution with translationally invariant mean field, summarized in Appendix B. This is done in the limit of low and high density in Section 3.2.4. The stability of the baryon crystal is shown numerically for all densities in Section 3.2.5.

3.2.1. Physical origin of the mean field ansatz

Apart from its use as a toy model in high energy physics, the GN model can serve to describe a variety of quasi-one-dimensional systems in condensed matter physics (see [37] for a review and further references). In particular, the massive GN_2 model describes electrons in a conducting polymer (*cis*-polyacetylene) in the vicinity of a half-filled band. Since the interpretation of the results in condensed matter physics is very different from high energy physics, we merely borrow the ansatz for the mean field and verify its self-consistency.

In order to find the right choice for the mean field σ in the HF equation (2.3), we follow references [38, 39] and extend the Schrödinger potential (3.4) to an array of infinitely many, equidistant potential wells. The lattice sum can be performed (see Eq. (6) in [38]) yielding a potential of the Lamé type

$$\sum_{n=-\infty}^{\infty}\frac{1}{\cosh^2(x-nd)} = \left(\frac{2\kappa\mathbf{K}'}{\pi}\right)^2\left[\frac{\mathbf{E}'}{\kappa^2\mathbf{K}'} - \mathrm{sn}^2\left(\frac{2\mathbf{K}'}{\pi}x\right)\right]. \tag{3.16}$$

It involves the complete elliptic integrals of first and second kind $\mathbf{E}$ and $\mathbf{K}$, the elliptic integrals $\mathbf{E}'$, $\mathbf{K}'$ with complementary elliptic modulus $\kappa' = \sqrt{1-\kappa^2}$ and the Jacobi elliptic

function $\mathrm{sn}(x,\kappa)$ where the argument κ will be suppressed in the following (see Appendix D). Comparing the spatial period of both sides of Eq. (3.16), we can relate d and κ via

$$d = \pi \frac{\mathbf{K}}{\mathbf{K}'} \ .$$

How does the fact that the single potential wells (3.4) are reflectionless manifest itself in the periodic extension (3.16)? This has been discussed in mathematical physics [40] and condensed matter physics [41] some time ago: The periodic potential has a single gap (or, in general, a finite number of gaps), in contrast to generic periodic potentials with infinitely many gaps. Thus reflectionless potentials generalize to "finite band potentials" as one proceeds from a single well to a periodic array. In the same way as the sech^2-potential is the unique reflectionless potential with one bound state, the sn^2-potential is the unique single gap potential.

Guided by these considerations, let us try to find the most general superpotential of the Lamé potential (plus an additive constant). After a scale transformation

$$\sigma(x) = A\tilde{\sigma}(\xi) \qquad \xi = Ax,$$

the Schrödinger potentials $U_\pm = \sigma^2 \pm \sigma'$ should assume the form of the Lamé potential (3.16) plus constant. Allowing for a translation in space between $U_\pm(x) = A^2 \tilde{U}_\pm(\xi)$, we have to solve the equations ($\xi_+ = \xi + b$)

$$\begin{aligned} \tilde{U}_+ &= \tilde{\sigma}^2 + \tilde{\sigma}' = 2\kappa^2 \mathrm{sn}^2 \xi_+ + \eta \\ \tilde{U}_- &= \tilde{\sigma}^2 - \tilde{\sigma}' = 2\kappa^2 \mathrm{sn}^2 \xi \quad + \eta, \end{aligned} \tag{3.17}$$

for $\tilde{\sigma}$ or, equivalently,

$$\begin{aligned} \tilde{\sigma}^2 &= \kappa^2 [\mathrm{sn}^2(\xi_+) + \mathrm{sn}^2 \xi] + \eta \\ \tilde{\sigma}' &= \kappa^2 [\mathrm{sn}^2(\xi_+) - \mathrm{sn}^2 \xi]. \end{aligned} \tag{3.18}$$

Differentiating the upper equation and dividing the result by the lower equation yields an ansatz for the scalar potential depending on the three real parameters A, κ, b

$$\tilde{\sigma}(\xi) = \frac{\mathrm{sn}\,\xi_+ \mathrm{cn}\,\xi_+ \mathrm{dn}\,\xi_+ + \mathrm{sn}\,\xi\,\mathrm{cn}\,\xi\,\mathrm{dn}\,\xi}{\mathrm{sn}^2 \xi_+ - \mathrm{sn}^2 \xi}. \tag{3.19}$$

By specializing Eq. (3.18) to $\xi = 0$ we can determine the constant η

$$\eta = \frac{1}{\mathrm{sn}^2 b} - 1 - \kappa^2.$$

The scale factor A is not constrained by these considerations. Thus we conclude that the ansatz (3.19) is the most general Dirac potential leading to a single gap Lamé potential (plus constant) in the corresponding second order equations. This makes it a good starting point for finding periodic, static solutions.

The ansatz (3.19) can be cast into the simpler form

$$\tilde{\sigma}(\xi) = \kappa^2 \mathrm{sn}\, b\, \mathrm{sn}\, \xi\, \mathrm{sn}(\xi + b) + \frac{\mathrm{cn}\, b\, \mathrm{dn}\, b}{\mathrm{sn}\, b}, \tag{3.20}$$

from which the symmetries can easily be read off. Apart from the translational symmetry in ξ and b with period $2\mathbf{K}$

$$\tilde{\sigma}(\xi, b) = \tilde{\sigma}(\xi + 2\mathbf{K}, b) = \tilde{\sigma}(\xi, b + 2\mathbf{K}),$$

it is antisymmetric under simultaneous reflections of ξ and b

$$\tilde{\sigma}(\xi, b) = \tilde{\sigma}(-b - \xi, b) = -\tilde{\sigma}(-\xi, -b).$$

From the Dirac HF equation (2.3) we see that $\sigma(x)$ and $-\sigma(-x)$ are equivalent. Therefore we find that the space of different configurations is parametrized by

$$A \geq 0, \quad 0 \leq b \leq \mathbf{K}, \quad 0 \leq \kappa \leq 1. \tag{3.21}$$

In the limit $\kappa \to 0$ the mean field ansatz becomes constant, since

$$\lim_{\kappa \to 0} \tilde{\sigma}(\xi) = \cot b,$$

Hence, the ansatz for σ is capable of parameterizing both a periodic crystal and a spatially homogeneous state.

3.2.2. Ground state energy

In the HF approach, the task is now to calculate the total energy of a mean field configuration (cp. Eq. (2.9)). For the self-consistent solution this equals the ground state energy density, written as

$$E_{\text{gs}} = E_1 + E_2.$$

E_1 is the sum (or rather integral) over single particle energies of all filled orbits (including the negative energy states in the Dirac sea) and E_2 the double counting correction. We first find the density of state for our ansatz and evaluate E_1.

When inserted into the Schrödinger type equation (3.2), our ansatz leads by construction to the single gap Lamé equation

$$\left[-\partial_\xi^2 + 2\kappa^2 \mathrm{sn}^2(\xi + (b \mp b)/2)\right] \phi_\pm = \mathcal{E}\phi_\pm. \tag{3.22}$$

The Lamé eigenvalues $\mathcal{E}$ are related to the Dirac energies E through

$$\mathcal{E} = \frac{E^2}{A^2} - \eta. \tag{3.23}$$

Note that Eq. (3.22) is the same as in the chiral limit [8]. The differences lie in the relation between Lamé and Dirac energies (3.23) and in the reconstruction of solutions of the original first order HF equations (2.3), where the shape of the potential enters. The finite bare mass also enters the self-consistency conditions (2.7), cf. Section 3.2.3.

As is well known from quasi-one-dimensional condensed matter systems, the physics behind the appearance of periodic structures is the Peierls instability — the system lowers its energy by generating dynamically an energy gap at the Fermi surface. This was already observed in the chiral limit of the GN model where the state of lowest energy has a completely filled

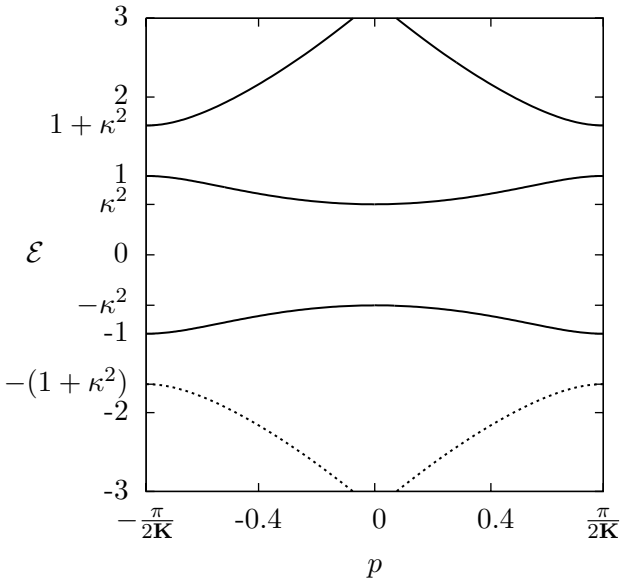

Figure 3.1.: The dispersion relation (3.18) for the Lamé potential for $\kappa = 0.8$ and $b = 1.7$. The Bloch momentum p is projected onto the Brillouin zone ranging from $-\pi/2\mathbf{K}$ to $\pi/2\mathbf{K}$. The filled single particle states for antimatter with density $\rho = A/2\mathbf{K}$ are marked as a dotted line.

(for matter) or empty (for antimatter) valence band. Assuming that the gap is located at the Fermi surface, the scale factor A takes on the same value as in the chiral limit

$$A = \frac{2p_f\mathbf{K}}{\pi},$$

with the Fermi momentum p_f related to the spatially averaged baryon density via $\rho = p_f/\pi$. The two real parameters which determine $\sigma(x)$ are the elliptic modulus κ and the shift b.

The solutions to the eigenvalue problem (3.22) are well known [42]. The eigenfunctions can be expressed in terms of H, Θ, and Z, the Jacobi eta, theta, and zeta functions

$$\phi_+(\xi) = \mathcal{N}\frac{\mathrm{H}(\xi+\alpha)}{\Theta(\xi)}\mathrm{e}^{-\mathrm{Z}(\alpha)\xi}, \tag{3.24}$$

with a normalization factor $\mathcal{N}$. To any Lamé-eigenvalue $\mathcal{E}$ there exist two complex conjugate eigenfunctions parameterized by $\pm\alpha$. For $\pm\alpha = \mathbf{K} + \mathrm{i}\mathbf{K}' \ldots \mathbf{K}$ one obtains the solutions of the lower band $\kappa^2 \leq \mathcal{E} \leq 1$ whereas $\pm\alpha = 0 \ldots \mathrm{i}\mathbf{K}'$ provides the upper band $\mathcal{E} \geq 1+\kappa^2$. The eigenfunctions are presented in the form anti-periodic function times complex phase. This gives them a definite Bloch momentum which is opposite for α and $-\alpha$. The energy eigenvalue together with the Bloch momentum give a parametric representation of the dispersion relation,

$$\mathcal{E} = 1 + \kappa^2\mathrm{cn}^2\alpha, \quad p = -\mathrm{i}\mathrm{Z}(\alpha) \pm \frac{\pi}{2\mathbf{K}}, \tag{3.25}$$

The offset $\pm\pi/(2\mathbf{K})$ to the momentum was added to give the periodic lowest energy solution $\alpha = \pm(\mathbf{K} + \mathrm{i}\mathbf{K}')$ zero Bloch momentum. The dispersion relation is illustrated in Fig. 3.1.

From Eq. (3.25) we can calculate the density of states and determine its high momentum asymptotics,

$$\begin{aligned}\frac{\mathrm{d}p}{\mathrm{d}\mathcal{E}} &= \frac{|\mathcal{E}-\kappa^2-\mathbf{E}/\mathbf{K}|}{2\sqrt{(\mathcal{E}-\kappa^2)(\mathcal{E}-1)(\mathcal{E}-1-\kappa^2)}},\\ \mathcal{E} &= p^2+2(1-\mathbf{E}/\mathbf{K})+\mathcal{O}(p^{-2}).\end{aligned} \tag{3.26}$$

With this we can now calculate the integral over single particle energies of all filled orbits

$$E_1 = -2A^2\int_{\mathcal{E}_<}^{\mathcal{E}_>}\frac{\mathrm{d}\mathcal{E}}{2\pi}\left|\frac{\mathrm{d}p}{\mathrm{d}\mathcal{E}}\right|\sqrt{\mathcal{E}+\eta}, \tag{3.27}$$

with the integration limits ($\Lambda/2$ is the UV cutoff)

$$\mathcal{E}_< = 1+\kappa^2, \qquad \mathcal{E}_> = \left(\frac{\Lambda}{2A}\right)^2+2u,$$

where we introduce

$$u = 1-\frac{\mathbf{E}}{\mathbf{K}}, \qquad \chi = \frac{\mathrm{dn}\,b}{\mathrm{sn}\,b}$$

for recurring expressions to ease the notation. We consider antimatter here, filling only the negative energy states below the gap. This yields the same ground state energy as for matter, albeit in a simpler way. The integration in Eq. (3.27) using Eq. (3.26) is more involved than in the massless case, but can be done along similar lines as in Ref. [43]. The result is best expressed in terms of incomplete elliptic integrals F, E, Π of the first, second and third kind (see Appendix D) as follows,

$$\begin{aligned}\frac{2\pi}{A^2}E_1 = &-\sqrt{\frac{(\mathcal{E}_>-\kappa^2)(\mathcal{E}_>-1-\kappa^2)(\mathcal{E}_>+\eta)}{(\mathcal{E}_>-1)}}+\chi(\kappa^2-2u)F(p,q)\\ &+\chi\,E(p,q)-\frac{\kappa^2}{\chi}(\eta+2u)\Pi(p,n,q),\end{aligned} \tag{3.28}$$

The arguments of the elliptic integrals are

$$n = \frac{1}{\mathrm{dn}^2 b}, \qquad p = \mathrm{dn}\,b\sqrt{\frac{\mathcal{E}_>-1-\kappa^2}{\mathcal{E}_>-1}}, \qquad q = \kappa'\frac{1}{\mathrm{dn}\,b}. \tag{3.29}$$

For the renormalization of the total energy we need the asymptotic behavior of E_1 for large $\mathcal{E}_>$. The first term in Eq. (3.28) yields an irrelevant quadratic divergence $-\Lambda^2/(8\pi)$ which can be dropped, as well as a finite term. In the 2nd and 3rd terms, we can replace p by $\tilde{p} = \mathrm{dn}\,b$ in $E(p,q)$ and $F(p,q)$, all corrections being $1/\mathcal{E}_>$ suppressed. The last term in Eq. (3.28) is more delicate, since $\Pi(p,n,q)$ has a logarithmic singularity at $p=\tilde{p}$. Expanding

$$p \approx \mathrm{dn}\,b-\frac{\kappa^2\mathrm{dn}\,b}{2\mathcal{E}_>} = \tilde{p}-\epsilon$$

and using a standard identity [44] in the form

$$\Pi(\tilde{p}-\epsilon,n,q) = \frac{1}{2}\sqrt{\frac{n}{(n-1)(n-q^2)}}\ln\frac{2(n-q^2)(n-1)}{\sqrt{n}(n^2-q^2)\epsilon}+F(\tilde{p},q)-\Pi\left(\tilde{p},\frac{q^2}{n},q\right)+\mathrm{O}(\epsilon), \tag{3.30}$$

we finally arrive at

$$\begin{aligned}\frac{2\pi}{A^2}E_1 = \kappa^2 - 2u - \frac{\eta}{2} + \chi\left[E(\tilde{p},q) + (\kappa^2-2u)F(\tilde{p},q)\right] \\ - (\eta+2u)\left[\ln\frac{\Lambda}{A\sqrt{2+\eta}} + \frac{\kappa^2}{\chi}\left(F(\tilde{p},q) - \Pi\left(\tilde{p},\kappa'^2,q\right)\right)\right].\end{aligned} \tag{3.31}$$

The logarithmic divergence of the sum over single particle energies (the $\ln\Lambda$ term in the 2nd line) will be cured once we add the double counting correction E_2, to which we now turn. For finite bare quark mass m_0 it is given by (cp. Eq. (2.10), $\ell = 2\mathbf{K}$ is the spatial period in ξ),

$$E_2 = \frac{1}{2Ng^2}\frac{1}{\ell}\int_0^\ell \mathrm{d}\xi (A\tilde{\sigma}(\xi) - m_0)^2.$$

We invoke the vacuum gap equation (2.14) to eliminate the bare coupling constant. We then find

$$E_2 = \frac{A^2\langle\tilde{\sigma}^2\rangle}{2\pi}\left(\gamma + \ln\frac{\Lambda}{m}\right) - \frac{Am\langle\tilde{\sigma}\rangle\gamma}{\pi}, \tag{3.32}$$

with the spatial averages

$$\langle\tilde{\sigma}^2\rangle = \eta + 2u \qquad \langle\tilde{\sigma}\rangle = \mathrm{Z}(\alpha) + \frac{\mathrm{cn}\,b\,\mathrm{dn}\,b}{\mathrm{sn}\,b}. \tag{3.33}$$

Eqs. (3.31) and (3.32) are the main result of this section. Upon adding up E_1 and E_2 to get the ground state energy density E_{gs}, the logarithmically divergent terms are cancelled and a finite result involving only physical parameters is obtained. It depends on the 4 parameters κ, b, p_f, γ. Out of these 4 parameters, p_f and γ are determined by the baryon density and the bare fermion mass, respectively, whereas κ and b are so far unspecified parameters of the trial potential. They will be determined in the following section by demanding self-consistency.

3.2.3. Self-consistency conditions

In the present section we check the self-consistency of the ansatz scalar potential (3.19). This ansatz contains two free parameters, κ and b. We proceed to show that the self-consistency condition (2.4) is satisfied provided that κ and b take on definite values depending on the density and the parameter γ. The main result of this section will be a pair of transcendental equations for κ and b, Eqs. (3.41), which are equivalent to the self-consistency equation.

The self-consistency condition for the scalar potential, Eq. (2.4) can be written as (cp. Eq. (3.12))

$$-\frac{\sigma}{\pi}(\gamma + \ln\frac{\Lambda}{m}) + \frac{\gamma m}{\pi} = \sum_\alpha^{\mathrm{occ.}} \bar{\psi}_\alpha(x)\psi_\alpha(x). \tag{3.34}$$

As for the single baryon, the task is to evaluate the scalar density $\bar{\psi}_\alpha\psi_\alpha$ for an arbitrary single particle solution of the HF equation and perform the sum over all occupied states. With ϕ_+ given in (3.24), ϕ_- follows from the Dirac equation

$$\phi_- = -\frac{1}{E}\left(\frac{\partial}{\partial x} + \sigma\right)\phi_+.$$

Since ϕ_- fulfills the same Lamé equation with a Schrödinger potential shifted by b (see Eq. (3.17)), it differs from $\phi_+(\xi+b)$ only by a complex phase. First, this enables us to impose the normalization condition

$$1 = \langle \psi^\dagger \psi \rangle = \langle |\phi_+|^2 \rangle + \langle |\phi_-|^2 \rangle = 2\langle |\phi_+|^2 \rangle,$$

which fixes the normalization factor in (3.24)

$$|\mathcal{N}|^2 = \frac{\mathbf{K}\kappa\kappa'}{\pi\Theta^2(\alpha)|\mathrm{dn}^2\alpha - \mathbf{E}/\mathbf{K}|}.$$

Second, this leads to the scalar density of a single mode, expressing the ξ-dependence in terms of $\tilde{\sigma}(\xi)$ with

$$\bar{\psi}\psi = \frac{\tilde{\sigma}\omega - (\eta+1)(\eta+\kappa^2)(\eta+1+\kappa^2)/\omega}{\mathcal{E} - \kappa^2 - \mathbf{E}/\mathbf{K}}. \tag{3.35}$$

For the present purpose it turns out to be convenient to decompose the potential in the form (3.19)

$$\tilde{\sigma} = \frac{\mathrm{sn}\,\xi_+ \mathrm{cn}\,\xi_+ \mathrm{dn}\,\xi_+}{\mathrm{sn}^2\xi_+ - \mathrm{sn}^2\xi} + \frac{\mathrm{sn}\,\xi\,\mathrm{cn}\,\xi\,\mathrm{dn}\,\xi}{\mathrm{sn}^2\xi_+ - \mathrm{sn}^2\xi} = \tilde{\sigma}_1 + \tilde{\sigma}_2.$$

Eq. (3.35) is written as

$$\bar{\psi}\psi = \frac{\tilde{\sigma}(\mathcal{E} - 1 - \kappa^2) + \kappa^2(\tilde{\sigma}_1 \mathrm{sn}^2\xi + \tilde{\sigma}_2 \mathrm{sn}^2\xi_+)}{\omega(\mathcal{E} - \kappa^2 - \mathbf{E}/\mathbf{K})}.$$

Now the sum over occupied states in (3.34) is obtained by summing over the upper band of negative energies as it was done for the HF energy in section 3.2.2

$$\sum_\alpha^{\text{occ.}} \bar{\psi}_\alpha \psi_\alpha = 2A \int_{\mathcal{E}_<}^{\mathcal{E}_>} \frac{\mathrm{d}\mathcal{E}}{2\pi} \left| \frac{\mathrm{d}k}{\mathrm{d}\mathcal{E}} \right| \bar{\psi}\psi = -\frac{A}{2\pi} \left[I_2 \tilde{\sigma} + \kappa^2 I_1 (\tilde{\sigma}_1 \mathrm{sn}^2\xi + \tilde{\sigma}_2 \mathrm{sn}^2\xi_+) \right], \tag{3.36}$$

with the integrals

$$I_1 = \frac{2}{\chi} F(p,q), \qquad I_2 = \frac{2\kappa^2}{\chi} \left(\Pi(p,n,q) - F(p,q) \right). \tag{3.37}$$

The arguments of the elliptic integrals are the same as above, see Eqs. (3.29). Using once again the identity (3.30) to isolate the logarithmic singularity of $\Pi(p,n,q)$ and taking the asymptotics with respect to Λ allows us to replace

$$\begin{aligned} F(p,q) &\to F(\tilde{p},q), \\ \Pi(p,n,q) &\to F(\tilde{p},q) - \Pi\left(\tilde{p},(\kappa')^2,q\right) + \frac{\chi}{\kappa^2} \ln \frac{\Lambda}{A\sqrt{2+\eta}}. \end{aligned} \tag{3.38}$$

Upon inserting the results (3.36–3.38) into the self-consistency condition (3.34), the $\ln\Lambda$ term drops out once again and we arrive at the finite equation

$$m\gamma = \mathcal{C}_1 \left[\tilde{\sigma} + \frac{\mathcal{C}_2}{\mathcal{C}_1} \left(\tilde{\sigma}_1 \mathrm{sn}^2\xi + \tilde{\sigma}_2 \mathrm{sn}^2\xi_+ \right) \right], \tag{3.39}$$

with coefficients

$$\frac{\mathcal{C}_1}{A} = \ln \frac{A\sqrt{2+\eta}}{m} + \gamma + \frac{\kappa^2}{\chi} \Pi\left(\tilde{p},(\kappa')^2,q\right), \qquad \frac{\mathcal{C}_2}{A} = -\frac{\kappa^2}{\chi} F(\tilde{p},q).$$

At first glance, it seems unlikely that Eq. (3.39) can be solved, since a constant term and two different functions of x appear. However, these functions are not linearly independent. Using properties of elliptic functions (see Appendix D), one can verify the following identity,

$$\tilde{\sigma} - \kappa^2 \mathrm{sn}^2 b \left(\tilde{\sigma}_1 \mathrm{sn}^2 \xi + \tilde{\sigma}_2 \mathrm{sn}^2 \xi_+ \right) = \frac{\mathrm{cn}\, b\, \mathrm{dn}\, b}{\mathrm{sn}\, b}. \tag{3.40}$$

Comparing Eqs. (3.39) and (3.40), the self-consistency condition may be turned into the following two x-independent conditions,

$$\frac{m\gamma}{\mathcal{C}_1} = \frac{\mathrm{cn}\, b\, \mathrm{dn}\, b}{\mathrm{sn}\, b}, \qquad \frac{\mathcal{C}_2}{\mathcal{C}_1} = -\kappa^2 \mathrm{sn}^2 b.$$

For $\gamma \neq 0$, these equations can be cast into the somewhat simpler form

$$\begin{aligned} 0 &= A\, \mathrm{cn}\, b\; F(\tilde{p}, q) - m\gamma\, \mathrm{sn}^2 b, \\ m\gamma &= A\, \mathrm{cn}\, b \left[\kappa^2\; \Pi\left(\tilde{p}, (\kappa')^2, q\right) + \chi \left(\gamma + \ln \frac{A\sqrt{2+\eta}}{m} \right) \right]. \end{aligned} \tag{3.41}$$

They determine κ and b for given p_f and γ.

After carefully identifying all the variables, the self-consistency equations (3.41) agree exactly with Eqs. (5,6) in [45], confirming the 1:1 mapping from the theory of non-degenerate conducting polymers to the massive GN model. If we can solve the pair of transcendental equations (3.41), we have found a solution of the HF equations and hence a candidate for the ground state of baryonic matter. Another solution of the HF equations is the translationally invariant one discussed in detail in Ref. [46] and summarized in Appendix B. Which solution is favored is then simply a question of the energy which can be computed from Eqs. (3.31,3.32). The numerical results will be presented in Sec. 3.2.5.

3.2.4. Analytical results for special cases

This section is devoted to testing the general formalism in simple special cases where the answer is known from other sources, i.e., the massless case and the low and high density limits.

Chiral limit

As a first and most trivial test, let us check the above formalism in the chiral limit ($\gamma = 0$) against previous results from Ref. [8]. Consider the self-consistency equations, Eqs. (3.41). The first equation can be solved by $b = \mathbf{K}$. Consequently,

$$\tilde{p} = \chi = \kappa', \quad q = 1, \quad \eta = -\kappa^2,$$

and the elliptic integrals are reduced to elementary functions,

$$\begin{aligned} F(\kappa', 1) &= \mathrm{artanh}\, \kappa', \\ \Pi(\kappa', \kappa'^2, 1) &= \frac{1}{2\kappa^2} \left(\kappa' \ln \frac{\kappa^2}{1+\kappa'^2} + \ln \frac{1+\kappa'}{1-\kappa'} \right). \end{aligned}$$

The second equation of Eqs. (3.41) then yields simply

$$A\kappa = m,$$

relating κ and p_f. Likewise, the ground state energy Eqs. (3.31,3.32) simplifies tremendously in the limit $\gamma \to 0$,

$$E = \frac{A^2}{4\pi}\left(4\frac{\mathbf{E}}{\mathbf{K}} - 2 + \kappa^2\right) - \frac{A^2}{2\pi}\left(2\frac{\mathbf{E}}{\mathbf{K}} - 2 + \kappa^2\right)\ln\frac{A\kappa}{m}.$$

Finally, in the limit $b \to \mathbf{K}$ the self-consistent potential simplifies to

$$\tilde{\sigma}(\xi) = \kappa^2\,\frac{\operatorname{sn}\xi\operatorname{cn}\xi}{\operatorname{dn}\xi}. \tag{3.42}$$

All of these formulae agree with the known results for $\gamma = 0$ [8]. Comparing these equations with the full calculation shows a significant increase in complexity due to the finite bare fermion mass.

Low density limit and single baryon

A second obvious way of testing the formalism is the low density limit, where we expect to recover the properties of single baryons in the massive GN model. We have to expand around $\kappa' = 0$. To leading order, we may neglect all power corrections in κ' but must keep the logarithmic singularity $\sim \ln\kappa'$ whenever it is present. In this way, we find

$$\tilde{p} \approx \operatorname{sech} b, \qquad q \approx 0,$$

and hence all incomplete elliptic integrals reduce to the same elementary function,

$$\left\{F(\tilde{p},q), E(\tilde{p},q), \Pi(\tilde{p},(\kappa')^2,q)\right\} \to \arcsin\tilde{p}.$$

The self-consistency conditions (3.41) become

$$\begin{aligned} 0 &= 2p_f\tilde{p}\arcsin\tilde{p}\ln\frac{4}{\kappa'} - \pi\gamma\tanh^2 b \\ \pi m\gamma &= 2p_f\tilde{p}\ln\frac{4}{\kappa'}\left\{\arcsin\tilde{p} + \frac{1}{\sinh b}\left[\gamma + \ln\left(\frac{2p_f\ln(4/\kappa')}{\pi m\tanh b}\right)\right]\right\}. \end{aligned}$$

These equations can be solved parametrically for b and κ' as follows,

$$b = \operatorname{artanh} y, \qquad \kappa' = 4\exp\left(-\frac{\pi m y}{2p_f}\right).$$

The parameter y is related to γ through the self-consistency condition for the single baryon (3.10) with completely filled valence level ($\nu = 1$).

Using our full expression for the energies E_1 and E_2, Eqs. (3.31,3.32), the limit $\kappa' \to 0$ yields the finite parts

$$\begin{aligned} E_1 &= -\frac{m^2}{4\pi} + \frac{mp_f}{\pi}\left(\frac{2y\gamma}{\pi} + \frac{2y}{\pi}\right), \\ E_2 &= -\frac{m^2\gamma}{2\pi} + \frac{mp_f}{\pi}\left(\frac{2y}{\pi} + \frac{2\gamma}{\pi}\operatorname{artanh} y\right). \end{aligned} \tag{3.43}$$

The logarithmically divergent pieces have been omitted, since they anyway cancel in the sum. The total energy density can then be represented as

$$E_{\rm gs} = E_1 + E_2 = E_{\rm vac} + \rho M_B \tag{3.44}$$

The vacuum energy density ($p_f = 0$) agrees with Eq. (2.18), $\rho = p_f/\pi$ is the mean baryon density and M_B is the baryon mass Eq. (3.11). This is indeed the expected low density behavior for widely spaced baryons and an important additional test of the formalism.

Finally, we check the shape of the scalar potential in the low density limit. Taking $\kappa \to 1$ in Eq. (3.20), we find

$$\lim_{\kappa\to 1} \tilde{\sigma}(\xi) = \coth b + \tanh \xi - \tanh(\xi + b).$$

This can be matched with the single baryon profile (2.27) if we shift ξ by $b/2$ and identify

$$A = my, \quad \xi = ymx, \quad b = \operatorname{arctanh} y.$$

In the two limits for the confinement parameter the baryon mass becomes

$$\begin{aligned} \frac{M_B}{m} &\approx \frac{2}{\pi} - \frac{\gamma}{\pi}\left(1 + \ln\frac{\gamma}{4}\right) \quad \text{for } \gamma \to 0, \\ \frac{M_B}{m} &\approx 1 - \frac{\pi^2}{24\gamma^2} + \frac{\pi^2}{12\gamma^3} \quad \text{for } \gamma \to \infty. \end{aligned} \tag{3.45}$$

This result should be compared to the critical chemical potential in the translationally invariant HF solution (Appendix B). In the limits $\gamma \to 0, \infty$, the baryon mass in Eq. (3.45) is below the massive Fermi gas result in Eqs. (B.9,B.10). One can easily check numerically that this is in fact true for arbitrary values of γ. This proves that the translationally invariant solution is always unstable against formation of a kink-antikink crystal.

High density limit and perturbation theory

In the high density limit $p_f \to \infty$, one would expect that all interaction effects can be treated perturbatively. As is well known, band formation in a periodic potential requires almost degenerate perturbation theory (ADPT). Here we closely follow a similar calculation carried out by us in the context of the massless GN model [47]. There are two differences: In the double-counting correction, we have to take into account the bare quark mass, and we allow for $\sigma_0 \neq 0$ in addition to $\sigma_{\pm 1} \neq 0$ [σ_ℓ are the Fourier components of the periodic potential $\sigma(x)$]. Thus our present ansatz for $\sigma(x)$ is

$$\sigma(x) = \sigma_0 + \sigma_1 \mathrm{e}^{\mathrm{i}2p_f x} + \sigma_{-1}\mathrm{e}^{-\mathrm{i}2p_f x} \tag{3.46}$$

The potential has a spatial period a equal to the inter-baryon distance, i.e., the inverse density

$$a = \frac{\pi}{p_f}.$$

This is the reason why the lowest non-vanishing momentum which appears in the Fourier expansion (3.46) is $2\pi/a = 2p_f$. Without loss of generality, we may assume that σ_0 and

$\sigma_1 = \sigma_{-1}$ are real (a phase in σ_1 corresponds to a translation). The sum over single particle energies (for the antimatter case) in 2nd order perturbation theory (PT) is given by

$$\begin{aligned} E_1 &= 2\int_{p_f}^{\Lambda/2} \frac{\mathrm{d}k}{2\pi}\left[-k - \frac{\sigma_0^2}{2k} - \frac{\sigma_1^2}{2(k+p_f)} - \sqrt{(k-p_f)^2+\sigma_1^2} + (k-p_f)\right] \\ &= -\frac{\Lambda^2}{8\pi} + \frac{p_f^2}{2\pi} - \frac{\sigma_1^2}{4\pi} - \frac{\sigma_0^2+2\sigma_1^2}{2\pi}\ln\frac{\Lambda}{2p_f} + \frac{\sigma_1^2}{2\pi}\ln\frac{\sigma_1}{p_f}. \end{aligned} \tag{3.47}$$

We had to invoke ADPT only for the term which would blow up in naive 2nd order PT,

$$-\frac{\sigma_1^2}{2(k-p_f)} \to -\sqrt{(k-p_f)^2+\sigma_1^2} + (k-p_f)$$

This "recipe" has been derived in Eq. (2.11) of Ref. [47] by simply comparing 2nd order degenerate and non-degenerate perturbation theory. In Ref. [47], the states which are almost degenerate in a periodic potential are explained in more detail, following the standard weak binding approximation from solid state physics (see e.g. [48]). The double-counting correction for the potential (3.46) becomes

$$E_2 = \frac{1}{2\pi}(\sigma_0^2+2\sigma_1^2)(\gamma + \ln\frac{\Lambda}{m}) - \frac{m\gamma}{\pi}\sigma_0. \tag{3.48}$$

Adding Eqs. (3.47) and (3.48) then yields the approximate energy density

$$2\pi\, E_{\mathrm{gs}} = -\frac{\Lambda^2}{4} + p_f^2 + \sigma_0^2\ln\frac{2p_f}{m} + \sigma_1^2\left(\ln\frac{4p_f\sigma_1}{m^2} - \frac{1}{2}\right) + \gamma\left(\sigma_0^2+2\sigma_1^2-2m\sigma_0\right).$$

Minimizing with respect to S_0 and S_1, we find

$$\sigma_0\left[\ln\frac{2p_f}{m}+\gamma\right] - m\gamma = 0, \qquad \sigma_1\left[2\gamma + \ln\frac{4p_f\sigma_1}{m}\right] = 0.$$

The first equation has the unique solution

$$\sigma_0 = \frac{m\gamma}{\gamma + \ln(2p_f/m)}$$

in agreement with the leading term in Eq. (B.3) of the appendix. The 2nd equation has two solutions: $\sigma_1 = 0$, corresponding to unbroken translational invariance as discussed in Appendix B, and

$$\sigma_1 = \frac{m^2}{4p_f}\mathrm{e}^{-2\gamma} \tag{3.49}$$

for the soliton crystal. Comparing the energy densities of these two solutions,

$$E_{\mathrm{gs}}(\sigma_1\neq 0) - E_{\mathrm{gs}}(\sigma_1 = 0) = -\frac{m^4}{64\pi p_f^2}\mathrm{e}^{-4\gamma} \tag{3.50}$$

we learn that the crystal is favored, but the energy difference decreases with increasing γ. Eqs. (3.49) and (3.50) agree with our previous results if, in addition to the high density limit, we take the chiral limit $\gamma \to 0$. Notice that if we write the parameter γ in terms of the physical fermion mass with and without a bare mass m_0 like in Eq. (2.16), the energy difference

$$E_{\mathrm{gs}}(\sigma_1\neq 0) - E_{\mathrm{gs}}(\sigma_1 = 0) = \frac{m[0]^4}{64\pi p_f^2}$$

becomes independent of the bare mass.

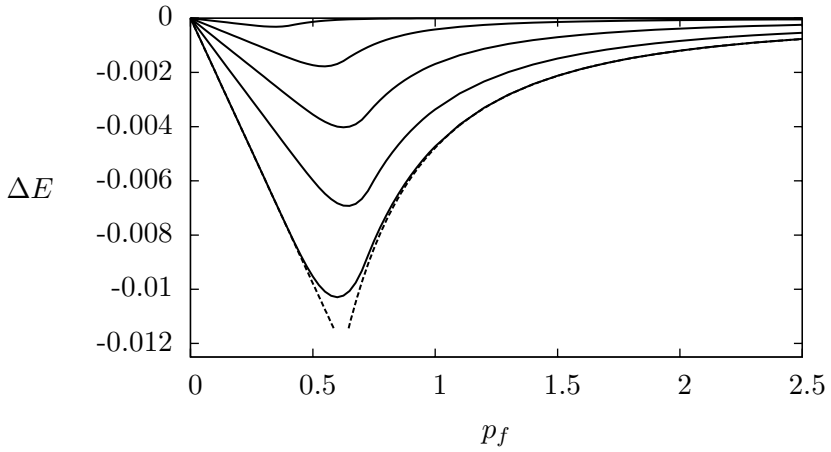

Figure 3.2.: Difference in energy density between crystal and translationally invariant Fermi gas. From top to bottom: $\gamma = 2.3, 0.75, 0.3, 0.1, 0.01$. Dashed curves: asymptotic behavior according to Eqs. (3.44) and (3.50), for $\gamma = 0.01$.

3.2.5. Numerical results

Before computing any observable, we have to solve the self-consistency equations (3.41). Choosing the mean density and the bare fermion mass or, equivalently p_f and γ, these two transcendental equations yield the two unknown parameters κ (elliptic modulus) and b (shift parameter) of the trial potential defined in Eqs. (3.13). Eqs. (3.41) always have two different solutions, a translationally invariant one ($\kappa = 1$) and a spatially modulated one ($0 < \kappa < 1$). In the case of the translationally invariant solution, there is an additional complication already familiar from the massless limit: At low densities, a mixed phase appears, characteristic of a first order phase transition. Therefore, one cannot simply take the HF energy at face value, but has to introduce a second variational parameter describing the amount of space filled with "droplets" of baryonic matter. Alternatively, one can work with a chemical potential and use the grand canonical potential at $T = 0$ as in Ref. [46], leading to the same results. More details are given in Appendix B.

The energy density of the crystal phase can be computed by inserting the self-consistent values for κ and b into Eqs. (3.31,3.32). We then find that the crystal is energetically favored at all densities and all bare quark masses. In the low and high density limits, this can be shown analytically, see Eqs. (3.45,B.10) for the limit $p_f \to 0$ and Eq. (3.50) for $p_f \to \infty$. In between, we have to compute the energy difference numerically (where "numerically" in this context simply means using floating point commands in Maple, thus getting any desired accuracy). Some illustrative results are shown in Fig. 3.2 for five different values of γ. Here and in the rest of this chapter we chose units in which the vacuum fermion mass $m = 1$. Together with the lowest curve (corresponding to $\gamma = 0.01$), we have also plotted two dashed curves corresponding to the (analytical) asymptotic behavior at small and large densities. We observe that the agreement of the full calculation with the asymptotic curves is excellent, with a narrow crossover region where the curve changes rather abruptly from $\sim p_f$ to $\sim p_f^{-2}$ behavior. On the basis of such calculations, we conclude that the lattice solution is stable at all densities and quark masses.

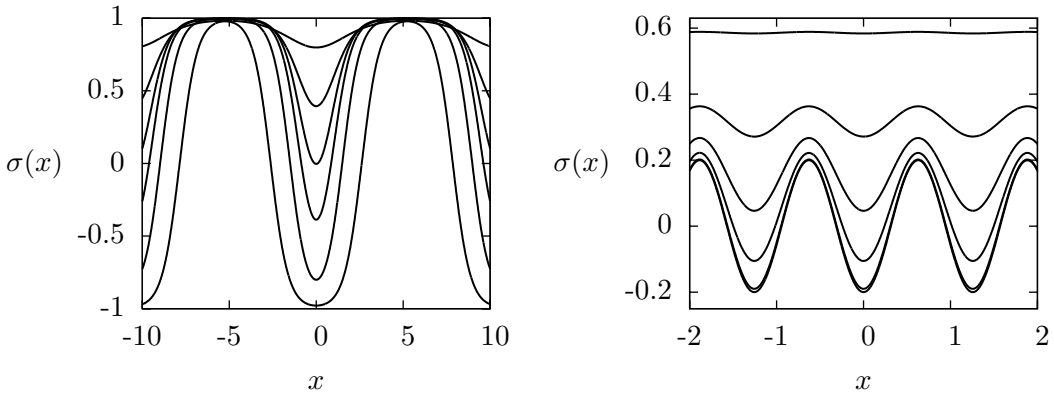

Figure 3.3.: Self-consistent scalar potential $\sigma(x)$ versus x for $p_f = 0.3$ (left) and $p_f = 2.5$ (right). From bottom to top: $\gamma = 0, 0.01, 0.1, 0.3, 0.75, 2.3$. Note the different scale on the x-axis.

Having established the stability of the crystal solution, let us now illustrate how a finite bare quark mass modifies the self-consistent scalar potential. This is exhibited in Fig. 3.3 at low and high density. The deepest curves always correspond to $\gamma = 0$, where the potential oscillates symmetrically around zero. This is actually a remnant of the original discrete chiral symmetry of the model. Translational invariance and the γ^5 transformation both break down, leaving an unbroken discrete symmetry (translation by half a period, combined with a γ^5 transformation). Since the massive GN model does not have discrete chiral symmetry in the first place, one would not expect the same behavior here. Indeed, the potentials now oscillate around a finite value, with a less symmetric shape. In the massive case, continuous translational invariance is broken down to a residual discrete translational invariance. As we turn on the symmetry violation parameter γ, the potential oscillates with decreasing amplitude around a value close to the mass M which the fermions would acquire in the translationally invariant solution, eventually leaving only a very weak modulation of a large scalar potential in the heavy fermion limit. It is surprising that such a variety of potential shapes in the Dirac equation can all be reduced to the standard single gap Lamé equation.

The last result which we should like to show is how the density varies with the chemical potential. The chemical potential at $T = 0$ can be obtained by differentiating the energy density with respect to the mean fermion density,

$$\mu = \frac{\partial E_{\rm gs}}{\partial \rho}, \qquad \rho = \frac{p_f}{\pi}.$$

If we assume unbroken translational invariance (Fig. 3.4 left), we find discontinuities in these curves, confirming the result of Ref. [46] about a first order phase transition. Repeating the same calculation for the crystal solution (which is the stable one), all the curves become continuous, signaling a 2nd order phase transition (Fig. 3.4 right). The critical chemical potential in this latter case coincides with the baryon mass, as expected on general grounds. By contrast, the first order transition in the translationally invariant solution happens at a chemical potential which has at best the meaning of an approximate baryon mass in a kind of droplet model, cf. Appendix B.

This completes the analytic description of the ground state of cold, dense matter in the massive GN_2 model. As compared to previous work on the massless case, the calculations became

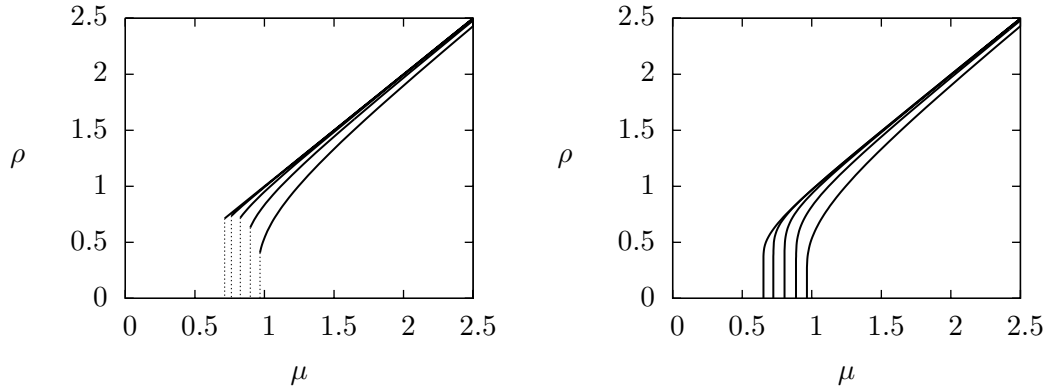

Figure 3.4.: Baryon density versus chemical potential for translationally invariant solution (left) and for the crystal solution (right), shown for (lines from left to right) $\gamma = 0.01, 0.1, 0.3, 0.75, 2.3$. The translationally invariant solution undergoes a first order phase transition with a sudden drop in μ indicated by dotted lines, whereas for the crystal solution a second order phase transition at $\mu_c = M_B$ is seen for all values of γ.

significantly more involved once the parameter γ was turned on. However, the problem of finding the single-particle spectrum of the HF Hamiltonian could still be reduced to the single gap Lamé equation, which made an analytical treatment possible. The main result of this chapter is the existence of a crystal with a periodic scalar condensate, favored over the translationally invariant solution for all baryon densities. The system undergoes a second order phase transition when the chemical potential is equal to the baryon mass, a theoretical constraint which is violated by the translationally invariant solution.

4. Model with continuous chiral symmetry

The 1+1 dimensional four-fermion interaction model with continuous chiral symmetry is the NJL_2 model, defined by the Lagrangian (2.2). In the chiral limit, the symmetry is broken spontaneously as the mean fields σ and π acquire a constant value somewhere on the circle of degenerate ground states $\sigma^2 + \pi^2 = m^2$. The bound states are obtained as topologically non-trivial excitations of the corresponding Goldstone boson [49]. This massless field is described by the chiral angle χ defined in Eq. (2.21). The baryon number induced by χ turns out to be equal to the winding number B_{top} in Eq. (2.20), which measures the number of times the mean field wraps around the circle of ground states [12]. This can be seen by choosing a mean field configuration restricted to $\sigma^2 + \pi^2 = m^2$ and with a chiral angle $\chi(x) = cx$. The HF Hamiltonian (2.5) can be written as

$$H = -\mathrm{i}\gamma^5\partial_x + m\mathrm{e}^{\mathrm{i}\gamma^5\chi(x)}\gamma^0\mathrm{e}^{-\mathrm{i}\gamma^5\chi(x)}.$$

By applying a chiral rotation it can be reduced to the Hamiltonian of free massive fermions

$$\mathrm{e}^{-\mathrm{i}\gamma^5\chi(x)}H\mathrm{e}^{\mathrm{i}\gamma^5\chi(x)} = -\mathrm{i}\gamma^5\partial_x + m\gamma^0 + \mu,$$

with a chemical potential $c = \mu$. The baryon number in a box of finite length L is then equal to the winding number

$$B_{\mathrm{top}} = \frac{1}{\pi}[\chi(+L/2) - \chi(-L/2)] = \frac{\mu}{\pi}L = \rho L.$$

Since the mean field configuration is obtained by a chiral rotation of the ground state, it is a self-consistent solution of the HF equations. Due to its helical shape it has been called the "chiral spiral" in Ref. [12]. This is illustrated by Fig. 4.1. For the single baryon $\mu = \pi/L$ so that the spiral is stretched over whole space. Thus, the mass of the baryon vanishes in the chiral limit.

In the massive NJL_2 model, like in massive GN_2, the new parameter γ appears after renormalization (see Section 2.3). In Ref. [24] it is shown, how it enters the mass of the "pion" in NJL_2. Since this latter quantity has a direct physical interpretation, we will express the dependence on the amount of chiral symmetry breaking in terms of the pion mass m_π. It is related to γ by

$$\gamma = \frac{\pi m_0}{Ng^2 m} = \frac{1}{\sqrt{\eta - 1}}\arctan\frac{1}{\sqrt{\eta - 1}}\ , \qquad \eta = \frac{4m^2}{m_\pi^2}. \tag{4.1}$$

In the massive model, self-consistent solutions with finite baryon number can no longer be obtained by chiral rotation of the vacuum, since the mean field is not restricted to the chiral circle. Moreover, one cannot apply the methods of supersymmetric quantum mechanics [34] like in GN_2, because the HF equations for the components of the Dirac spinor cannot be decoupled. Consequently, one has to consider other methods for a description of baryons

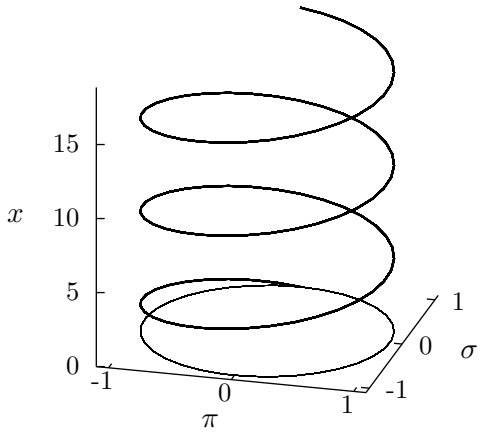

Figure 4.1.: Illustration of the "chiral spiral" for $\mu = 1$ (in units of the vacuum fermion mass m). The circle of degenerate ground states is indicated by the thin line.

and dense baryonic matter in NJL_2. In the vicinity of the chiral limit we identified the derivative expansion, introduced in Section 2.5 as one possibility to approximate the ground state energy density and the baryon number. In this chapter, we will apply this technique to describe baryons (Section 4.1) and dense matter (Section 4.2).

4.1. Baryons using the derivative expansion

In the search for baryons in both the 't Hooft model (large N QCD_2) and the NJL_2 model, Salcedo et al. [49] compared a lattice HF calculation with a variational ansatz in which the chiral phase of the fermions serves as effective low energy field. In the limit of small but finite bare quark masses, the authors find a sine-Gordon theory, the two-dimensional analog of the Skyrme model. In this approximation, the relevant length scale over which the minimum potential varies is given by $1/m_\pi$, the inverse pion mass. This suggests that the theoretical instrument of choice should be the derivative expansion, at least in the vicinity of the chiral limit. We will see that the sine-Gordon equation is nothing but the leading order term of such a derivative expansion. Moreover, the calculation of higher order corrections can be done in closed analytical form, so that we will get a quantitative understanding of the baryons in a reasonable range of bare mass parameters, although not for arbitrary mass. This is an example where one can study in all detail how a Skyrme-type description of baryons emerges from an underlying fermionic theory.

We now specialize the general setup of the derivative expansion (see Section 2.5) to the NJL_2 model. The HF Hamiltonian (2.5) is cast into the form

$$H = -\mathrm{i}\gamma^5\partial_x + M(x)\mathrm{e}^{\mathrm{i}\gamma^5\chi(x)}\gamma^0\mathrm{e}^{-\mathrm{i}\gamma^5\chi(x)} \qquad (\sigma = M\cos 2\chi,\ \pi = -M\sin 2\chi). \tag{4.2}$$

In the chiral limit, we have $M(x) = m$. In this section, the γ-matrices will be taken in the representation

$$\gamma^0 = \sigma_1, \qquad \gamma^1 = -\mathrm{i}\sigma_2, \qquad \gamma^5 = \sigma_3.$$

Next we identify the operators K and I from Eq. (2.26)

$$H = K + I = \begin{pmatrix} -\mathrm{i}\partial_x & 0 \\ 0 & \mathrm{i}\partial_x \end{pmatrix} + \begin{pmatrix} 0 & \phi \\ \phi^* & 0 \end{pmatrix} \quad \text{with} \quad \phi = M\mathrm{e}^{2\mathrm{i}\chi}. \tag{4.3}$$

Note that compared to the Hamiltonian of GN_2, the real field σ is replaced by the complex field ϕ. We want to expand around the vacuum case where $\chi = 0$ and $M = m$. A natural way of decomposing H^2 into H_0^2 and V is

$$H_0^2 = -\partial_x^2 + m^2 \qquad V = \begin{pmatrix} M^2 - m^2 & (2M\chi' - \mathrm{i}M')\mathrm{e}^{2\mathrm{i}\chi} \\ (2M\chi' + \mathrm{i}M')\mathrm{e}^{-2\mathrm{i}\chi} & M^2 - m^2 \end{pmatrix}. \tag{4.4}$$

For the calculation of the energy (2.25), only the odd part of the resolvent contributes. In the expansion of the resolvent in powers of V (2.27), the terms of order V^0 and V^1 contain divergences, whereas all higher order terms are finite. We regularize by evaluating the trace in momentum space, summing over states with $|p| < \Lambda/2$ only. In our renormalization scheme, the non-trivial divergent part will be cancelled by the double counting correction term (2.10) which now reads

$$E_{\mathrm{dcc}} = \int \mathrm{d}x \, \frac{M^2 - 2m_0 M \cos 2\chi + m_0^2}{2Ng^2}. \tag{4.5}$$

The term of order V^0 just leads to the vacuum energy. The resolvent in this order is given by

$$\mathrm{Tr}' \, zG = \int \mathrm{d}x \int_{-\Lambda/2}^{\Lambda/2} \frac{\mathrm{d}p}{2\pi} \frac{2z}{p^2 + m^2 - z^2},$$

denoting the trace with cutoff by Tr'. The integral over the spectral density (2.22) and the vacuum part of the double counting correction (4.5) give

$$E_{(0)} + E_{\mathrm{dcc}}(M = m, \chi = 0) = -\int \mathrm{d}x \left[\int_{-\Lambda/2}^{\Lambda/2} \frac{\mathrm{d}p}{2\pi} \sqrt{p^2 + m^2} + \frac{(m - m_0)^2}{2Ng^2} \right].$$

With the gap equation (2.14) and dropping the trivial divergence $-\Lambda^2/8\pi$, this yields the renormalized vacuum energy from Eq. (2.18). This can be expressed in terms of the pion mass defined in Eq. (4.1). Using the function

$$F(y) = \frac{4}{y\sqrt{4 - y^2}} \arctan \frac{y}{\sqrt{4 - y^2}} = 1 + \frac{1}{6}y^2 + \frac{1}{30}y^4 + \frac{1}{140}y^6 + \ldots,$$

Eq. (2.18) becomes

$$E_{(0)}^{\mathrm{ren}} = -\frac{m^2}{4\pi} - \frac{m_\pi^2}{8\pi} F(m_\pi/m).$$

This already shows that an expansion for small quark masses should be thought of as an expansion in the ratio of pion mass to (dynamical) quark mass in the NJL_2 model. The bare quark mass m_0 goes to 0 in the limit $\Lambda \to \infty$ and cannot appear in any physical quantity.

For the term of order V^1 in the energy, we have to compute the integral over the spectral density plus the remaining part of the double counting correction (4.5). Since we expand around $M = m$, we set $M = m + \lambda(x)$, and get

$$E_{(1)} = -\frac{1}{\pi} \int_{-\infty}^{0} \mathrm{d}E \, E \, \mathrm{Im} \, \mathrm{Tr}' \, zGVG + \int \mathrm{d}x \, \frac{M^2 - 2m_0 M \cos 2\chi + m_0^2 - (m - m_0)^2}{2Ng^2}.$$

The integrations over E and p can easily be carried out. Owing to the gap equation, all divergences cancel and the unphysical quantities (Ng^2, m_0, Λ) can again be eliminated in favor of m_π and m with the result

$$E_{(1)} = \frac{m_\pi^2}{4\pi} F(m_\pi/m) \int \mathrm{d}x \left[\left(1 + \frac{\lambda}{m}\right)(1 - \cos 2\chi) + \frac{\lambda^2}{2m^2} \right].$$

All higher order terms in the expansion (2.27) are free of UV divergences. The traces and integrals are calculated with computer algebra (we used MAPLE). The result for the energy density coming from these higher order terms is a polynomial in λ, χ and their derivatives. Before we give the result for the energy, we check whether the topological form of the baryon number prevails in the derivative expansion.

The leading order contribution in the derivative expansion of the baryon number (2.24) comes from the Tr$IGVG$ term in Eq. (2.27) and can easily be shown to be equal to the winding number B_{top} in Eq. (2.22). We have computed the next three orders in the derivative expansion, using MAPLE. We found that the result does not get any correction whatsoever and therefore presumably holds to all orders. Although many terms are produced in the integrand (the baryon density) by our algorithm, they can be nicely combined into total derivatives of functions which vanish at infinity and therefore do not affect the lowest order topological result.

On the basis of the effective sine-Gordon theory [49] for the NJL$_2$ model, the mass of the baryon with fermion number N is expected to approach $2m_\pi/\pi$ for $m_\pi \to 0$. Our goal is to compute corrections to this result up to order m_π^{12}/m^{12}. These can be used to analyze the convergence behavior of the series. The higher order terms require a substantial number of terms in the derivative expansion and correspondingly involved algebraic expressions. To simplify the notation, let us set $m = 1$ from now on. The result for the derivative expansion of the energy density keeping terms relevant up to order m_π^6 can be written in the compact form

$$\begin{aligned} 2\pi\mathcal{E} = &-\frac{m_\pi^2}{2} F(m_\pi) \left[(1+\lambda)(\cos 2\chi - 1) - \frac{1}{2}\lambda^2 \right] + (\chi')^2 - \frac{1}{6}(\chi'')^2 + \frac{1}{30}(\chi''')^2 \\ &- \frac{1}{140}(\chi^{IV})^2 - \frac{1}{45}(\chi'')^4 + \lambda^2 + \frac{1}{12}(\lambda')^2 - \frac{1}{120}(\lambda'')^2 + \frac{1}{3}\lambda^3 - \frac{1}{6}\lambda(\lambda')^2 \\ &- \frac{1}{12}\lambda^4 + \frac{1}{3}\lambda(\chi'')^2 + \frac{1}{15}\lambda(\chi''')^2 + \frac{1}{5}\lambda\chi''\chi^{IV} - \frac{1}{2}\lambda^2(\chi'')^2. \end{aligned} \tag{4.6}$$

We have subtracted the vacuum contribution and simplified the result as much as possible with the help of partial integrations (only the energy $\int \mathrm{d}x\, \mathcal{E}$ is uniquely defined in this approach). The terms relevant up to order m_π^{12} are also calculated by computer algebra and are not shown here. To appreciate the complexity of expression (4.6), one should compare it with the leading order terms only,

$$2\pi\mathcal{E} = (\chi')^2 - \frac{m_\pi^2}{2}(\cos 2\chi - 1),$$

which reproduce exactly the sine-Gordon theory and represent the state of the art prior to this work.

Before we minimize the energy, let us illustrate the result in Eq. (4.6) to give a more intuitive picture. We choose a constant mean field and calculate the energy density. The result is

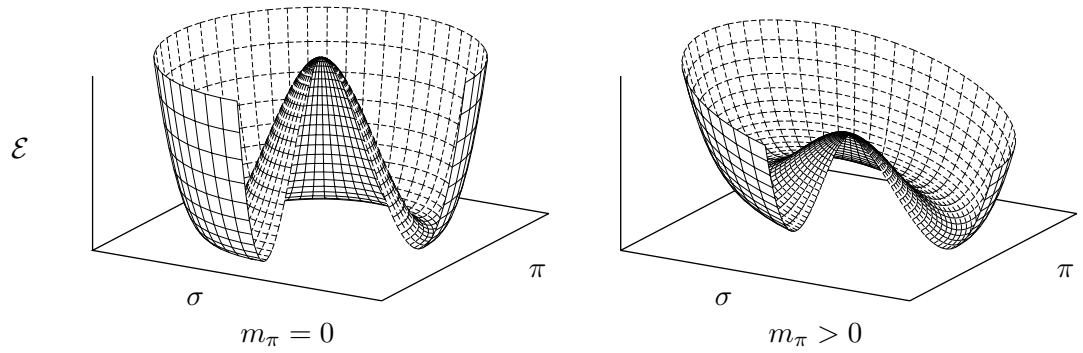

Figure 4.2.: Plot of the energy density in Eq. (4.6) for $\chi' = \lambda' = 0$ in the chiral limit (left) and with bare fermion mass (right). The "Mexican hat" shaped potential is tilted as the chiral symmetry is broken explicitly.

shown in Fig. 4.2. In the chiral limit, the mean field can wind around the circle of minima. The single baryon is stretched over whole space, so that the spatial gradient vanishes and the baryon becomes massless. This is different for explicitly broken chiral symmetry. In the right plot one can see how the potential is tilted as the pion mass m_π is turned on. The mean field of the single baryon will now minimize the size of the region where the potential is large, while keeping the spatial gradient small due to the derivative terms in (4.6). The interplay between these effects will lead to the shape of the mean field in the following calculation.

We vary the energy with respect to χ and λ. In order to solve the resulting differential equations, we expand $F(m_\pi)$ and assume the following Taylor series for χ and λ,

$$\chi \approx \sum_{n=0}^{6} m_\pi^{2n} \chi_n, \qquad \lambda \approx \sum_{n=1}^{6} m_\pi^{2n} \lambda_n \tag{4.7}$$

The coefficients χ_n and λ_n in turn are taken to depend only on $\xi = m_\pi x$, so that each derivative with respect to x increases the power of m_π by one. All of these assumptions can be justified *a posteriori* by showing that they are the simplest ones which lead to a consistent approximate solution of the differential equations. This procedure yields a set of inhomogeneous differential equations for χ_n and algebraic equations for λ_n. Up to next to leading order, we get (where now $' = \mathrm{d}/\mathrm{d}\xi$)

$$\chi_0'' = \frac{1}{2} \sin 2\chi_0 \tag{4.8a}$$

$$\lambda_1 = \frac{1}{4} (\cos 2\chi_0 - 1) \tag{4.8b}$$

$$\chi_1'' - \chi_1 \cos 2\chi_0 = \frac{1}{2} \left(\lambda_1 + \frac{1}{6} \right) \sin 2\chi_0 - \frac{1}{6} \chi_0^{IV}. \tag{4.8c}$$

The higher order equations are of the same type: The λ_n are given algebraically in terms of coefficients of lower order, whereas the χ_n are determined by a second order differential equation with the homogeneous part $\chi_n'' - \chi_n \cos 2\chi_0$. Up to order m_π^6, the equations are given

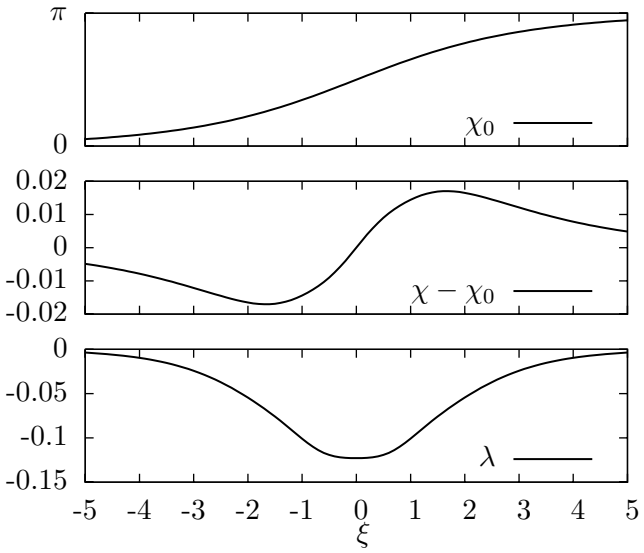

Figure 4.3.: Result for χ and λ in the derivative expansion up to order m_π^{12} with scaled x-dependence $\xi = m_\pi x$ and $m_\pi = 0.5$ in units where $m = 1$. The dotted line in the topmost plot shows the sine-Gordon kink χ_0, which is the leading order result.

in Appendix E. They can be solved successively in orders of m_π. Our analytical results for baryon number 1 are ($\operatorname{sech}\xi = 1/\cosh\xi$) in next to leading order

$$\chi_0 = 2\arctan \mathrm{e}^{\xi} \tag{4.9a}$$

$$\lambda_1 = -\frac{1}{2}\operatorname{sech}^2\xi \tag{4.9b}$$

$$\chi_1 = \frac{1}{8}\sinh\xi\operatorname{sech}^2\xi. \tag{4.9c}$$

The higher order coefficients are calculated with MAPLE. The result can be found in Appendix E. In the course of this calculation, we had to decide what to do with the homogeneous solution of the differential equations for χ_n. Physically, they reflect the fact that there is a flat direction in function space due to the breaking of translational invariance by the baryon. We have made the choice that χ is odd under $\xi \to -\xi$, a requirement which fixes the position of the baryon in space and leads to a unique solution of the differential equations.

We see that the leading order result (keeping only χ_0) agrees with the sine-Gordon theory, whereas the higher order corrections yield systematic corrections to it. Inserting Eqs. (4.9) into Eqs. (4.7), the scalar and pseudoscalar potentials can be written as a power series in m_π^2, i.e., the ratio of pion mass to physical quark mass (remember that we have chosen units such that $m = 1$), with smooth coefficient functions depending only on $m_\pi x$. The result is plotted in Fig. 4.3 for $m_\pi = 0.5\,m$. As expected from the intuitive picture in Fig. 4.2, the spatial region, where $\chi \neq 0, \pi$ and $\lambda \neq 0$ becomes smaller for increasing pion mass.

Inserting the results (4.9) into the expression for the energy density (4.6) and integrating over

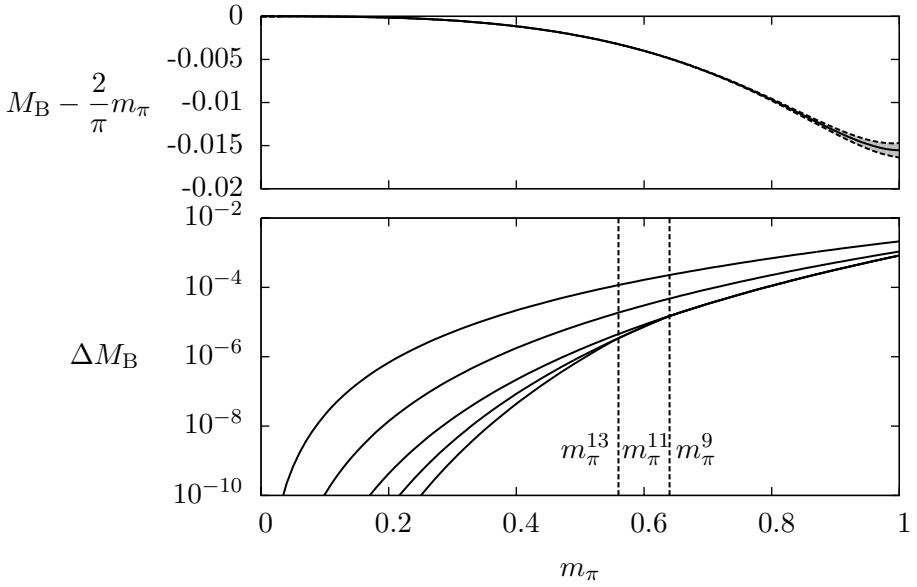

Figure 4.4.: *Upper plot:* Correction to the leading order in the result for the baryon mass (4.10) versus pion mass up to $m_\pi = 1$ (in units of m). *Lower plot:* Accuracy set by the highest order term, which is smaller than its preceeding term. From top to bottom, the precision for the expansion up to orders $m_\pi^5, m_\pi^7, m_\pi^9, m_\pi^{11}, m_\pi^{13}$.

space, we finally get the following chiral expansion for the baryon mass in the NJL_2 model,

$$\frac{M_B}{N} = \frac{2m_\pi}{\pi}\left[1 - \frac{m_\pi^2}{36} - \frac{m_\pi^4}{300} - \frac{m_\pi^6}{588} + \frac{12437\ m_\pi^8}{9525600} - \frac{8146151\ m_\pi^{10}}{2561328000} + \frac{287583896861\ m_\pi^{12}}{28049615193600} + \mathrm{O}(m_\pi^{14})\right]. \tag{4.10}$$

The leading order result $2m_\pi/\pi$ agrees with the sine-Gordon theory. The result up to order m_π^6 was published in [25].

The higher order corrections in Eq. (4.10) have been calculated in order to analyze the convergence behavior of the series. The accuracy of the derivative expansion is indicated by the highest order. For $m_\pi \gtrapprox 0.56$ the 13th order term is larger than the term $\sim m_\pi^{11}$, i.e., the expansion is only reliable up to 11th order. For $m_\pi \gtrsim 0.64$ the m_π^9 term is an indicator of the accuracy of the approximation. In Fig. 4.4 the correction to the sine-Gordon result is plotted versus m_π. The lower plot shows the absolute value of the term which sets the accuracy. At small values for the pion mass, the precision of the result can be increased by including higher order terms. At larger values, higher orders do not improve the result. This shows that the chiral expansion (4.10) has the convergence properties of an asymptotic series.

4.2. Dense matter

In leading order of the expansion in m_π/m, the chiral angle χ is described by the sine-Gordon equation (4.8a). For the single baryon we chose the kink solution (4.9a), which has winding

number 1. In order to describe dense matter, we now consider periodic solutions of the sine-Gordon equation. A solution which leads to a finite baryon number density is the kink crystal found in Ref. [12]

$$\chi_0 = \frac{\pi}{2} + \mathrm{am}(z,\kappa) \qquad \left(z = \frac{m_\pi}{\kappa} x\right), \tag{4.11}$$

where am is the Jacobi amplitude. One can check that χ_0 fulfills the sine-Gordon equation using identities for Jacobi elliptic functions in Appendix D. This solution leads to a baryon density equal to the winding number density. Due to the periodicity $\mathrm{am}(z+n2\mathbf{K}) = \mathrm{am}(z) + n\pi$ for $n \in \mathbb{Z}$, the topological baryon density is

$$\rho = \frac{m_\pi}{2\kappa\mathbf{K}}. \tag{4.12}$$

Using the results of the derivative expansion, we can now calculate the next to leading order correction to the energy density calculated in [12] by solving the minimum equations (4.8). Note that the parameter κ (elliptic modulus) which determines the baryon density introduces an additional scale. Hence, the derivative expansion cannot be interpreted as an expansion in the pion mass only and is merely reliable at low densities. The result for λ_1 in Eq. (4.8b) is

$$\lambda_1 = -\frac{1}{2}\mathrm{cn}^2 z, \tag{4.13}$$

from which the equation for χ_1 can be deduced (where now $' = \mathrm{d}/\mathrm{d}z$)

$$\chi_1'' + \kappa^2\chi_1(1 - 2\mathrm{sn}^2 z) = \frac{\mathrm{sn}\, z\, \mathrm{cn}\, z}{6}\ (\kappa^2 + 3\kappa^2 \mathrm{sn}\, z^2 - 4). \tag{4.14}$$

The solution is

$$\chi_1 = \frac{1}{8}\mathrm{dn}\, z\, \mathrm{cn}\, z - \frac{\kappa'^2}{12\kappa^2}\frac{\mathbf{K}}{\mathbf{E}}\left(\mathrm{dn}\, z\, \mathrm{Z}(z) - \kappa^2\, \mathrm{sn}\, z\, \mathrm{cn}\, z\right) + C\mathrm{dn}\, z \tag{4.15}$$

where $\mathrm{dn}\, z$ is a solution to the homogeneous equation. Like in the single baryon case, the non-periodic part of the general solution was dropped, leaving a single integration constant C. Higher order corrections to this result have not yet been evaluated. In Fig. 4.5 χ and λ are plotted in next to leading order. The right plot illustrates how the "chiral spiral" in Fig. 4.1 is distorted when chiral symmetry is broken explicitely.

The total energy density with respect to the vacuum in next to leading order becomes

$$E = \rho\left[\frac{m_\pi}{\pi\kappa}(2\mathbf{E} - \mathbf{K}\kappa'^2) - \frac{m_\pi^3}{36\pi k^3}\left((3\kappa^4 - 5\kappa^2 + 2)\mathbf{K} + (4k^2 - 2)\mathbf{E}\right) + \mathrm{O}(m_\pi^5)\right]. \tag{4.16}$$

In the limit $\kappa \to 1$, the coefficients χ_0, χ_1 and λ_1 reduce to the single baryon solution in Eq. (4.9) and the total energy density reduces to $E = \rho M_B$, with the baryon mass M_B from Eq. (4.10) up to order m_π^3. The term of linear order in m_π coincides with the result in Ref. [12], the derivative expansion gives the next to leading order. In Fig. 4.6 the energy density (4.16) is compared to the translationally invariant solution of the HF problem (see Appendix B), which shows that for small densities and pion masses, the crystal is energetically favorable.

Finally we can say that the derivative expansion leads to a consistent picture of baryons and dense matter in massive NJL_2, where the validity of the calculation is restricted to small values of the pion mass and small densities. Without explicitly solving the Dirac equation we have obtained the first few terms beyond the sine-Gordon theory results in Refs. [49],[12]. In effect, the derivative expansion can be regarded as a kind of bosonization where a chiral angle field χ and a radial field λ carry all the dynamical information. The emergence of the Skyrme picture is put on very solid grounds in this case.

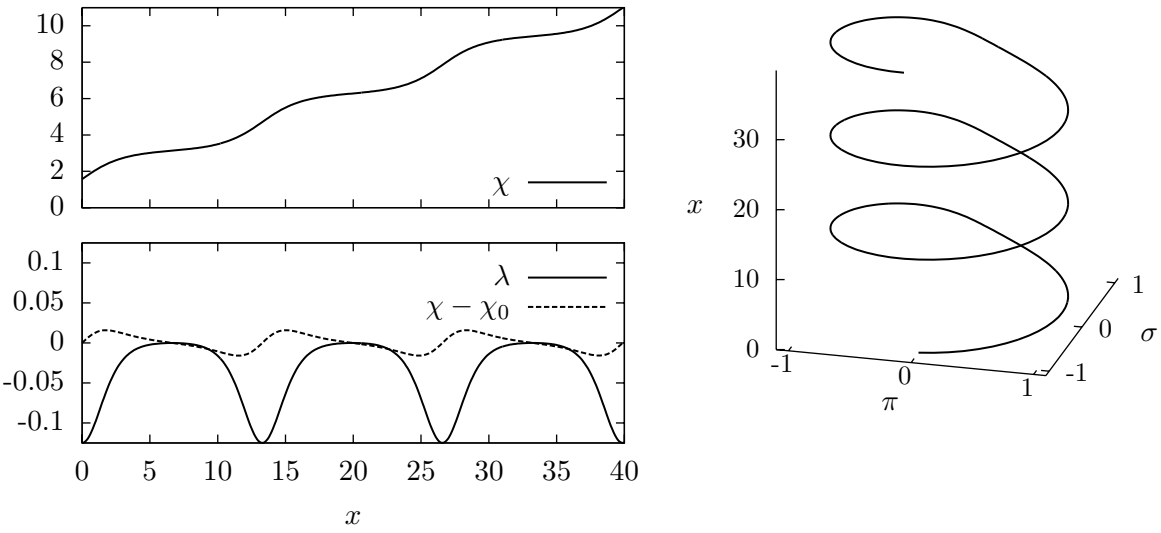

Figure 4.5.: *Left*: Result for χ and λ in the derivative expansion up to order m_π^2 for density $\rho = 0.075$ ($\kappa = 0.99$ and $m_\pi = 0.5$). *Right*: The distorted "chiral spiral" for the same baryon density.

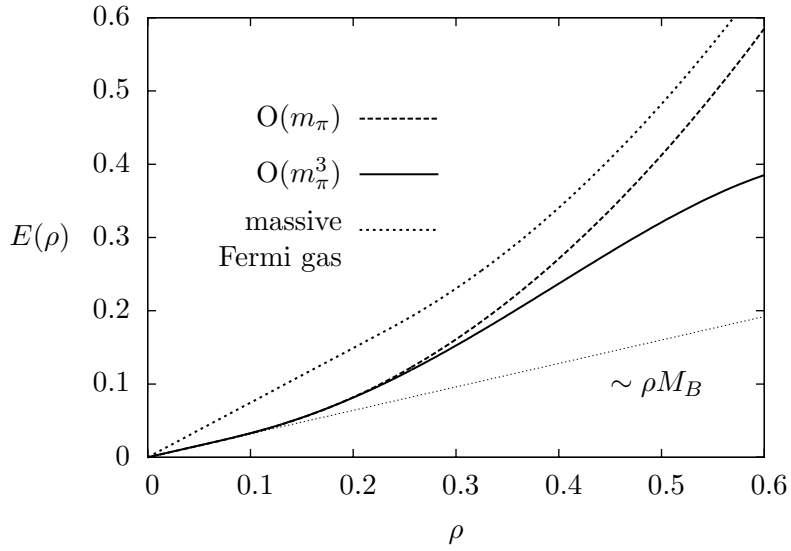

Figure 4.6.: Energy density (4.16) for dense baryonic matter in the NJL_2 in the derivative expansion for $m_\pi = 0.5$ ($\gamma = 0.065$) versus baryon density ρ. The chiral spiral is energetically favorable to the translationally invariant solution (dotted line, see Appendix B) at all densities shown. At densities $\rho \gtrapprox 0.4$ the derivative expansion is not reliable as the term of order m_π^3 changes the result significantly.

Part II.

2+1 dimensional models

5. Gross-Neveu model in 2+1 dimensions

In Chapter 3 the GN model in 1+1 dimensions was used as a toy model for relativistic quark matter. As the restriction to one spatial dimensions is unphysical, the question arises, how this analysis can be extended to higher dimensions. However, one cannot choose the physical 3+1 dimensional space without giving up renormalizability. As a compromise between physical significance and the restriction to renormalizable theories, in this chapter, we consider dynamical symmetry breaking in the 2+1 dimensional GN model.

A further motivation to study GN_3 is its application in condensed matter physics. Like its little brother, the model is used to describe electrons near the Fermi surface of a half-filled band in quasi-two-dimensional systems. In particular, the superconducting electrons in some high-temperature superconductors are confined to planes determined by the lattice structure of the material (CuO_2 planes) [50, 18, 51]. Another recent example for an application are carbon nanotubes [52].

As described in Sections 2.2 and 2.3 we can use the same tools of relativistic HF theory as in the 1+1 dimensional case. The HF Hamiltonian of GN_3 is given in (2.6) with $\phi_1 = \phi_2 = 0$ and $\phi_3 \equiv \phi$

$$H = -\mathrm{i}\gamma^0(\gamma^1\partial_1 + \gamma^2\partial_2) + \gamma^0\tau_3\phi(x_1, x_2).$$

Since the Hamiltonian is diagonal in isospin space, it is sufficient to find a self-consistent solution for the upper isospin component by solving the eigenvalue problem for the two-component Hamiltonian

$$H = -\mathrm{i}\gamma^0(\gamma^1\partial_1 + \gamma^2\partial_2) + \gamma^0\phi(x_1, x_2). \tag{5.1}$$

The self-consistency condition (2.8) becomes

$$\langle\bar{\psi}\psi\rangle = -\frac{\phi}{Ng^2}. \tag{5.2}$$

Total energy and baryon density, i.e., fermion density divided by N, have to be doubled to get the quantities for the full theory. The gap equation (2.15) has to be modified to

$$\frac{2}{Ng^2} = \frac{1}{\pi}(\Lambda - m) \tag{5.3}$$

as the isospin degeneracy of the vacuum states is removed.

If translational invariance of the ground state is assumed, the HF equations can be solved self-consistently, where $\phi = \text{const.}$ plays the role of a dynamical fermion mass. In this case, the behavior of the total energy and the baryon density is well known [13, 15]. In Appendix C the results of this calculation are summarized.

In the following, we consider spatially inhomogeneous mean field configurations and discuss their stability by comparing the total energy with the translationally invariant case. On

the basis of the mean field of the baryon and dense matter in GN_2 (Sections 3.1 and 3.2) it is possible to find self-consistent solutions of the 2+1 dimensional model. These extend the 1+1 dimensional solutions, maintaining translational symmetry in one spatial direction. Surprisingly, these solutions are degenerate to the massive Fermi gas.

5.1. The self-consistent baryon stripe solution

For GN_3, the question of existence of localized multi-fermion bound states is still open. The inverse scattering analysis which was used to find the baryon in GN_2 (see Section 3.1 and Ref. [23]) cannot be applied easily in 2+1 dimensions. If a bound state exists, we expect the chiral condensate to be rotationally symmetric $\phi(r)$. Even in such a symmetric case, a self-consistent solution to the HF equations (5.1) is not known. In this chapter we consider mean field configurations depending on one spatial coordinate only ($\phi = \phi(x_2)$). This leads to fermion states which are localized in the x_2 direction and form "stripe" structures in the two-dimensional plane.

A HF solution involving a one-dimensional structure was found by Bietenholz et. al. [53]. They extend the single baryon solution in Section 3.1 to 2+1 dimensions, prove its self-consistency and show that the total energy is the same as in the translationally invariant solution. The motivation of this analysis is to study the dimensional reduction of the dynamics of fermions moving along this "baryon stripe", which in this context should be considered as a "brane world". In the following, we state some results of Ref. [53] and put it into the context of translational symmetry breakdown. In Section 5.2 we generalize the result to the "stripe phase" solution, which is inspired by the baryon crystal in GN_2, cf. Section 3.2.

In Ref. [53], the profile in the x_2 direction is chosen to be equal to the single baryon solution of GN_2 in Eq. (3.3) with $\phi(x_2) = \sigma(x_2)$, which contains the variational parameter y. For this configuration the single particle spectrum consists of bulk states with energies $\pm\sqrt{p_1^2 + p_2^2 + m^2}$ and states of fermions propagating along the kink-anti-kink walls with energies $\pm\sqrt{p_1^2 + m^2(1-y^2)}$, originating from the two discrete states of the 1+1 dimensional baryon solution [22]. The spectrum for $y = 0.8$ is shown in Fig. 5.1.

Bietenholz et. al. proved the self-consistency (5.2) of the baryon stripe. For the calculation, the system is enclosed in a finite volume $[0, L_1] \times [0, L_2]$, where the limit $L_1, L_2 \to \infty$ is taken in the end. A given (full) occupation of valence state energy levels up to the Fermi momentum p_f is then equivalent to choosing the baryon density $\rho = p_f/(L_2\pi)$. Self-consistency now leads to the restriction of the variational parameter to $y = p_f/m$.

The renormalized total energy per length L_1 of the baryon stripe is found in section 5.4 of Ref. [53], where it plays the role of the brane tension. Using the self-consistency condition and subtracting the vacuum energy, one gets the simple expression

$$\frac{E - E_{(0)}}{L_1} = \frac{ym^2}{\pi} = \frac{p_f m}{\pi}, \tag{5.4}$$

which can be written in terms of the baryon density as

$$\frac{E - E_{(0)}}{L_1 L_2} = \rho\, m.$$

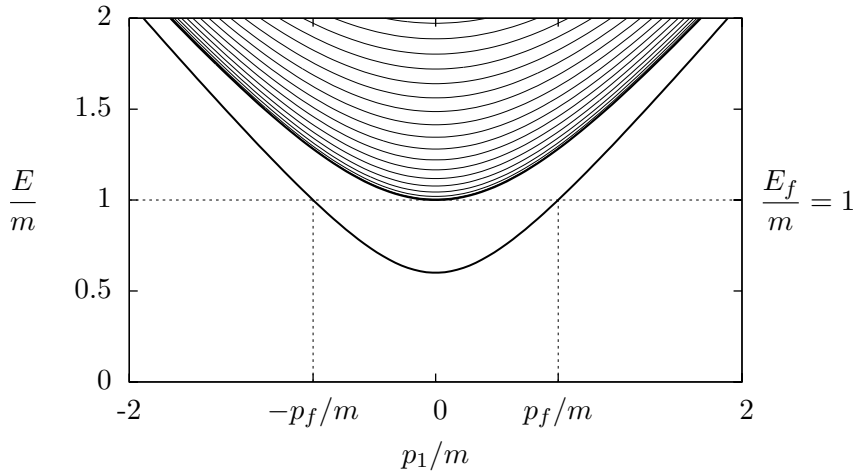

Figure 5.1.: Energy spectrum of fermions in the self-consistent baryon stripe potential ($y = 0.8$, $p_f = 0.8\,m$). The lower line shows energies of states localized at the stripe with $E = \sqrt{p_1^2 + m^2(1-y^2)}$, the upper lines indicate the bulk spectrum $E = \sqrt{p_1^2 + p_2^2 + m^2}$ with $p_2/m = 0.0 \ldots 1.7$.

This is the same result as in the translationally invariant HF solution described in Appendix C, cf. Eq. (C.1). As we only consider large L_2, the baryon density is well below the critical density $m^2/(4\pi)$ at which chiral symmetry is restored when assuming translational symmetry. Hence, the massive Fermi gas with the same occupation of positive energy states, i.e., the same baryon density, is energetically degenerate to the baryon stripe. The finite binding energy for the baryon profile in the x_2-direction is cancelled by the extra energy needed to fill the momentum states in the x_1-direction.

Unless there would be another self-consistent solution with lower energy, we may conclude that the GN_3 model at finite density $0 \leq \rho \leq m/(L_2\pi)$ has a degenerate ground state. The system has neither an advantage nor a disadvantage in breaking translational symmetry by forming a one-dimensional structure. The following section will generalize this result to densities up to the critical density $m^2/(4\pi)$. In this regime the massive Fermi gas solution is degenerate to x_2-periodic structures.

Finally, we would like to mention an alternative derivation of the total energy result in Eq. (5.4). It is based on the dimensional argument that the energy per length L_1 will be proportional to m^2 because the vacuum fermion mass m is the only physically meaningful mass scale. In Appendix F, we use this argument due to Feinberg [35] to confirm the result in Eq. (5.4).

5.2. The stripe phase configuration

The self-consistent baryon stripe can only hold fermions up to the density $m/(L_2\pi)$. Above this density, the massive Fermi gas described in Appendix C is the only solution to the HF equations known so far. The existence of the baryon crystal in GN_2 (see Section 3.2) now leads to the question of the stability of its extension to 2+1 dimensions. The main result of

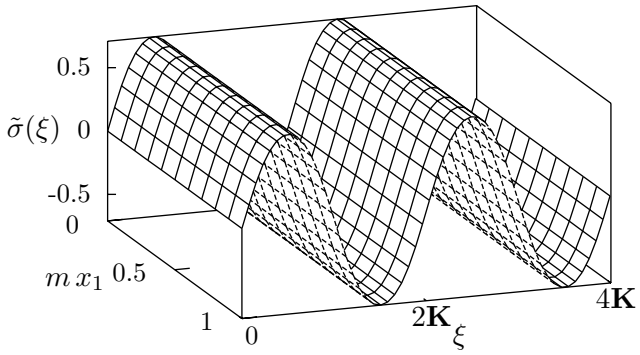

Figure 5.2.: Stripe phase ansatz for the scalar potential in GN_3 in Eq. (5.5) with the parameter $\kappa = 0.96$ (corresponds to density $\rho = 0.06\,m^2$).

this section will be to show that this "stripe phase" configuration is a self-consistent solution which is again degenerate to the massive Fermi gas up to the critical density $m^2/4\pi$.

The scalar potential of the "stripe phase" is defined by the 2+1 dimensional extension of Eq. (3.42). This ansatz involves Jacobi elliptic functions (see Appendix D) and depends on two variational parameters A and κ. We set

$$\phi(x_2) = A\tilde{\sigma}(Ax_2) = A\kappa^2 \frac{\mathrm{sn}(Ax_2)\,\mathrm{cn}(Ax_2)}{\mathrm{dn}(Ax_2)}. \tag{5.5}$$

The shape of this ansatz is illustrated in Fig. 5.2. The baryon stripe is obtained as a special case in the limit $\kappa \to 1$, where we have to set $A = m$ and $y \to 1$.

5.2.1. Self-consistency of the stripe phase

Using the results from 1+1 dimensions, one can check self-consistency at given baryon density (determined by the filling of positive energy states), and derive a constraint for the parameters A and κ from the self-consistency condition (5.2). This requires the solution of the eigenvalue problem for the Hamiltonian (5.1). We first choose the gamma matrices analogous to the 1+1 dimensional case (3.1)

$$\gamma^0 = -\sigma_1, \qquad \gamma^1 = \mathrm{i}\sigma_2, \qquad \gamma^2 = \mathrm{i}\sigma_3,$$

which makes it easier to take over results from Section 3.2 and the treatment of baryons in massless GN_2 at finite temperature in Ref. [54]. Using the ansatz $\psi(x_1, x_2) = \mathrm{e}^{\mathrm{i}p_1 x_1}\psi(x_2)$ the Hamiltonian reads

$$H = \begin{pmatrix} p_1 & \partial_2 - \phi(x_2) \\ -\partial_2 - \phi(x_2) & -p_1 \end{pmatrix}.$$

By squaring the Hamiltonian one gets equations for the upper and lower components $\psi_\pm(x_2)$ of the spinor eigenfunctions. These are the Lamé equations (3.22)

$$\left[-\partial_\xi^2 + 2\kappa^2 \mathrm{sn}^2(\xi + (\mathbf{K} \mp \mathbf{K})/2)\right] \psi_\pm = \mathcal{E}\psi_\pm,$$

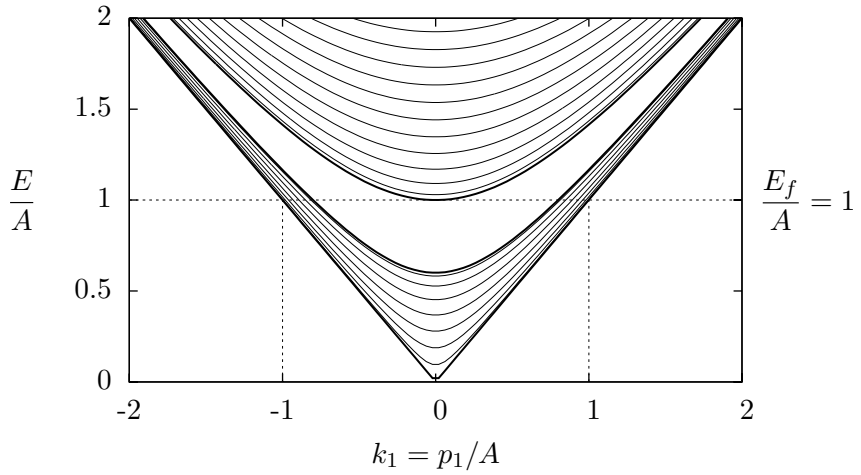

Figure 5.3.: Energy spectrum of fermions in the "stripe phase" potential with $\kappa = 0.8$ (baryon density $\rho \approx 0.073$). The lines in the lower band correspond to Bloch momenta $p = 0 \ldots \pi/2\mathbf{K} \approx 0.787$ (in steps of 0.1), the upper band is shown for $p = \pi/2\mathbf{K} \ldots 1.9$. The Fermi energy E_f is taken from the self-consistency condition Eq. (5.11)

with $\xi = Ax_2$. The difference to the 1+1 dimensional case lies in the relation between the Lamé eigenvalues and the Dirac energies $E = A\omega$ ($k_1 = p_1/A$)

$$\mathcal{E} = \omega^2 + \kappa^2 - k_1^2.$$

The Lamé eigenfunctions can be found in Eq. (3.24), the spectrum of the Lamé equation is given by Eq. (3.25). In order to ease the notation in the following, we write the energies ω in terms of the Dirac energies in the 1+1 dimensional case $\tilde{\omega}$

$$\omega^2 = \tilde{\omega}^2 + k_1^2. \tag{5.6}$$

$\tilde{\omega}$ now lies in the two energy bands $0 \ldots \kappa' = \sqrt{1-\kappa^2}$ and $1 \ldots \infty$. Compared to the 1+1 dimensional case, each state now becomes a hyperbola of states with different momenta k_1. The spectrum is plotted in Fig. 5.3. The lines show states with different values of the dimensionless Bloch momentum p of the x_2-direction. In the limit $\kappa \to 1$ the lower Lamé band shrinks to a single valence state $\tilde{\omega} = 0$ and the spectrum is reduced to the baryon stripe spectrum shown in Fig. 5.1 with $y = 1$.

In order to show self-consistency, first $\bar{\psi}\psi$ is calculated for each energy mode. By integrating over all occupied states up to the Fermi energy E_f we prove that Eq. (5.2) holds. The final result of this section will be Eq. (5.11) which restricts E_f and the parameter A. The second parameter κ is determined by the baryon density in Eq. (5.14).

The divergence in the energy integral is handled in the renormalization scheme developed in Section 2.3. However, due to the specific shape of the spectrum of the stripe phase, it turns out to be more convenient to choose a slightly different regularization method. Instead of the symmetric cut-off procedure $|\mathbf{p}| < \Lambda$, we cut off momenta with $|p_k| > \lambda$. The self-consistency condition in the vacuum, leads to the gap equation

$$\frac{1}{Ng^2} = 2\lambda \ln\left(1+\sqrt{2}\right) - \frac{\pi}{2}m. \tag{5.7}$$

The result for physically meaningful quantities will not depend on the regularization method.

For the normalization of the eigenspinors one requires that the mean fermion density is

$$\langle\psi^\dagger\psi\rangle = 1 = \frac{1}{2\mathbf{K}}\int_0^{2\mathbf{K}} \mathrm{d}\xi \left(|\psi_+|^2 + |\psi_-|^2\right). \tag{5.8}$$

One first finds a relation between the supersymmetric partner eigenfunctions $\psi_\pm$. Since ψ_- fulfills the same Lamé equation with a potential shifted by a half period ($\mathrm{sn}^2\xi \mapsto \mathrm{sn}^2(\xi+\mathbf{K})$), it is necessary that $\psi_-(\xi+\mathbf{K}) = c\psi_+(\xi)$ with a complex factor c. This factor can be determined using the coupled equations for the upper and lower component given by the eigenvalue equation of the single particle Hamiltonian in (5.1) and the symmetry $\tilde{\sigma}(\xi+\mathbf{K}) = -\tilde{\sigma}(\xi)$. The result is

$$c^2 = \frac{\omega - k_1}{\omega + k_1}\mathrm{e}^{2\mathrm{Z}(\alpha)\mathbf{K}},$$

where the parameter α is related to the Bloch momentum by Eq. (3.25). The condition (5.8) becomes

$$1 = \frac{1}{2\mathbf{K}}\int_0^{2\mathbf{K}} \mathrm{d}\xi\, |\psi_+|^2 \left(1 + \frac{\omega - k_1}{\omega + k_1}\right).$$

$|\psi_+|^2$ can be obtained by squaring the solution of the Lamé equation (3.24). The result is taken from the 1+1 dimensional case [54]

$$|\psi_+|^2 = |\mathcal{N}|^2 \frac{\pi\Theta^2(\alpha)}{2\mathbf{K}\kappa\sqrt{1-\kappa^2}} \left|\mathrm{dn}^2(\alpha,\kappa) - \mathrm{dn}^2(\xi,\kappa)\right|.$$

The spatial average of this expression is calculated to get the normalization factor

$$|\mathcal{N}|^2 = \frac{\omega + k_1}{\omega}\frac{\mathbf{K}\kappa\kappa'}{\pi\Theta^2(\alpha)|\tilde{\omega}^2 - \mathbf{E}/\mathbf{K}|},$$

and

$$|\psi_+|^2 = \frac{\omega + k_1}{2\omega}\frac{\tilde{\omega}^2 - \mathrm{dn}^2(\xi)}{\tilde{\omega}^2 - \mathbf{E}/\mathbf{K}}.$$

With this result, $\bar{\psi}\psi$ can be calculated, where we again take over results from Ref. [54]

$$\begin{aligned}\bar{\psi}\psi &= -(\psi_+^*\psi_- + \psi_-^*\psi_+) \\ &= \frac{1}{\omega + k_1}\left(\psi_+^*(\partial_\xi + \tilde{\sigma})\psi_+ + \left[(\partial_\xi + \tilde{\sigma})\psi_+\right]^*\psi_+\right) \\ &= \frac{\tilde{\omega}}{\omega}\frac{\tilde{\omega}}{\tilde{\omega}^2 - \mathbf{E}/\mathbf{K}}\tilde{\sigma}(\xi).\end{aligned} \tag{5.9}$$

This is the contribution to chiral condensate of a single energy mode. For the calculation of the ground state expectation value $\langle\bar{\psi}\psi\rangle$, we integrate this expression over all negative energy states and the positive energy states up to the Fermi energy $E_f = \omega_f A$

$$\langle\bar{\psi}\psi\rangle = P_{\mathrm{neg}} + P_{\mathrm{pos}}.$$

The negative energy part is regularized and becomes ($p_2 = pA$, $\tilde{\lambda} = \lambda/A$)

$$P_{\mathrm{neg}} = \frac{1}{(2\pi)^2}\int_{-\lambda}^{\lambda}\mathrm{d}p_2\int_{-\lambda}^{\lambda}\mathrm{d}p_1\,\bar{\psi}\psi = -\frac{A\phi(x_2)}{\pi^2}\int_0^{\tilde{\lambda}}\mathrm{d}p\int_0^{\tilde{\lambda}}\mathrm{d}k_1\frac{\tilde{\omega}^2}{(\tilde{\omega}^2 - \mathbf{E}/\mathbf{K})\sqrt{\tilde{\omega}^2 + k_1^2}}.$$

With the density of states (3.26), we derive

$$\frac{\mathrm{d}p}{\mathrm{d}\tilde{\omega}} = \frac{|\tilde{\omega}^2 - \mathbf{E}/\mathbf{K}|}{W}, \qquad \text{with} \qquad W = \sqrt{|(\tilde{\omega}^2 - \kappa'^2)(\tilde{\omega}^2 - 1)|}, \tag{5.10}$$

so that the integral over p can be transformed into an integral over $\tilde{\omega}$. Now

$$\begin{aligned} P_{\mathrm{neg}} &= -\frac{A\phi(x_2)}{\pi^2}\left[-\int_0^{\kappa'}\frac{\mathrm{d}\omega}{W} + \int_1^{\tilde{\lambda}}\frac{\mathrm{d}\omega}{W}\right]\int_0^{\tilde{\lambda}}\mathrm{d}k_1\,\frac{\omega^2}{\sqrt{\omega^2+k_1^2}} \\ &= -\frac{A\phi(x_2)}{\pi^2}\left[-\int_0^{\kappa'}\frac{\mathrm{d}\omega}{W} + \int_1^{\tilde{\lambda}}\frac{\mathrm{d}\omega}{W}\right]\omega^2\,\mathrm{arcsinh}(\tilde{\lambda}/\omega) \\ &\equiv -\frac{A\phi(x_2)}{\pi^2}\Big[P_{\mathrm{lb}} + P_{\mathrm{ub}}\Big], \end{aligned}$$

where in the second step the integral over k_1 was solved, leaving a one-dimensional integral over the two energy bands which can be evaluated for large λ. In the first integral one can assume $\omega \ll \tilde{\lambda}$ and separate the logarithmically divergent part ($\mathrm{arsinh}(1/\epsilon) = \ln 2/\epsilon + \epsilon^2/4 + \mathcal{O}(\epsilon^3)$). We get the lower band contribution

$$P_{\mathrm{lb}} = \int_0^{\kappa'}\frac{\mathrm{d}\omega}{W}\,\omega^2\ln\omega - \ln(2\tilde{\lambda})\int_0^{\kappa'}\frac{\mathrm{d}\omega}{W}\,\omega^2.$$

We expect P_{neg} to have only a linear divergence in λ so that the logarithmic term should be cancelled by a contribution in the upper band.

The calculation of the asymptotics of P_{ub} is more difficult, because the integrand cannot be expanded in orders of $\tilde{\lambda}$. We solve this by splitting the integral over the upper band into an integral from 1 to $\sqrt{\tilde{\lambda}}$ ($\omega \ll \tilde{\lambda}$) and one from $\sqrt{\tilde{\lambda}}$ to $\tilde{\lambda}$ ($\omega \ll 1$). Now, both integrals can be expanded in orders of $\tilde{\lambda}$, leading to

$$\begin{aligned} \int_1^{\sqrt{\tilde{\lambda}}}\frac{\mathrm{d}\omega}{W}\,\omega^2\,\mathrm{arsinh}(\tilde{\lambda}/\omega) &= \int_1^{\sqrt{\tilde{\lambda}}}\frac{\mathrm{d}\omega}{W}\,\omega^2(\ln(2\tilde{\lambda}) - \ln\omega) + \mathcal{O}\left(\lambda^{-1/2}\right) \\ \int_{\sqrt{\tilde{\lambda}}}^{\tilde{\lambda}}\frac{\mathrm{d}\omega}{W}\,\omega^2\,\mathrm{arsinh}(\tilde{\lambda}/\omega) &= \int_{\sqrt{\tilde{\lambda}}}^{\tilde{\lambda}}\mathrm{d}\omega\,\mathrm{arsinh}(\tilde{\lambda}/\omega) + \mathcal{O}\left(\lambda^{-1/2}\right). \end{aligned}$$

With this expansion, the divergent terms can be split from the integral over the upper band. It can be shown analytically that the logarithmic divergent term is cancelled by the divergence in the integral over the lower band by writing the sum of both integrals as the real part of an integral in the complex plane. The result for the negative energy part is

$$P_{\mathrm{lb}} + P_{\mathrm{ub}} = -\frac{\pi}{2}\mathbf{E} + 2\tilde{\lambda}\ln(1+\sqrt{2}).$$

The integral over the positive energy states is given by

$$\begin{aligned} P_{\mathrm{pos}} &= -\frac{A\phi(x_2)}{\pi^2}\int_0^{\kappa'}\frac{\mathrm{d}\omega}{W}\int_0^{k_{\max}(\omega)}\mathrm{d}k_1\,\frac{\omega^2}{\sqrt{\omega^2+k_1^2}} = \\ &= -\frac{A\phi(x_2)}{\pi^2}\int_0^{\kappa'}\frac{\mathrm{d}\omega}{W}\,\omega^2\,\mathrm{arsinh}\left(\sqrt{\omega_f^2-\omega^2}/\omega\right), \end{aligned}$$

with the maximum value $k_{\max}(\omega)^2 + \omega^2 = \omega_f^2$ for the momentum k_1 in direction parallel to the stripes. We restricted the Fermi energy to values within the Lamé band gap: $\kappa' \leq \omega_f \leq 1$. One now merges the contributions to $\langle\bar{\psi}\psi\rangle$ and renormalizes the linearly divergent part by substituting it with the coupling constant and the dynamical fermion mass using the gap equation (5.7). The result is

$$\langle\bar{\psi}\psi\rangle = -\frac{\phi(x_2)}{Ng^2} - \frac{A\phi(x_2)}{\pi^2}\left[\int_0^{\kappa'} \frac{\mathrm{d}\omega}{W}\,\omega^2\,\mathrm{arsinh}\Big(\sqrt{\omega_f^2-\omega^2}/\omega\Big) - \frac{\pi}{2}\mathbf{E} + \frac{\pi}{2}\frac{m}{A}\right]$$

The first integral can be given in closed form if we assume that the Fermi level is at the upper edge of the energy gap of the Lamé spectrum, i.e., $\omega_f = 1$, cf. Fig. 5.1. We get

$$\int_0^{\kappa'} \frac{\mathrm{d}\omega}{W}\,\omega^2\,\mathrm{arsinh}\big(\sqrt{1-\omega^2}/\omega\big) = \frac{\pi}{2}(\mathbf{E}-1).$$

The result for the self-consistency condition is now independent of κ

$$\langle\bar{\psi}\psi\rangle = -\frac{\phi(x_2)}{Ng^2} - \frac{A\phi(x_2)}{2\pi}\left(1-\frac{m}{A}\right).$$

This is fulfilled for the choice of the parameter

$$A = m. \tag{5.11}$$

Due to $\omega_f = 1$ the Fermi energy becomes

$$E_f = A\omega_f = m.$$

Eq. (5.11) is the same condition derived for the "baryon stripe" in Ref. [53]. The second parameter κ of our ansatz will be fixed by the choice of baryon density (see Eq. (5.14)).

5.2.2. Energy density

We now calculate the total energy density $\mathcal{E}$ of the stripe phase. We divide $\mathcal{E}$ into three contributions

$$\mathcal{E} = \mathcal{E}_{\mathrm{dcc}} + \mathcal{E}_{\mathrm{neg}} + \mathcal{E}_{\mathrm{pos}},$$

the double counting correction and the integral over negative and positive energies. $\mathcal{E}_{\mathrm{dcc}}$ is calculated using the result for the spatial average of ϕ^2 along the x_2 direction in Eq. (3.33)

$$\mathcal{E}_{\mathrm{dcc}} = \frac{1}{2Ng^2L_1L_2}\int \mathrm{d}x_1 \int \mathrm{d}x_2\,\phi^2(x_2) = \frac{A^2(2u-\kappa^2)}{2Ng^2}, \tag{5.12}$$

with the κ-dependent parameter $u = 1-\mathbf{E}/\mathbf{K}$. The coupling constant in the above expression is eliminated using the gap equation (5.7), which leads to a linear divergence.

The other contributions to the energy are

$$\mathcal{E}_{\mathrm{neg}} = -\frac{A^3}{\pi^2}\int_0^{\tilde{\lambda}} \mathrm{d}p \int_0^{\tilde{\lambda}} \mathrm{d}k_1 \sqrt{\omega^2+k_1^2}$$
$$\mathcal{E}_{\mathrm{pos}} = \frac{A^3}{\pi^2}\int_{\mathrm{occ.}} \mathrm{d}p \int_{\mathrm{occ.}} \mathrm{d}k_1 \sqrt{\omega^2+k_1^2}.$$

Using the same techniques as in the preceding section, we isolate the divergent parts of the integrals. Our calculation shows that the linear divergence in the double counting correction term (5.12) is cancelled by the integral over the upper band, leaving the same λ^3 divergence as in the vacuum energy density (2.12). The renormalized expression for $\mathcal{E}$ is

$$\frac{\mathcal{E}_{\text{ren}}}{A^3} = -\frac{(2u-\kappa^2)m}{4\pi A} + \frac{1}{12\pi}\left[2\left(2-\kappa^2-\frac{3}{2}\frac{\mathbf{E}}{\mathbf{K}}\right)\mathbf{E} - (1-\kappa^2)\mathbf{K}\right] - \frac{1}{2\pi^2}\int_0^{\kappa'} \mathrm{d}\omega\, \frac{\omega^2 - \mathbf{E}/\mathbf{K}}{W}\left[\omega_f\sqrt{\omega_f^2-\omega^2} + \omega^2 \ln\frac{\sqrt{\omega_f^2-\omega^2}+\omega_f}{\omega}\right], \quad (5.13)$$

where we did not make use of the self-consistency condition (5.11) yet. In the limit $\kappa \to 1$ the above expression becomes $-1/12\pi$, the vacuum energy density.

Next, we will compare the energy density (5.13) to that of the translationally invariant solution in Eq. (C.1). We have to choose the same baryon density ρ in both solutions to decide if it is energetically favorable to break translational symmetry. Since $\langle\psi^\dagger\psi\rangle = 1$ is fixed due to the normalization, the baryon density of the stripe phase is

$$\rho = \frac{A^2}{4\pi^2}\int \mathrm{d}p \int \mathrm{d}k\, \langle\psi^\dagger\psi\rangle = -\frac{A^2}{\pi^2}\int_0^{\kappa'}\frac{\mathrm{d}\omega}{W}\left(\omega^2 - \frac{\mathbf{E}}{\mathbf{K}}\right)\sqrt{\omega_f^2-\omega^2}.$$

We now use the self-consistency condition (5.11), filling energy states up to the lower edge of the upper Lamé band ($\omega_f = 1$). We get

$$\rho(\omega_f = 1) = -\frac{A^2}{4\pi}\left(1-\kappa^2-2\frac{\mathbf{E}}{\mathbf{K}}\right). \quad (5.14)$$

When the parameter κ is changed from 1 to 0, one obtains densities ranging from 0 to $m^2/(4\pi)$, the critical density at which chiral symmetry is restored ($\phi(\kappa = 0) = 0$).

With this self-consistent choice of parameters the integrals in the energy density in Eq. (5.13) can be given in closed form. The result is

$$\mathcal{E}_{\text{ren}} = -\frac{m^3}{12\pi} + \rho\, m, \quad (5.15)$$

which equals the translationally invariant result in Eq. (C.1). Thus we conclude that the stripe crystal is energetically degenerate to the massive Fermi gas configuration.

In Fig. 5.4 the self-consistent "stripe phase" configuration is plotted for different baryon densities.

In order to get a further check of the self-consistency condition $m = A$, we derive it by minimizing a thermodynamic potential, requiring that positive energy states are filled up to Fermi energy $E_f = A$. With a chemical potential as a Lagrange multiplier fixing the baryon density, Eq. (5.13) gives

$$\mathcal{E}_{\text{ren}} - \mu\rho = -\frac{A^2}{4\pi}\left[(2u-\kappa^2)(m-\mu) - \frac{2}{3}A + \mu\right].$$

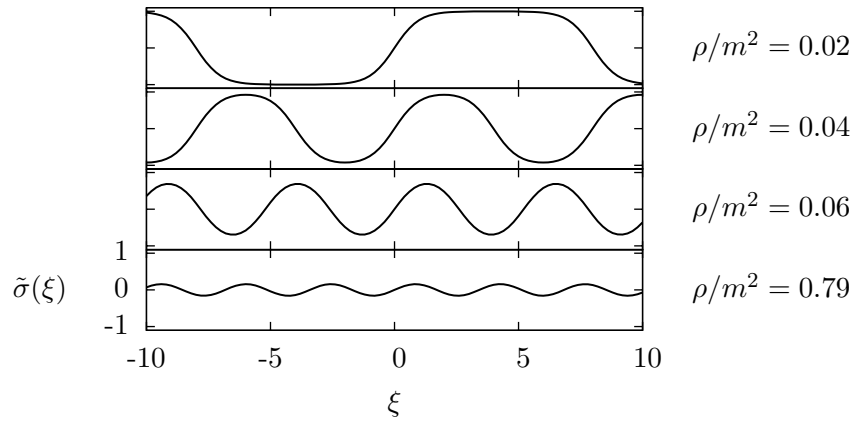

Figure 5.4.: Self-consistent stripe crystal configuration in the $x_2 = \xi/m$ direction for various baryon densities ρ/m^2. In the low density limit, the self-consistent baryon stripe solution is obtained, at the critical density $\rho/m^2 = 1/4\pi \approx 0.0796$, chiral symmetry is restored

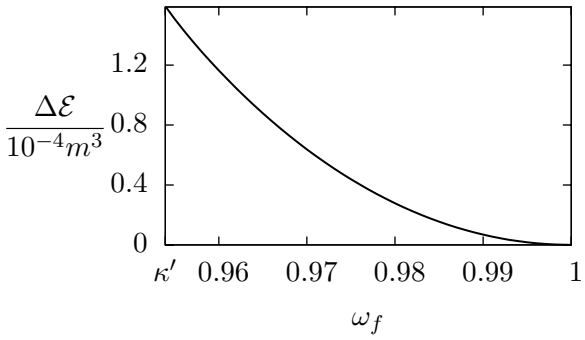

Figure 5.5.: Energy difference between the stripe crystal and the Fermi gas configuration for fixed $\kappa = 0.3$ and $A = m$ varying the band filling ω_f from κ' to 1.

The minimum conditions are

$$0 = \frac{\partial(\mathcal{E}_{\text{ren}} - \mu\rho)}{\partial(2u - \kappa^2)} = -\frac{A^2}{4\pi}(m - \mu)$$
$$0 = \frac{\partial(\mathcal{E}_{\text{ren}} - \mu\rho)}{\partial A} = -\frac{A}{2\pi}\left[(2u - \kappa^2)(m - \mu) - A + \mu\right],$$

which is fulfilled if the self-consistency condition (5.11) holds. Moreover, one can show that the stripe crystal is energetically less favorable compared to the Fermi gas if we fill the valence states up to a Fermi energy $\omega_f < 1$. This fact is illustrated in Fig. 5.5.

Finally, we emphasize that there is no physics argument to restrict the mean field to the one-dimensional structures investigated in this section. If translational symmetry is broken, we expect fermions to be localized in rotationally symmetric bound states ("baryons"). At finite fermion density they might form a two-dimensional lattice. Due to the complexity of the HF problem in 2+1 dimensions, we could not yet give a definite answer to the question of the existence of baryons in GN_3.

In 1+1 dimensions, the mechanism which drives the breakdown of translational symmetry was identified as Overhauser effect [55] with gap formation at the Fermi surface. In 2+1 dimensions the stripe phase does not lead to a gap in the spectrum, whereas two-dimensional structures might minimize the energy in this way. The marginally bound state found in this section in our view is an argument in favor of such a translational symmetry breakdown.

In the next chapter, we will search for localized baryons in the NJL_3 model. Because the continuous chiral symmetry of this model simplifies the calculation of the total energy, we will be able to identify the rotationally symmetric baryon as a marginally bound state of fermions.

6. Nambu-Jona-Lasinio model in 2+1 dimensions

In the preceding section we looked for bound states in the GN_3 model. Our analysis was restricted to one-dimensional structures, because it would be extremely difficult to calculate the total energy for an arbitrary mean field. The derivative expansion as a technique to circumvent the diagonalization of the single-particle Hamiltonian cannot be expected to be valid in this model. This expectation can be motivated with the following argument. Like in the GN_2 model the baryon (if existent) has to carve out a finite region in space, where the chiral condensate is suppressed. Because of the resulting increase in total energy, the size of the baryon is minimized, bounded from below by the cost of gradient energy. As a consequence, we have no reason to expect that the mean field of the baryon is slowly varying in space. This argument is confirmed by the self-consistent solution for the baryon in GN_2, so that we have to conclude that the derivative expansion cannot be applied for the models with discrete chiral symmetry. This is different in the NJL models, where the mean field of the baryon can wind itself around a continuum of ground states so that translational symmetry is broken without suppressing the condensate. Hence, the derivative expansion can be applied to calculate the total energy of the baryon. The analysis of baryons in the NJL_2 model can be found in Chapter 4, the calculation for the 2+1 dimensional model will be presented in the following. In analogy to the 1+1 dimensional case, we will first show that the topological charge of the mean field induces a finite baryon number through a spectral flow. The mass of an infinitely large chiral soliton will turn out to be equal to the vacuum fermion mass, leading to the conclusion that the single baryon has zero binding energy. This is very different from the NJL_2 model where the baryon is massless. In Section 6.2, we use numerical diagonalization of the HF Hamiltonian to show that solitons with large spatial variations do not lead to a true bound state.

6.1. Baryons in the derivative expansion

If a stable baryon exists in NJL_3, we expect its mean field to be rotationally symmetric and wrapping around the sphere of degenerate ground states ($\boldsymbol{\phi}^2 = m^2$) with topological charge 1. Such a configuration is the so called "hedgehog field", given in polar coordinates ($x_1 = r\cos\alpha$, $x_2 = r\sin\alpha$) by

$$\boldsymbol{\phi} = m \begin{pmatrix} \cos\alpha \, \sin f(r) \\ \sin\alpha \, \sin f(r) \\ \cos f(r) \end{pmatrix} . \tag{6.1}$$

The radial profile function $f(r)$ has to be an integer multiple of π at $r = 0$ and $r \to \infty$, so that the field configuration is localized and has finite classical energy. The topological charge

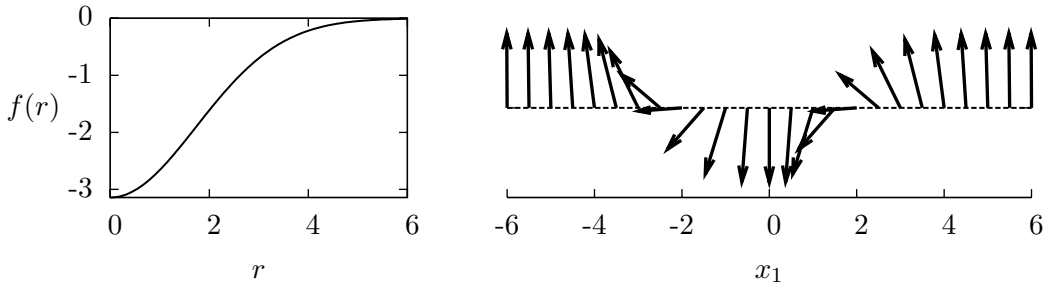

Figure 6.1.: *Left*: Radial soliton profile from Eq. (6.2) with size parameter $\lambda = 6$. *Right*: Plot of the resulting hedgehog field in Eq. (6.1) on the x_1 axis. The nonzero components ϕ_1 and ϕ_3 can be shown in a planar plot.

is calculated with Eq. (2.23),

$$B_{\text{top}} = -\frac{1}{2}[\cos f(\infty) - \cos f(0)] = \begin{cases} +1 & f(\infty) = \pi \quad f(0) = 0 \\ -1 & f(\infty) = 0 \quad f(0) = \pi \end{cases}.$$

One might expect configurations with wrapping number 2 to be characterized by $f(\infty) = 2\pi$. However, such a field can be deformed continuously into the vacuum. Instead, higher topological charges are obtained by replacing $\alpha \mapsto \alpha B_{\text{top}}$ in Eq. (6.1).

As a test case we want to choose a radial profile function with $B_{\text{top}} = -1$ depending on a size parameter λ. In units where the vacuum fermion mass $m = 1$, we write

$$f(r) = -\pi \mathrm{e}^{-r^2/\lambda}. \tag{6.2}$$

This profile and the resulting hedgehog field are illustrated in Fig. 6.1. When the size parameter λ is large compared to the vacuum fermion mass, we can approximate the baryon number and the total energy using the derivative expansion introduced in Section 2.5.

In order to apply the derivative expansion, we first have to split the squared Hamiltonian into a free and an interacting part. We expand around the constant field $\boldsymbol{\phi}^2 = m^2$ and set

$$\begin{aligned} H &= K + I, & K &= -\mathrm{i}\gamma^0\gamma^k\partial_k, & I &= \gamma^0\boldsymbol{\phi}\cdot\boldsymbol{\tau} \\ H^2 &= H_0^2 + V, & H_0^2 &= p^2 + m^2, & V(x) &= \mathrm{i}(\gamma^k\partial_k\boldsymbol{\phi})\cdot\boldsymbol{\tau}. \end{aligned} \tag{6.3}$$

Here, we already assumed that $\boldsymbol{\phi}$ is confined to the sphere of ground states $\boldsymbol{\phi}^2 = m^2$.

Total energy and baryon number are calculated by means of the resolvent in Eq. (2.27), written in the form

$$R(z) = \int \mathrm{d}^2x \ \mathrm{tr}\left[\gamma^0\gamma^k(r_K)_k + Ir_I + zr_z\right], \tag{6.4}$$

with contributions from the building blocks $\mathrm{Tr}\,(K + I + z)(GV)^nG$. The trace tr refers to spin and isospin indices. Up to order V^4 we get the results

$$\begin{aligned} (r_K)_k &= -\frac{\mathrm{i}}{3}\mathcal{G}_3(\partial_k V)V + \frac{\mathrm{i}}{4}\mathcal{G}_4\left[2(\partial_k V)V^2 + V(\partial_k V)V\right] \\ r_I &= \mathcal{G}_1 - \mathcal{G}_2 V + \mathcal{G}_3 V^2 + \frac{1}{2}\mathcal{G}_4\left[(\Delta V)V + V(\Delta V) + (\partial_l V)(\partial_l V)\right] - \mathcal{G}_4 V^3 + \mathcal{G}_5 V^4 \\ r_z &= \mathcal{G}_1 - \mathcal{G}_2 V + \mathcal{G}_3 V^2 + \frac{1}{2}\mathcal{G}_4(\Delta V)V - \mathcal{G}_4 V^3 + \mathcal{G}_5 V^4, \end{aligned} \tag{6.5}$$

with the integrals of propagators

$$\mathcal{G}_n = \int \frac{\mathrm{d}^2 p}{(2\pi)^2} G^n. \tag{6.6}$$

Each V and each extra derivative is counted as an additional order in the expansion. The traces in spin and isospin space in Eq. (6.4) are given in Appendix G.

The baryon number is calculated using Eq. (2.24). In second order of the derivative expansion, the baryon number is equal to the topological charge (2.23). The fourth order terms can be written as a total derivative and therefore do not contribute to the baryon number. This result was also obtained in Ref. [31] for a 2+1 dimensional nonlinear σ model. Note that in NJL_3 the restriction $\boldsymbol{\phi}^2 = m^2$ is a variational ansatz for the mean field motivated by the chiral spiral solution in 1+1 dimensions, whereas in the model in [31], this constraint is fixed for the σ model background.

The total energy is calculated from Eq. (2.25), where the zeroth and first order terms in r_z lead superficially to divergences. For the hedgehog potential, the first order term vanishes due to the trace in spin and isospin space, leaving as only divergence the zeroth order term, i.e., the vacuum. Therefore the mass of the hedgehog configuration is a finite quantity. Note that the double counting correction term of the hedgehog configuration (2.10) is equal to the vacuum double counting correction due to $\boldsymbol{\phi}^2 = m^2$.

The mass of the hedgehog configuration becomes

$$M_\mathrm{B} = \int \mathrm{d}^2 x \left[\frac{(\nabla\boldsymbol{\phi})^2}{8\pi m} - \frac{(\Delta\boldsymbol{\phi})^2}{96\pi m^3} + \frac{\left[(\nabla\boldsymbol{\phi})^4 + 4(\partial_1\boldsymbol{\phi}\times\partial_2\boldsymbol{\phi})^2\right]}{128\pi m^5} + \mathcal{O}(\partial^6\boldsymbol{\phi}) \right]. \tag{6.7}$$

The above result is the 2+1 dimensional analog of the total energy in NJL_2 calculated in Section 4.1. Just like in 1+1 dimensions it leads to a description of baryons reminiscent of the Skyrme model. The chiral soliton in Eq. (6.1) is akin to the "baby Skyrmion" introduced in Ref. [56]. Moreover, taking the chiral limit ($m_\pi = 0$) in the NJL_2 model, we see that the leading order term in Eq. (6.7) $(\nabla\boldsymbol{\phi})^2$ corresponds to the term $(\chi')^2$ in Eq. (4.6). In this order, the energy is minimized by the "chiral spiral" characterized by the chiral field $\chi = \mu x$. The single baryon configuration $\mu = \pi/L$ becomes massless, as the mean field winds slowly around the circle of degenerate ground states. The situation is different in 2+1 dimensions, where the chiral soliton (6.1) acquires a finite mass. This can be explained by the scale invariance of the leading order term $(\nabla\boldsymbol{\phi})^2$, which gives a finite contribution to the total energy, independent of the size of the soliton. The optimal shape of the soliton is found by minimization of the scale invariant term. We insert Eq. (6.1), leading to

$$\int \mathrm{d}^2 x \, \frac{(\nabla\boldsymbol{\phi})^2}{8\pi m} = \frac{m}{4} \int \mathrm{d}r \left[\frac{\sin^2 f}{r} + (f')^2 r \right].$$

The minimum condition

$$r\, f'' + f' = \frac{\cos f \sin f}{r}$$

is solved by the radial profile function

$$f = \pm 2 \arctan \frac{r}{\lambda} + n\pi, \qquad n \in \mathbb{Z}, \tag{6.8}$$

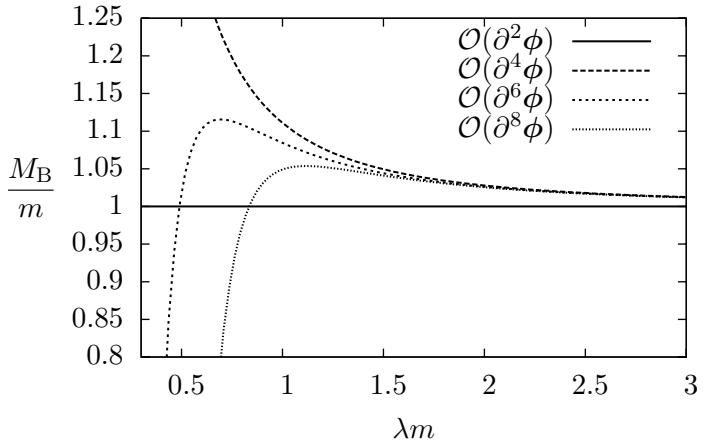

Figure 6.2.: Baryon mass in Eq. (6.9) vs. size parameter λ of the radial profile (6.8) in different orders of the derivative expansion.

with the scale parameter λ. The solution leads to the topological baryon number $(-1)^n$ and to the total energy

$$M_\mathrm{B} = m + \frac{1}{9m\lambda^2} - \frac{2}{75m^3\lambda^4} - \frac{26}{735m^5\lambda^6} + \mathcal{O}(\lambda^{-8}). \tag{6.9}$$

The terms $\sim \lambda^{-4}$ and $\sim \lambda^{-6}$ have been calculated by extending the result in Eq. (6.7) to higher orders using computer algebra. Note that these extra terms can only be evaluated for radial profiles where surface terms in the basic procedure for the derivative expansion (2.29) vanish.

For an infinitely wide soliton ($\lambda \to \infty$) the contributions of higher derivative terms in Eq. (6.9) vanish. In this limit, the leading order of the derivative expansion yields the exact result $M_\mathrm{B} = m$. This equals the mass of the translationally invariant HF solution $\boldsymbol{\phi}^2 = m^2$, where a single valence state (zero momentum) in the positive energy spectrum is filled completely. It is easy to show that this result can be taken over to configurations with winding numbers $B_\mathrm{top} > 1$, characterized by the radial profile

$$f = \pm 2 \arctan\left(\frac{r}{\lambda}\right)^{B_\mathrm{top}} + n\pi, \qquad n \in \mathbb{Z},$$

and lead to the baryon mass $M_\mathrm{B} = mB_\mathrm{top}$.

From the above calculation we conclude that in NJL_3 there exist baryons in the form of chiral solitons with zero binding energy. Clearly, we cannot rule out the existence of a bound state outside the range of validity of the derivative expansion. In Fig. 6.2 we plot the baryon mass versus the scale parameter in different orders of the derivative expansion. The derivative expansion seems to be valid for $\lambda \gtrapprox 1.5$, where higher orders do not change the result significantly. For small solitons the total energy in Eq. (6.9) gets dominated by these contributions and eventually becomes negative. If the derivative expansion was to be trusted in this regime, we would have to interpret this result as a vacuum instability. This problem also arises in the derivative expansion of the effective action of a non-linear sigma model in 3+1 dimensions, see Ref. [57]. The authors suggest a numerical calculation to determine if the skyrmion is stable. In the following section, we will present such a calculation for the NJL_3 model. It

shows no sign of the instability observed in the derivative expansion result, i.e., the energy of small sized solitons is above the vacuum fermion mass.

6.2. Numerical search for stable baryons

The derivative expansion of the total energy cannot answer the question of stability of small-sized topological solitons. In this section the single particle Hamiltonian

$$H = -\mathrm{i}\gamma^0\gamma^k\partial_k + m\gamma^0\boldsymbol{\phi}\cdot\boldsymbol{\tau}$$

is diagonalized numerically to calculate the mass of such configurations. The result has to be compared with the mass of a translationally invariant HF solution with the same baryon number. Since the spectrum with constant mean field is that of free massive fermions, this mass is equal to m. For the numerical calculation we will work in units where $m = 1$.

In principle, our procedure can be applied to the GN_3 model as well. However, in this model it is not possible to renormalize the total energy by subtracting the vacuum energy like it can be done in NJL_3 for configurations with $\boldsymbol{\phi}^2 = 1$. There will always remain a divergence $\sim (\phi_3^2 - m^2)\,\Lambda$ in the difference, so that it is numerically difficult to extract the finite part. We therefore restrict our calculation to the model with continuous chiral symmetry.

The soliton mass is calculated with an accuracy limited by the number of basis states. These are obtained by confining the theory to a disc of finite radius, analogous to the numerical procedure in 1+1 dimensions [7, 47]. Within this limited precision we found no bound state for small sized soliton configurations. We used various shapes of the radial profile function. In the following subsections we will present the details of our numerical methods and its results.

6.2.1. Basis and matrix elements

First we derive a set of suitable basis states for the diagonalization. In the discussion of chiral solitons in the 3+1 dimensional NJL model [58, 59], the basis states are defined as eigenstates of parity and total angular momentum. We would like to proceed in a similar manner.

The parity transformation P defined in Eq. (A.11) of the discussion of fermions in 2+1 dimensions in Appendix A commutes with the Hamiltonian H for the hedgehog potential in Eq. (6.1). Therefore for each eigenspinor of H the parity transformed spinor is an eigenvector of H as well, since

$$H\psi(x_1, x_2) = E\psi(x_1, x_2) \quad \Rightarrow \quad H\tau_1\gamma^1\psi(-x_1, x_2) = E\tau_1\gamma^1\psi(-x_1, x_2).$$

This will lead to a twofold degeneracy in the single particle spectrum.

Apart from parity symmetry, the Hamiltonian is symmetric under rotations. This leads to the invariance of the total angular momentum or grand spin operator [28], consisting of angular momentum, Dirac spin and isospin,

$$M_3 = -\mathrm{i}\partial_\alpha + \frac{\gamma^0}{2} + \frac{\tau_3}{2}.$$

Since H commutes with M_3 we will diagonalize the Hamiltonian in subspaces with grand spin n.

With the choice for the γ matrices

$$\gamma^0 = \sigma_3, \qquad \gamma^k = \mathrm{i}\sigma_k,$$

the eigenfunctions of M_3 are ($n = 0, \pm 1, \pm 2, \ldots$)

$$\psi_n = \mathrm{e}^{\mathrm{i}\alpha n} \begin{pmatrix} g_1(r)\mathrm{e}^{-\mathrm{i}\alpha} \\ g_2(r) \\ g_3(r) \\ g_4(r)\mathrm{e}^{+\mathrm{i}\alpha} \end{pmatrix} \qquad \begin{matrix} \tau = 1 & \gamma = 1 \\ \tau = 1 & \gamma = 2 \\ \tau = 2 & \gamma = 1 \\ \tau = 2 & \gamma = 2 \end{matrix} \quad .$$

The Dirac and isospin indices of the four-dimensional representation are indicated on the right. Unlike in 3+1 dimensions, these single particle states have no definite parity since with the definition of parity (A.11), P does not commute with M_3.

The eigenstates of H are now labeled by their grand spin n. The radial Hartree-Dirac equations are obtained by applying H to ψ_n, leading to

$$\begin{aligned} Eg_1 &= \frac{n}{r} g_2 + \partial_r g_2 + \phi_3 g_1 + F g_3 \\ Eg_2 &= \frac{n-1}{r} g_1 - \partial_r g_1 - \phi_3 g_2 - F g_4 \\ Eg_3 &= \frac{n+1}{r} g_4 + \partial_r g_4 - \phi_3 g_3 + F g_1 \\ Eg_4 &= \frac{n}{r} g_3 - \partial_r g_3 + \phi_3 g_4 - F g_2, \end{aligned} \tag{6.10}$$

where $F(r)$ is the related to the radial profile of the hedgehog field, cp. (6.1)

$$F(r) \equiv \sin f(r), \quad \phi_3(r) = \cos f(r).$$

The upper two equations in Eq. (6.10) with $F = 0$ yield the equations for the GN_3 model with the HF Hamiltonian in Eq. (5.1).

As basis states for the numerical diagonalization, we take the solution of the vacuum equations with $\phi_3 = 1$ (in units of the vacuum fermion mass m) and $F(r) = 0$. This is just the Dirac equation with mass ϕ_3. After that we will impose a boundary condition on a circle $r = R$ to obtain a discrete spectrum. Including states up to a momentum cutoff $\bar{k}$ leads to a finite number of basis states. In the following, the procedure leading to the basis states is outlined, details are given in Appendix H.

The vacuum equations lead to Bessel differential equations. Hence, the vacuum eigenstates involve Bessel functions $J_n(kr)$ with momentum k, related to the energy by $E^2 = k^2 + m^2$. These states are discretized by the boundary condition $J_n(k_{n,j}R) = 0$ on a circle with radius R. The index $j = 1, 2, \ldots$ is related to the jth zero of the nth Bessel function by $k_{n,j} = \alpha_{n,j}/R$. The zeros of the Bessel functions show the symmetry $\alpha_{-n,j} = \alpha_{n,j}$ because $J_{-n}(\alpha_{n,j}) = (-1)^n J_n(\alpha_{n,j}) = 0$. Therefore the states with the corresponding discrete momenta are degenerate $E_{-n,j} = E_{n,j}$. The dependence of the discretized momenta on the quantum numbers n and j is illustrated in Fig. 6.3, where $k_{n,j}$ is plotted depending on j for several values of the total angular momentum n. Note that in order to consider all states

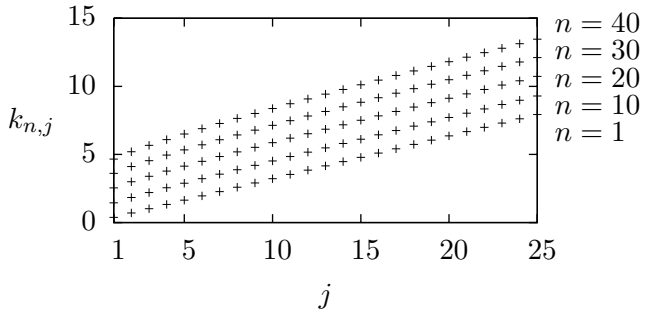

Figure 6.3.: Discrete momenta $k_{n,j}$ of the eigenstates of the Dirac Hamiltonian with boundary conditions on a disc with radius $R = 10$ for values of the total angular momentum $n = 1, 10, 20, 30, 40$.

below a relatively low momentum cutoff (~ 5 in units of m), states with large grand spin n (~ 40) have to be taken into account.

The set of commuting operators $H[\boldsymbol{\phi} = (0, 0, 1)]$, M_3 is completed by the isospin $\tau_3/2$. States with isospin $\pm 1/2$ are labeled by $s = \pm 1$. The normalized basis states are then characterized by the grand spin $n = 0, \pm 1, \pm 2, \ldots$, the momentum quantum number $j = 1, 2, \ldots$, the sign of the energy eigenvalue $\eta = \pm 1$ and the isospin $s = \pm 1$, writing

$$\psi_{n,j,\eta,1} = \mathrm{e}^{\mathrm{i}n\alpha} \begin{pmatrix} C_1 \frac{k_{n,j}}{\eta E - 1} J_{n-1}(k_{n,j} r) \mathrm{e}^{-\mathrm{i}\alpha} \\ C_1 J_n(k_{n,j} r) \\ 0 \\ 0 \end{pmatrix} \quad \psi_{n,j,\eta,-1} = \mathrm{e}^{\mathrm{i}n\alpha} \begin{pmatrix} 0 \\ 0 \\ C_{-1} \frac{k_{n,j}}{\eta E + 1} J_n(k_{n,j} r) \\ C_{-1} J_{n+1}(k_{n,j} r) \mathrm{e}^{+\mathrm{i}\alpha} \end{pmatrix}, \quad (6.11)$$

with $E = \sqrt{k_{n,j}^2 + 1}$ and energy ηE. The normalization constants C_s are fixed by the constraint $\|\psi_{n,j,k,s}\|^2 = 1$, which leads to

$$C_s(n, j, \eta) = \frac{1}{R J_{n+1}(\alpha_{n,j})} \sqrt{\frac{E - \eta s}{2\pi E}}. \quad (6.12)$$

For the numerical calculation we choose states with momentum $k_{n,j} < \bar{k}$.

We now calculate the matrix elements. The interaction term reads

$$\gamma^0 \boldsymbol{\phi} \cdot \boldsymbol{\tau} = \begin{pmatrix} \phi_3 & 0 & F\mathrm{e}^{-\mathrm{i}\alpha} & 0 \\ 0 & -\phi_3 & 0 & -F\mathrm{e}^{-\mathrm{i}\alpha} \\ F\mathrm{e}^{\mathrm{i}\alpha} & 0 & -\phi_3 & 0 \\ 0 & -F\mathrm{e}^{\mathrm{i}\alpha} & 0 & \phi_3 \end{pmatrix}.$$

With the abbreviations

$$\begin{array}{llll} C = C_s(n, j, \eta) & C' = C_{s'}(n, j', \eta') & k = \alpha_{n,j}/R & k' = \alpha_{n,j'}/R \\ J_n = J_n(\alpha_{n,j} r/R) & J'_n = J_n(\alpha_{n,j'} r/R) & E = \sqrt{k^2 + 1} & E' = \sqrt{k'^2 + 1}, \end{array}$$

the matrix elements for fixed n are

$$\begin{aligned}\langle j', \eta', s'|\gamma^0 \boldsymbol{\phi}\cdot\boldsymbol{\tau}|j,\eta,s\rangle = 2\pi CC' \int_0^R \mathrm{d}r\, r \Bigg[\frac{k'}{\eta' E' - s'} \frac{k}{\eta E - s} J'_{n-\delta_{s',1}} J_{n-\delta_{s,1}} \\ - J'_{n+\delta_{s',-1}} J_{n+\delta_{s,-1}} \Bigg] \left[(s\phi_3 - F)\delta_{s,s'} + F\right].\end{aligned} \tag{6.13}$$

Since the interaction preserves the grand spin M_3, it does not mix states with different n. The matrix element of the full Hamiltonian with fixed n now is given by

$$\langle j', \eta', s'|H(n)|j,\eta,s\rangle = \delta_{j,j'}\delta_{\eta,\eta'}\delta_{s,s'}\eta E + \langle j', \eta', s'|\gamma^0 \tilde{\boldsymbol{\phi}}\cdot\boldsymbol{\tau}|j,\eta,s\rangle, \tag{6.14}$$

with $\tilde{\phi}_3 = \phi_3 - 1$, because the vacuum term is absorbed into the free massive Hamiltonian. For the numerical diagonalization of H these matrix elements are calculated using numerical integration in Eq. (6.13). Since the integrand involves Bessel functions, this will be the most time-consuming step of the calculation.

The Hamiltonian is symmetric under parity transformations $H = PHP$, leading to a twofold degeneracy in the spectrum. This can be seen by applying a parity transformation on the basis states (6.11). We get

$$P\psi_{n,j,k,s} = \mathrm{i}(-1)^n \eta \psi_{-n,j,k,-s}.$$

Hence submatrices with opposite grand spin $M_3 = \pm n$ are related by

$$\langle j', \eta', s'|H(-n)|j,\eta,s\rangle = \eta\eta' \langle j', \eta', -s'|H(n)|j,\eta,-s\rangle.$$

Since P is a one-to-one mapping of basis states with grand spin n to states with $-n$, the submatrices $H(n)$ and $H(-n)$ have the same eigenvalues.

6.2.2. Calculation of baryon number and mass

As described in Section 2.4, the baryon number of the topological soliton is determined by the asymmetry in the spectrum (2.20). In the numerical approach, this asymmetry can be read off by counting the number of positive and negative eigenvalues. According to Section 6.1, for slowly varying soliton configurations the resulting spectral asymmetry B should be equal to the topological charge B_{top} in Eq. (2.23).

The spectral asymmetry is illustrated in Fig. 6.4. The states with opposite isospin which are degenerate in the vacuum split up. The energy of one state with grand spin $n = 0$ can change sign due to the hedgehog mean field.

Each field configuration $\boldsymbol{\phi}$ has a counterpart with opposite spectral asymmetry. Since the expression for the topological charge (2.23) changes the sign when $-\boldsymbol{\phi}$ is inserted, this inverted field should lead to the inverted spectral asymmetry. In fact, this can be shown directly, since the transformation inverts the spectrum by

$$H(\boldsymbol{\phi})\psi = E\psi \qquad \Rightarrow \qquad H(-\boldsymbol{\phi})\gamma^0\psi = -E\gamma^0\psi.$$

This is related to the charge conjugation symmetry described in Appendix A. We can use the transformation behavior of the bilinears in Table A.1 to show that for every self-consistent

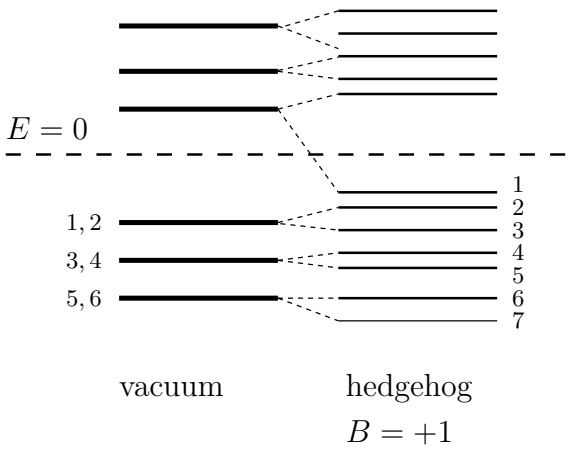

Figure 6.4.: Illustration of the spectrum of the vacuum and the hedgehog Hamiltonian. For mean field configurations with finite topological charge, one eigenstate with grand spin $n = 0$ can change sign. This is the spectral asymmetry which induces a finite fermion number. The numbers at the negative energy levels indicate the eigenvalue numbering in Eq. (6.16).

solution, there exists a self-consistent solution with scalar condensates $-\boldsymbol{\phi}$, charge conjugated spinors, and inverted single particle spectrum, i.e.,

$$\begin{aligned} H(\boldsymbol{\phi})\psi = E\psi \qquad & \phi_a = -g^2\langle\bar{\psi}\tau_a\psi\rangle \\ \Rightarrow H(-\boldsymbol{\phi})\psi_C = -E\psi_C \qquad & \phi_a = -g^2\langle\bar{\psi_C}\tau_a\psi_C\rangle. \end{aligned}$$

Hence a configuration $\boldsymbol{\phi}$ with $B = 1$ will be referred to as a baryon, the mean field $-\boldsymbol{\phi}$ with $B = -1$ as the corresponding antibaryon.

The sum over energy eigenvalues with a hedgehog configuration $\boldsymbol{\phi}^2 = 1$ has the same divergent part as the vacuum. Hence the mass of such fields can be calculated by subtracting the sum over vacuum energies, leading to a finite result without the need to go through the renormalization procedure in Section 2.3. In our numerical procedure, the difference of the two spectra is approximated by the sum over differences of the discrete energy eigenvalues. The matrix in Eq. (6.14) is diagonalized using basis states up to the cutoff momentum $\bar{k}$. The mass becomes

$$M_\mathrm{B} = E(\boldsymbol{\phi}) - E(m) \approx \sum_{\substack{l, E_l<0 \\ k_l<\bar{k}}} (E_l - E_l^0). \tag{6.15}$$

For large cutoff momenta $\bar{k}$ and large sizes of the disc R, this should approach the continuum result for the mass.

Due to the spectral asymmetry, one has to be careful to include the right eigenvalues in the sum in Eq. (6.15). We used the numbering scheme shown in Fig. 6.4. After sorting the negative eigenvalues of both the hedgehog and the vacuum spectrum with increasing absolute value, the baryon mass is calculated by

$$M_\mathrm{B} = \begin{cases} \sum_{l=1}^{l_\mathrm{max}} (E_l - E_{l+1}^0) - E_1^0 & \text{for } B = -1 \\ \sum_{l=1}^{l_\mathrm{max}} (E_l - E_l^0) & \text{for } B = 0 \\ \sum_{l=1}^{l_\mathrm{max}} (E_{l+1} - E_l^0) + E_1 & \text{for } B = 1, \end{cases} \tag{6.16}$$

which replaces Eq. (6.15).

Due to the trace in isospin and Dirac space, the trace of the Hamiltonian vanishes in the continuum. When $\bar{k}$ and R are large enough, this should be also true for the discretized spectrum, i.e., the sum over positive and negative energies of the hedgehog spectrum should vanish. One important consequence of this fact is that the baryon has the same mass as the antibaryon with inverted mean field $\boldsymbol{\phi} \to -\boldsymbol{\phi}$. The difference of the two masses is the difference of the two spectra. Since charge conjugation inverts the spectrum of the Hamiltonian, this difference vanishes.

As the Hamiltonian commutes with the grand spin operator, it is possible to calculate the contribution to the baryon mass for each submatrix with grand spin n. This also ensures that energies with the same grand spin are compared to the vacuum, when truncating the spectrum with a momentum cutoff.

6.2.3. Perturbation theory

In order to save computing power, we want to approximate high energy eigenvalues using perturbation theory. The interaction term $\gamma^0 \tilde{\boldsymbol{\phi}} \cdot \boldsymbol{\tau}$ in Eq. (6.14) is taken as the small perturbation. Unfortunately, in first order this method is not applicable when summing over the difference to the vacuum spectrum in Eq. (6.16) because the perturbation of the eigenvalues falls off too slowly in the range of momenta we used in our calculation. Second order perturbation theory involves the calculation of all matrix elements. Since the most time-consuming step of the calculation are the numerical integrals in matrix elements, there is no significant benefit compared to exact diagonalization.

We apply first order degenerate perturbation theory and diagonalize the interaction term in the four-dimensional eigenspaces. Since the perturbation is diagonal in the angular momentum basis, we only need to find the eigenvalues of a 2×2 matrix. The energy level n, j, η then splits up with the first order perturbation

$$E^{(1)} = \frac{1}{2}\left(V_{++} + V_{--} \pm \sqrt{(V_{++} - V_{--})^2 + 4V_{+-}^2}\right), \qquad V_{s's} = \langle j, \eta, s | \gamma^0 \tilde{\boldsymbol{\phi}} \cdot \boldsymbol{\tau} | j, \eta, s' \rangle.$$

An analysis of the asymptotics of the matrix elements $V_{s's}$ using Eq. (6.13) shows that the absolute value of $E^{(1)}$ vanishes with $|E^{(1)}| \sim 1/k \sim 1/\sqrt{l}$ where k is the momentum and l the eigenvalue counter when sorting the eigenvalues in ascending order. This means that when we use the perturbations $E^{(1)}$ to calculate the baryon mass, the sum in Eq. (6.15) will not be absolutely convergent. In order to show that the sum diverges we have to evaluate the perturbations explicitly. We do this by analyzing the UV behavior of $E^{(1)}$ for the radial profile in Eq. (6.2). For high momenta the eigenvalue differences $\Delta E_l = E_l^{(1)}$ in the submatrix with grand spin $n = 0$ form an alternating series due to the splitting of isospin states illustrated in Fig. 6.4. We can add up consecutive pairs of values to yield a series with definite sign. The absolute value of the result is plotted in Fig. 6.5 with logarithmic scales. In the momentum range we can reach in our calculation, this vanishes like $\sim 1/l$ for perturbation theory and $\sim 1/l^2$ for the numerical result. Hence, the sum over the perturbation diverges and we have to conclude that in our numerical scheme first order perturbation theory is not applicable to the calculation of the baryon mass.

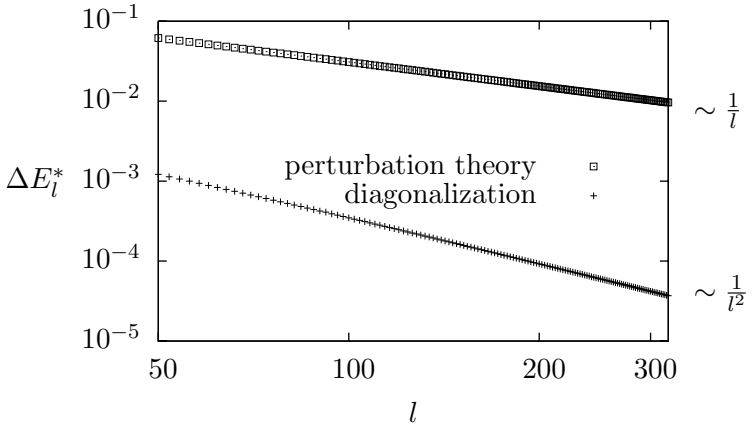

Figure 6.5.: The sum over 2 consecutive eigenvalue differences: $\Delta E_l^* = \Delta E_{2l} + \Delta E_{2l+1}$. *Upper points*: perturbation theory $\sim 1/l$. *Lower points*: Numerical diagonalization $\sim 1/l^2$. The profile Eq. (6.2) was used with $\lambda = 2$, $R = 10$ and $\bar{k} = 60$. The first 50 eigenvalues are omitted to show the UV behavior of the calculation.

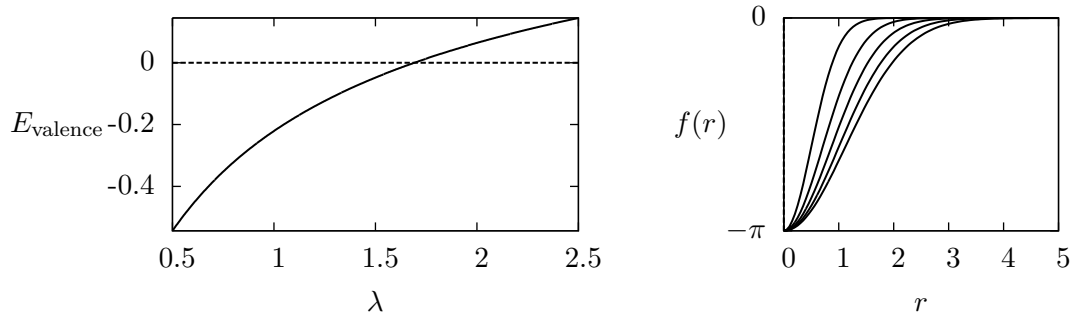

Figure 6.6.: *Left:* Energy of the valence state for different values of the size parameter λ ($R = 5$). At $\lambda < 1.69$ the valence state becomes negative and the spectral asymmetry vanishes. *Right:* Radial profile with $\lambda = 0.5, 1.0, 1.5, 2.0, 2.5$. ($\bar{k} = 14$)

6.2.4. Size-dependence of spectral asymmetry

From the derivative expansion calculation in Section 6.1, we know that for large sized solitons the spectral asymmetry is determined by the topological charge $B = B_{\text{top}}$. This can now be checked in the numerical calculation. We determine the spectral asymmetry for the radial profile in Eq. (6.2) and vary the size parameter λ. The result for the valence state is shown in Fig. 6.6. It turns out that the spectral asymmetry vanishes when the size of the soliton is decreased below $\lambda = 1.69$. This confirms that the derivative expansion is not valid for small sized solitons. A similar behavior of the valence state was found in the discussion of a non-linear σ model [28].

The spectral flow has an important consequence for the calculation of the hedgehog mass. For small-sized solitons the baryon number will no longer be fixed by its topological charge. In order to check if such a configuration describes a bound state of fermions, one has to include the positive valence state in the sum over single particle energies.

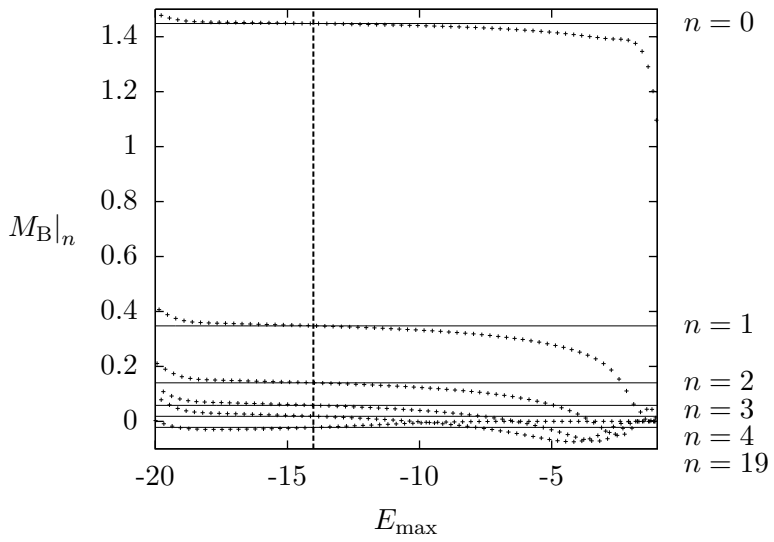

Figure 6.7.: Sum over eigenvalue differences for submatrices with grand spin $n = 0, 1, 2, 3, 4, 19$ from top to bottom (radial profile (6.2), $\lambda = 2$, $R = 20$, $\bar{k} = 20$). The vertical line shows the cutoff in energy $E_{\max} = -0.7\sqrt{\bar{k}^2 + m^2}$, used to calculate the mass contribution of each spin (indicated by the horizontal lines).

6.2.5. Effects of finite size and momentum cutoff

In this section, we discuss the effects of the choice of the finite basis we used for numerical diagonalization. Since we want to compare the numerical result for the baryon mass with continuum values, the value of M_B should not change when disc size R and momentum cutoff $\bar{k}$ are increased.

We first observe that the finite cutoff $\bar{k}$ in momentum space leads to an error in the high-momentum eigenvalues, because the mixing with the nearby states above the cutoff is ignored by the calculation. This should not affect the baryon mass, when we cut off the sum in Eq. (6.16) at energies $E_l > E_{\max} > -\bar{k}$. In Fig. 6.7 the result for the contributions to the baryon mass from different grand spin n submatrices $M_B|_n$ is plotted versus the maximum energy $E_{\max}$ considered in the sum. Again, we used the test case profile (6.2). $M_B|_n$ approaches a stable value as the maximum energy is increased. The momentum cutoff error can be observed as a slight increase of $M_B|_n$ at high momenta. This error can be avoided safely by cutting off the sum over energy differences with $E_{\max} = -0.7\sqrt{\bar{k}^2 + m^2}$.

The mass contribution of each grand spin resulting from this calculation is plotted in Fig. 6.8. The values are compared with the result for the corresponding antibaryon configuration $\boldsymbol{\phi} \to -\boldsymbol{\phi}$ ($f \to f + \pi$). We observe that higher spin eigenvalues contribute small amounts to the total mass, but add up and change the contribution from lower spins $n = 0, \ldots, 5$ significantly (± 0.3). Therefore spins up to $n \approx 40$ have to be taken into account to get the value for the total mass $M_B(B = -1) = 1.458$ and $M_B(B = +1) = 1.448$. Since the mass of baryon and antibaryon would be equal in an exact continuum calculation (see Section 6.2.2) the difference between these values in our numerical calculation serves as a good measure for the accuracy of the result for M_B. However, this difference should not be confused with an error bar. The

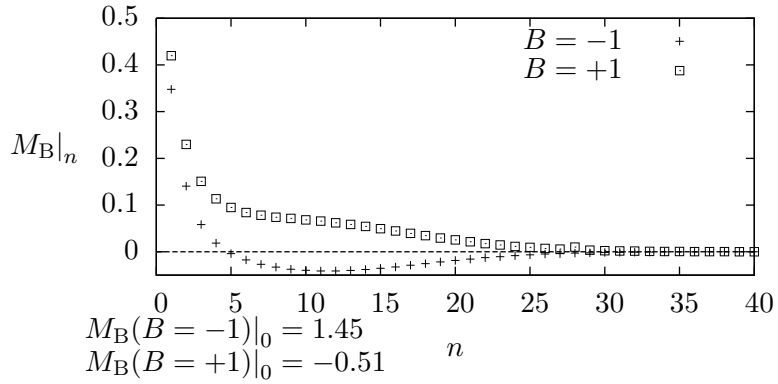

Figure 6.8.: Mass contribution of each grand spin for a hedgehog with radial profile (6.2) and its corresponding antibaryon. ($\lambda = 2$, $R = 20$, $\bar{k} = 20$).

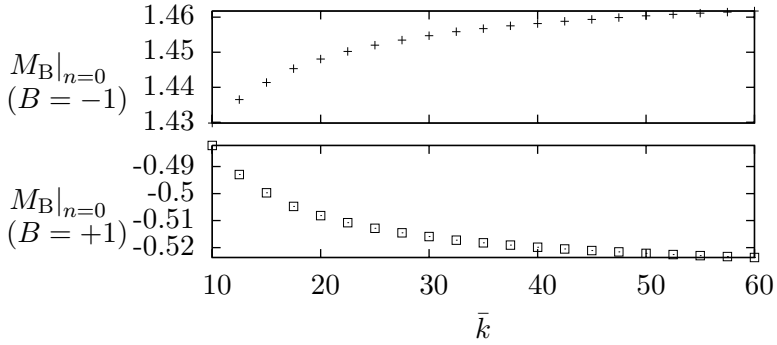

Figure 6.9.: Contribution to the baryon and to the antibaryon mass from the $n = 0$ submatrix, depending on the momentum cutoff $\bar{k}$. ($\lambda = 2$, $R = 20$, $E_\mathrm{max} = -0.7\sqrt{\bar{k}^2 + m^2}$)

main drawback of the diagonalization method is that the error made by the restriction to a finite number of basis states can only be observed by a change of the baryon mass result as R and $\bar{k}$ are increased.

Next, we analyze how the mass contribution of a single grand spin n changes as the momentum cutoff is increased. The behavior of the $n = 0$ mass contribution for cutoffs $\bar{k} = 10 \ldots 60$ is shown in Fig. 6.9, including the calculation for the $B = +1$ soliton. For given radius $R = 20$ the result approaches a stable value as $\bar{k}$ is increased. In Fig. 6.10, $M_\mathrm{B}|_{n=0}$ is plotted versus E_max, which illustrates how the accuracy is improved by increasing the momentum cutoff $\bar{k}$. The sudden increase of $M_\mathrm{B}|_{n=0}$ which occurs at $E_\mathrm{max} \approx \bar{k}$ stems from the momentum cutoff error.

The second requirement for the validity of the numerical result for the hedgehog mass is the stability against an increase of the disc size R. In Fig. 6.11 we plot M_B for our test case profile (6.2) using different values of R. The lower points show the mass of the corresponding antibaryon configuration. For large R, the two values approach the common value $M_\mathrm{B} = 1.45$. Above $R \gtrapprox 20$ the result does not change significantly so that M_B can be expected to approximate the continuum value.

The number of basis states grows quadratically with R and $\bar{k}$. The number of matrix elements

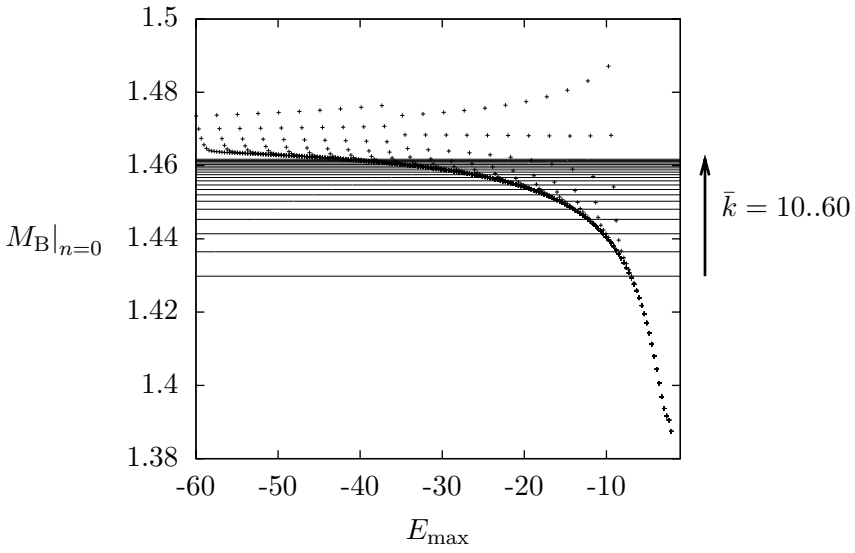

Figure 6.10.: The $n = 0$ contribution to the baryon mass versus the $E_{\max}$. Results for $\bar{k} = 10 \ldots 60$ (in steps of 2.5) are shown in a single plot. Horizontal lines indicate the mass contributions calculated with $E_{\max} = -0.7\sqrt{\bar{k}^2 + m^2}$. ($\lambda = 2$, $R = 20$)

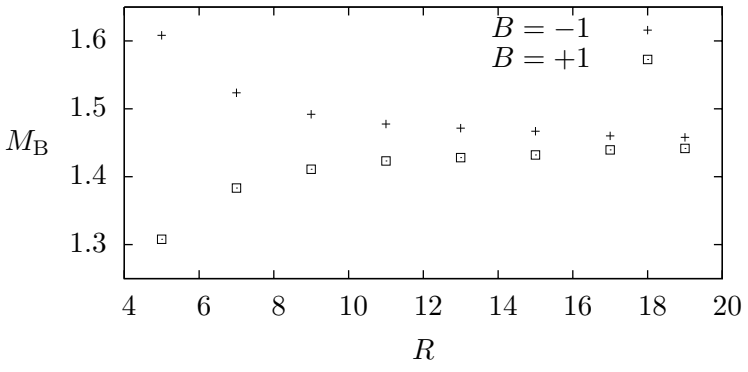

Figure 6.11.: Baryon mass M_B for the test case Eq. (6.2) compared to the corresponding antibaryon mass. ($\lambda = 2$, $\bar{k} = 20$, $E_{\max} = -0.7\sqrt{\bar{k}^2 + m^2}$)

to be calculated by numerical integration thus grows $\propto R^4\bar{k}^4$. This limits the accuracy which can be achieved by this numerical technique.

The convergence of the M_B for large numbers of basis states clearly depends on size and shape of the hedgehog field. If the radial profile f rapidly approaches an integer multiple of π, the limitation to a finite area $r < R$ will be a good approximation. Hence, for profiles with an exponential behavior like the test case in Eq. (6.2), we get the most accurate results for the baryon mass. However, for a soliton with very large spatial variations, we need to take into account higher momentum states by increasing $\bar{k}$. This sets a lower bound to the soliton size for which the baryon mass can be calculated.

6.2.6. Results for the baryon mass

We now turn to the results for the baryon mass, using different radial profile functions and sizes. First, we compare the numerical method to the derivative expansion in Section 6.1. We choose three different radial profiles with exponential behavior, depending on a size parameter λ. The derivative expansion in Eq. (6.7) can be applied if λ is chosen in a regime, where the second and fourth order term do not differ significantly. In Fig. 6.12, the derivative expansion and the numerical results are plotted versus λ. We included the mass of the corresponding antibaryon, which gives an impression of the accuracy of the numerics. The data points for two different choices of the parameter R show how the precision is increased by including a higher number of basis states. With an acceptable error, the numerics matches the derivative expansion result.

For small sized solitons, the derivative expansion leads to small hedgehog masses (see Fig. 6.2 in Section 6.1). Since the expansion does not converge in this regime, we cannot trust the result. With the numerical diagonalization procedure, we can now search for bound states with such rapidly varying mean fields. In Fig. 6.13, we show the baryon mass for small solitons with the radial profile (6.2). In order to obtain reliable results, we had to increase the momentum cutoff $\bar{k}$ whereas we could choose a smaller disc size R. The decrease of the baryon mass for small parameters λ predicted by the derivative expansion is not observed in our calculation. The figure shows the opposite behavior, i.e., small hedgehogs are not favored energetically.

In Section 6.1, it was shown that the radial profile in Eq. (6.8) minimizes the second order derivative expansion result for the total energy. The baryon mass was calculated in orders of the inverse of the size parameter λ (see Eq. (6.9)). Since this minimum profile leads to a potential which does not decrease exponentially for large r, we cannot numerically calculate the associated mass for values of λ where we could compare the result to Eq. (6.9). Instead we choose a very small size for the minimal soliton, so that it fits into the disc of a radius R for which the numerical procedure can be applied. In Fig. 6.14 we plot the results of our calculation. Like for the exponentially decaying potential, we observe an increase in energy with decreasing soliton size. In contrast, the derivative expansion calculation predicts values well below $M_\mathrm{B} = m$ (see Fig. 6.2).

The numerical calculation presented in this section confirms that the derivative expansion breaks down for small sized solitons. We used several ansätze for the radial profile function and found an increase of the mass for smaller solitons. For slowly varying potentials, the derivative expansion agrees with the numerical calculation, whereas the decrease of the total energy

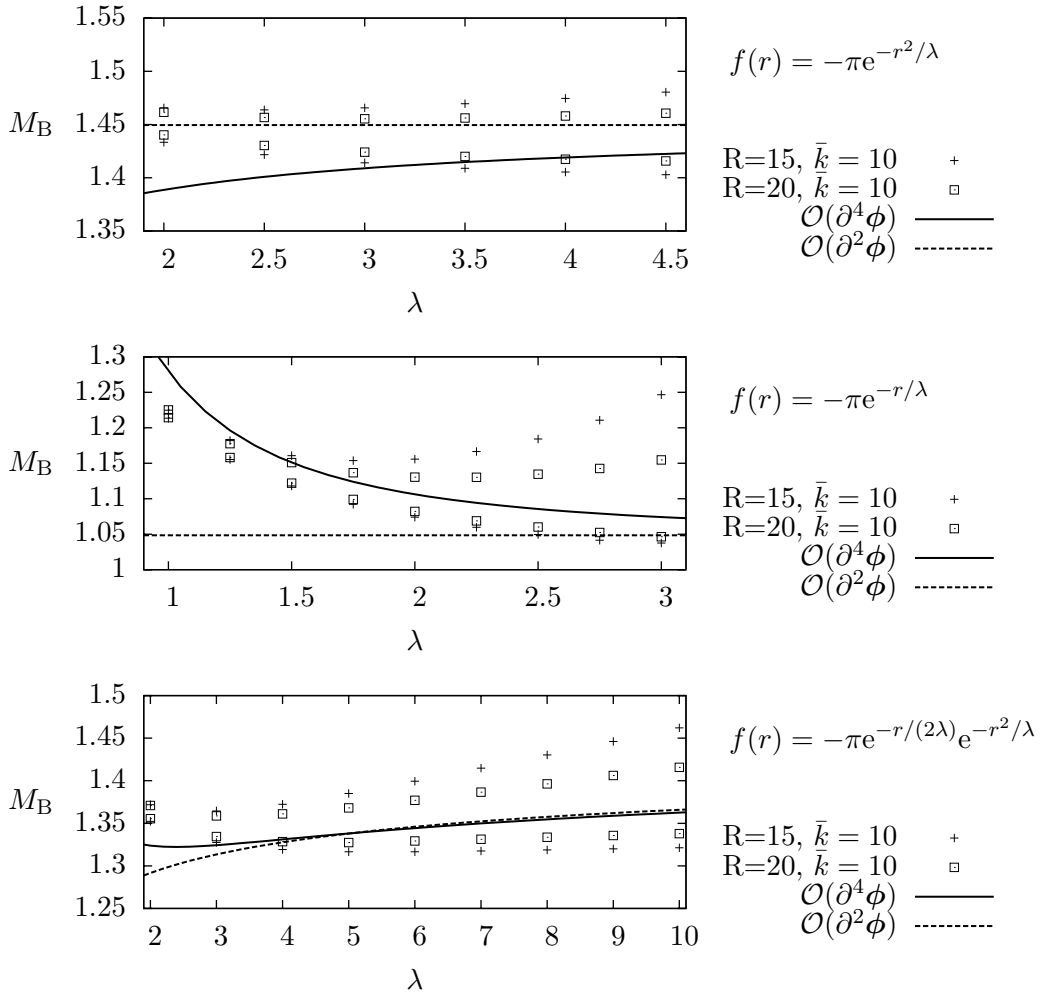

Figure 6.12.: Numerical result for the baryon mass compared to the derivative expansion in Eq. (6.7). Due to the discretization of the basis, the mass for the soliton with $B = -1$ is larger than for $B = +1$.

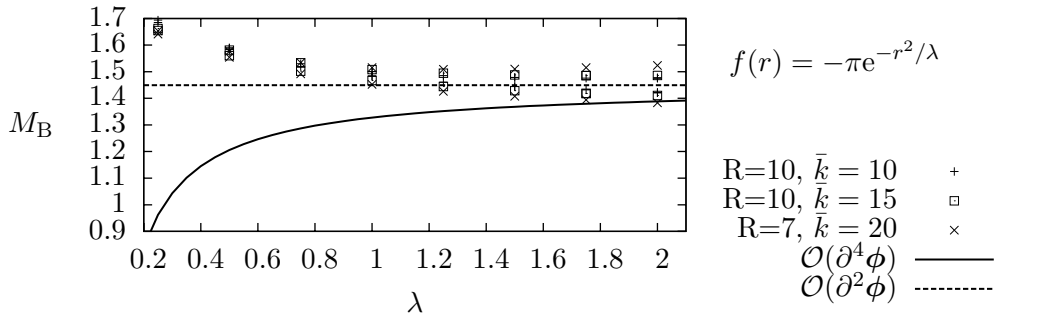

Figure 6.13.: Numerical result for the baryon mass for small sized soliton configurations. Note the change of parameters R and $\bar{k}$ as compared to Fig. 6.12.

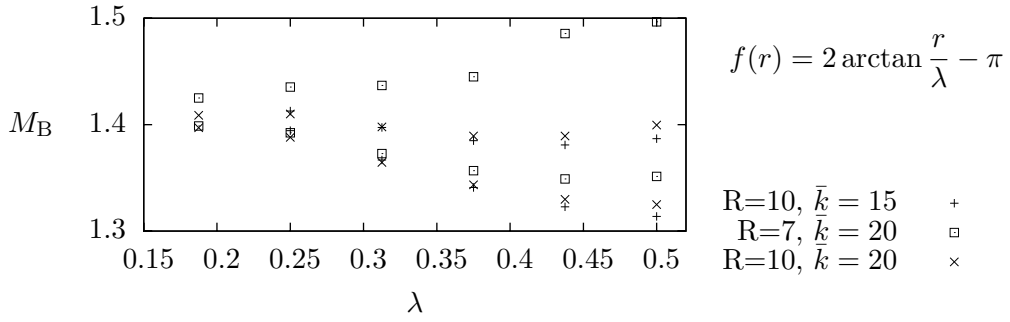

Figure 6.14.: Numerical result for the baryon mass for the profile in Eq. (6.8).

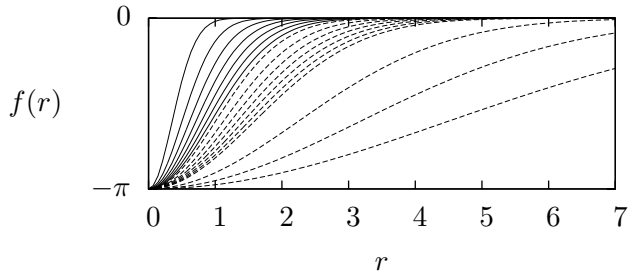

Figure 6.15.: Radial profile (6.2) for different values of λ. *Solid lines:* Mass calculation accessible to the numerical calculation. *Dashed lines:* Derivative expansion applicable.

below the vacuum fermion mass observed in the derivative expansion result is apparently due to the limits of this approximation. In addition, we tested several other trial functions for the radial profile and found no configuration that was favored against the translationally invariant HF solution. We also observed an increase of the total energy for configurations involving large gradients.

Within the limitations given by the numerical procedure, we can rule out the existence of a soliton bound state of small sizes not accessible to the derivative expansion. The range of sizes where we can calculate the soliton mass is illustrated in Fig. 6.15 for the specific radial profile in Eq. (6.2). For size parameters $\lambda \gtrapprox 2$ we can use the derivative expansion result, for solitons down to size $\lambda = 0.2$ we apply numerical diagonalization to get the total energy with acceptable error. Since the total energy is increasing as we tune down λ (cf. Fig. 6.13), we do not expect a bound state for even smaller fields.

Summarizing, we have presented a numerical HF calculation of the baryon in the NJL_3 model. Due to computational limitations, our results should be taken as exploratory. In order to significantly improve the accuracy, one would either have to invest a factor of 100 more of computing power, or perhaps use other techniques. An alternative to diagonalization could be the numerical technique used in [60] to calculate the effective action of QCD in a rotationally symmetric instanton background. This method is based on the calculation of determinants of one-dimensional differential operators rather than numerical diagonalization and thus does not suffer from problems due to discretization of the one-particle basis.

7. Conclusions and Outlook

In this thesis we discussed baryons and baryonic matter in simple four-fermion interaction theories, the GN model and the NJL model in 1+1 and 2+1 space-time dimensions. The models are designed as toy models for dynamical symmetry breaking in strong interaction physics. For each model, we investigated the existence of baryons as localized bound states of fermions and, if possible, calculated their mass. In the 2+1 dimensional models we could not find stable baryonic solutions, whereas for the 1+1 dimensional models baryons exist and lead to breakdown of translational symmetry at finite density. The latter result was obtained including a bare mass of the fermions.

In order to find the ground state for given baryon number or baryon density, we used a mean field method which was formulated in the language of many particle physics and is equivalent to the Hartree-Fock approximation. The models in this work are defined in the 't Hooft limit $N \to \infty$, $Ng^2 = \text{const.}$, where the Hartree-Fock method becomes exact. In addition, the 't Hooft limit circumvents no-go theorems which rule out some cases of spontaneous symmetry breakdown in low dimensions. The basic task of the Hartree-Fock method was then to minimize the total energy as a functional of the mean field for a given baryon number or baryon density. The mean field served as an order parameter for chiral symmetry and, if spatially varying, for translational symmetry. In some special cases, the total energy could be calculated analytically by summing over energies of single particles in the presence of the mean field. When such a self-consistent solution could not be found, we applied the derivative expansion technique. This lead to a closed expression for the energy in terms of the mean field, valid for slowly varying fields.

For the GN model in 1+1 dimensions, we generalized earlier work on the massless model to the case where chiral symmetry is broken explicitly by a bare mass term in the Lagrangian. In the process of renormalization the bare mass m_0 was replaced by a physical constant γ, whereas the relation between the coupling constant and the cutoff merely set the scale of the theory. As a result the massive GN model can be considered as a one parameter family of physical theories, the point $\gamma = 0$ corresponding to the massless case. For $\gamma > 0$, we first had to find a self-consistent solution for the single baryon, which was found with the mean field of the partially filled baryon in the chiral limit. In order to describe baryonic matter, we used an ansatz from a related problem in condensed matter physics. The Hartree-Fock energies were found analytically because the eigenvalue problem could be reduced to a Lamé type equation. This lead to a self-consistent solution for dense baryonic matter, namely a crystal of equally spaced baryons.

Next, we discussed the 1+1 dimensional version of the NJL model with bare mass fermions. The parameter γ could be directly related to a quantity with a direct physical interpretation, the mass of the pion m_π. For small m_π earlier studies predicted a sine-Gordon theory, the two-dimensional analog of the Skyrme model where baryon number is generated through a topologically non-trivial pion field configuration. In this limit, the relevant length scale over

which the potential varies is given by $1/m_\pi$. Hence, we could use the derivative expansion to calculate the total energy in powers of derivatives of the mean field, leading to a systematic improvement of the sine-Gordon result. Minimizing the total energy, the mass of the single baryon was obtained as a power series in m_π. The expansion exhibits the convergence properties of an asymptotic series. In leading order of m_π, dense matter can be described by a periodic solution of the sine-Gordon equation. Our work improved this result in next to leading order using the derivative expansion.

In the 2+1 dimensional GN model, we could not find an exact solution for the single baryon, expected to be rotationally symmetric. Instead we performed an exploratory calculation, testing whether the finite density ground state breaks translational symmetry in one spatial direction. This approach was inspired by an earlier calculation which extended the single baryon solution of the 1+1 dimensional model by choosing the mean field to be translationally invariant in one direction. The result was shown to be self-consistent and energetically degenerate to the massive Fermi gas solution. We could derive the same result for a 2+1 dimensional extension of the one-dimensional baryon crystal. In this "stripe phase" fermions are restricted in one spatial dimension by the periodic crystal mean field, but are free to move in the other direction parallel to the stripes. The finite binding energy gained in one direction is cancelled by the extra energy needed to fill the momentum states in the other direction. With the "stripe phase" we have found a state which is degenerate with the translationally invariant solution up to the baryon density $m^2/4\pi$ where chiral symmetry is restored. We see this degeneracy as an argument in favor of the possibility of a spontaneous breakdown of translational symmetry at finite density.

With the usual trick to generalize chiral symmetry to odd space-time dimensions, one can define the 2+1 dimensional version of the NJL model. We applied the derivative expansion technique to calculate the total energy as a functional of the three component mean field and its derivatives. In analogy to the 1+1 dimensional case, this led to a description of baryons as chiral solitons reminiscent of the Skyrme model. The crucial difference to the 1+1 dimensional model is that the leading term of the expansion is independent of the scale of the soliton, resulting in a finite contribution to the baryon mass even for arbitrarily slowly varying mean fields. We identified the radial profile minimizing the energy and calculated a vanishing binding energy in the limit of an infinitely wide soliton. For small sized solitons, the derivative expansion predicted energies well below the vacuum fermion mass. As the approximation could not be trusted below a certain spatial scale, we applied a numerical technique to explore the possibility of a stable baryon in this regime. For given radial profile, we diagonalized the Hartree-Fock Hamiltonian in a discrete basis and summed over the spectrum to calculate the total mass. The results confirmed the breakdown of the derivative expansion for large gradients and showed an increase in total energy for smaller solitons. From this finding we concluded that the NJL model does not possess a stable soliton solution, at least in the range of spatial scale we could reach by numerical calculation and the derivative expansion.

Clearly, the four-fermion models discussed in this thesis cannot describe baryonic matter in the real world. The reasons are the unrealistic restrictions to low dimensions and the large N limit, which are needed to allow for an analytical treatment. Despite these drastic simplifications, the models lead to phenomena akin to findings in more realistic, higher-dimensional theories. The emergence of an inhomogeneous ground state at high densities observed in the 1+1 dimensional GN model is also discussed in QCD in form of a crystalline superconductor [9] or via the Overhauser effect [61]. Moreover, the description of baryons as

chiral solitons found in the low-dimensional NJL models is reminiscent of the Skyrme model of nuclear physics. The analytic derivation of these important phenomena in simple interacting quantum field theories gives insights into the mechanisms behind them.

Some of the methods which proved to be useful for the solution of four-fermion toy models at finite density can now be applied to more general problems. For instance, the mean field method can also be used at finite temperature. Like in QCD, one could ask questions about the phase diagram at temperature T and chemical potential μ. In the Hartree-Fock approach this means that we have to minimize the grand canonical potential for each value of T, μ as a functional of the mean field. In the case of the massive GN model in 1+1 dimensions this has been studied recently [62, 63]. It turns out that the mean field ansatz from zero temperature (Section 3.2) is sufficient to compute the whole phase diagram. The result is a self-consistent solution of the finite temperature Hartree-Fock problem, featuring a baryon crystal phase at low temperatures and finite density.

The derivative expansion method used in Sections 4.1, 6.1 is also a valuable tool at finite temperature. It can be applied to calculate the grand canonical potential in powers of derivatives of the mean field. The result is a Ginzburg-Landau effective theory containing all information on the thermodynamic ground state in regions of the phase diagram where the mean field is slowly varying. In the GN model in 1+1 dimensions this calculation reproduces the results known from the exact Hartree-Fock solution. In the 1+1 dimensional NJL model, the method has been applied recently. The minimization of the effective action and the derivation of a phase diagram are subject of current research [64]. Moreover, this analysis is not restricted to low dimensions and could possibly be generalized to more realistic models.

Part III.

Appendix

A. Fermions in low dimensions

This appendix reviews important definitions for the description of Dirac fermions in 1+1 and 2+1 space-time dimensions. More information on the 1+1 dimensional case can be found in Ref. [65], for further reading on 2+1 dimensions, the reader is referred to Refs. [16, 15, 17].

1+1 dimensions

Dirac spinors are defined by a spinor representation of the Lorentz group, which in 1+1 dimensions consists only of boosts. Since there are no rotations and hence no spin, Dirac spinors have only two components (particle/ antiparticle degrees of freedom). The free Dirac equation reads

$$(\mathrm{i}\gamma^\mu\partial_\mu - m)\psi = 0 \tag{A.1}$$

where the 2×2 dimensional γ matrices satisfy the Dirac algebra

$$\{\gamma^\mu,\gamma^\nu\} = 2g^{\mu\nu}. \tag{A.2}$$

They can be chosen proportional to the Pauli spin matrices σ_a (cp. Eq. (3.1)). The hermitian matrix $\gamma^5 = \gamma^0\gamma^1$ generates chiral transformations $\psi \mapsto \mathrm{e}^{\mathrm{i}\alpha\gamma^5}\psi$. Together with the transformations $\psi\mapsto \mathrm{e}^{\mathrm{i}\alpha}\psi$, this defines the chiral symmetry group, which is preserved by the Lagrangian of the NJL model in its 1+1 dimensional formulation in Eq. (2.2). A mass term $\sim\bar\psi\psi$ breaks chiral symmetry explicitly.

For completeness, we give the discrete symmetries of the Dirac equation in 1+1 dimension. The following representation for the γ matrices is used

$$\gamma^0 = \sigma_1 \qquad \gamma^1 = -\mathrm{i}\sigma_2 \qquad \gamma^5 = \gamma^0\gamma^1 = \sigma_3. \tag{A.3}$$

The parity transformation is defined by

$$(x_P) = (t,-x^1), \quad \psi_P(x_P) = \gamma^0\psi(x),$$

from which we conclude that the bilinear $\bar\psi\psi$ is a scalar and $\bar\psi\gamma^5\psi$ a pseudoscalar.

Charge conjugation can be defined by $\psi_C = \gamma^5\psi^*$. In the representation (A.3), $\bar\psi\psi$ is odd under charge conjugation, whereas $\bar\psi\mathrm{i}\gamma^5\psi$ is even.

2+1 dimensions

The Poincaré group in 2+1 dimensions consists of 3 translations, 2 boosts and 1 rotation. Its generators form the Poincaré algebra:

$$[P_\mu,P_\nu] = 0 \tag{A.4}$$
$$[J^\mu,J^\nu] = \mathrm{i}\epsilon^{\mu\nu\rho}J_\rho \tag{A.5}$$
$$[J^\mu,P^\nu] = \mathrm{i}\epsilon^{\mu\nu\rho}P_\rho, \tag{A.6}$$

where P_μ generates translations in space and time, J_0 generates spatial rotations, and J_1 and J_2 Lorentz boosts in the 2 and 1 direction, respectively. Single particle states are defined by irreducible representations of this group. These are characterized by the value of its Casimir operators

$$(P^2 - m^2)\,\psi = 0, \qquad (P \cdot J + sm)\,\psi = 0. \tag{A.7}$$

The value of the spin s can be chosen arbitrarily, leading to a description for particles with arbitrary spin and statistics ("anyons") [16].

For $s = -1/2$, the Lorentz group can be represented by two-component Dirac spinor with 2×2 γ-matrices which satisfy (A.5) with $J^\mu = \gamma^\mu/2$. In 2+1 dimensions this is equivalent to the Dirac algebra (A.2), which has two inequivalent representations

$$\begin{aligned} \gamma^0 &= +\sigma_3, \qquad \gamma^1 = +\mathrm{i}\sigma_1, \qquad \gamma^2 = +\mathrm{i}\sigma_2 \\ \gamma^0 &= -\sigma_3, \qquad \gamma^1 = -\mathrm{i}\sigma_1, \qquad \gamma^2 = -\mathrm{i}\sigma_2. \end{aligned} \tag{A.8}$$

This is due to the fact that there exists no analog of γ^5 in 2+1 dimensions, i.e., no matrix which anticommutes with all γ matrices. Hence, there also exists no generator of chiral transformations in 2+1 dimensions.

As in 3+1 dimensional space, the Dirac equation (A.1) should be invariant under parity transformations. However, in the two-dimensional plane, inverting both spatial coordinates is equal to a rotation by 180^o. A parity transformation which is inequivalent to a rotation can defined by inverting one axis. In the first of the two representations (A.8) this is

$$(x_P) = (t, -x^1, x^2), \quad \psi_P(x_P) = -\mathrm{i}\gamma^1\psi(x) = \sigma_1\psi(x). \tag{A.9}$$

When this transformation is applied to the Dirac equation the mass term acquires an extra minus sign. A common workaround [16, 17, 15] to this problem is to join the two inequivalent representations of the Dirac algebra above to form a four-dimensional reducible representation. The two representations are labeled by an additional "isospin" index. The Dirac equation becomes

$$(\mathrm{i}\gamma^\mu\partial_\mu - m\tau_3)\psi(x) = 0. \tag{A.10}$$

In this notation, the τ matrices act on the isospin degrees of freedom, with $\tau_a = \sigma_a$. Parity invariance of the Dirac equation is recovered by defining the transformation (A.9) to act both in spin and isospin space

$$\psi_P(x_P) = -\mathrm{i}\tau_1\gamma^1\psi(x). \tag{A.11}$$

Lorentz transformations do not act on isospin

$$\psi(x) \mapsto \psi'(x') = \mathrm{e}^{\mathrm{i}\omega_\mu J^\mu}\psi(x') = \mathrm{e}^{\mathrm{i}\omega_\mu\gamma^\mu/2}\psi(x).$$

The isospin matrix in the Eq. (A.10) does not change the covariance of this equation.

The isospin matrices are the analog of the matrix γ^5 in 1+1 dimensions. They generate continuous "chiral" transformations

$$\psi \mapsto \mathrm{e}^{\mathrm{i}\theta_a\tau_a}\psi = \left(\cos\theta + \mathrm{i}\frac{\sin\theta}{\theta}\theta_a\tau_a\right)\psi \qquad (\theta^2 = \theta_a\theta_a). \tag{A.12}$$

The Lagrangian of free massless particles is invariant under chiral transformations as well as under formations $\psi \to \mathrm{e}^{\mathrm{i}\alpha}\psi$. The resulting "chiral" symmetry group $U(1) \otimes SU(2) = U(2)$

	$\bar{\psi}\psi$	$\bar{\psi}\tau_1\psi$	$\bar{\psi}\tau_2\psi$	$\bar{\psi}\tau_3\psi$	$\bar{\psi}\gamma^\mu\psi$
P	-1	-1	$+1$	$+1$	$(+1,-1,+1)$
C	-1	$+1$	-1	-1	$(+1,+1,+1)$

Table A.1.: Transformation of bilinears in 2+1 dimensions under discrete symmetries.

is generated by the τ_a and the identity matrix. The analog of the chirally symmetric four-fermion interaction of the NJL model in 1+1 dimensions is the NJL_3 interaction term

$$(\bar{\psi}\tau_1\psi)^2 + (\bar{\psi}\tau_2\psi)^2 + (\bar{\psi}\tau_3\psi)^2. \tag{A.13}$$

Chiral invariance can be confirmed by applying (A.12).

A mass term $\bar{\psi}\tau_3\psi$ breaks chiral symmetry $U(2)$ down to $U(1)\times U(1)$. The two remaining symmetries

$$\psi \to \mathrm{e}^{\mathrm{i}\alpha}\psi, \qquad \psi \to \mathrm{e}^{\mathrm{i}\tau_3\alpha}\psi,$$

correspond to the conservation of fermion number and the 3-component of isospin. In addition to the terms in (A.13) the bilinear $\bar{\psi}\psi$ is invariant under isospin rotations. It is a parity-violating candidate for a mass term in the Lagrangian

Apart from Lorentz and parity symmetry, the Dirac equation in 2+1 dimensions is invariant under time inversion (T) and charge conjugation (C). We derive the form of the latter discrete symmetry in analogy to the 3+1 dimensional case [66]. We define the charge conjugated spinor by

$$\psi_C = C\gamma^0\psi^*,$$

with the charge conjugation matrix C. The effect of this transformation is the change of sign of the charge e in the Dirac equation for a particle in external electromagnetic field, i.e.,

$$[(\mathrm{i}\partial_\mu - eA_\mu)\gamma^\mu - m]\,\psi(x) = 0 \tag{A.14}$$

$$[(\mathrm{i}\partial_\mu + eA_\mu)\gamma^\mu - m]\,\psi_C(x) = 0. \tag{A.15}$$

This leads to the condition

$$C\gamma^\mu C^{-1} = -(\gamma^\mu)^{\mathrm{T}}, \qquad C\tau_3 C^{-1} = \tau_3.$$

A possible choice is $C = \gamma^1\gamma^0\tau_3$. In addition, C converts positive energy solutions into negative ones, because

$$H\psi = E\psi \quad \Rightarrow \quad H\psi_C = -E\psi_C.$$

The transformation properties for the various bilinears are shown in Table A.1. Note that all above bilinears are real (except $\bar{\psi}\gamma^k\psi$ which is imaginary), because the matrices defining them are hermitian (antihermitian).

B. Translationally invariant solution for 1+1 dimensional models

For the sake of comparison with the states with broken translation symmetry, we also need results for the translationally invariant HF solution which is the same in both GN_2 and NJL_2. These results are found in the work of Barducci et. al. [46] and extended here.

In order to decide whether a periodic or "crystal" solution is energetically favorable, we need the energy density of the massive Fermi gas. This quantity is calculated in the same way as in the vacuum Eq. (2.11). Positive (negative) energy levels up (down) to the Fermi momentum p_f are occupied (unoccupied) to study matter (antimatter) at baryon density $\rho = p_f/\pi$. The energy density per flavor is

$$E = -2\int_{p_f}^{\Lambda/2} \frac{\mathrm{d}p}{2\pi}\sqrt{p^2+M^2} + \frac{(M-m_0)^2}{2Ng^2}.$$

Eliminating the bare coupling constant with the help of the vacuum gap equation (2.14), the logarithmic divergence disappears and we are left with ($\epsilon_f^2 = p_f^2 + M^2$)

$$E = -\frac{\Lambda^2}{8\pi} - \frac{M^2}{4\pi} + \left(\frac{M^2}{2\pi} - \frac{Mm}{\pi}\right)\gamma + \frac{p_f\epsilon_f}{2\pi} + \frac{M^2}{2\pi}\ln\frac{p_f+\epsilon_f}{m},$$

M can be obtained by minimizing E with respect to M,

$$(M-m)\gamma + M\ln\frac{p_f+\epsilon_f}{m} = 0. \tag{B.1}$$

The difference between energy density and vacuum energy density is finite,

$$E - E_0 = -\frac{(M^2-m^2)}{4\pi} - \frac{(Mm-m^2)}{2\pi}\gamma + \frac{p_f\epsilon_f}{2\pi}$$

This last equation is only valid at the minimum, since we have made use of Eq. (B.1) to simplify the expression.

In general, Eq. (B.1) can only be solved numerically. In some limiting cases, one can solve it by a series expansion for M and compute the corresponding energy. Consider the following limits:

- $\gamma \to \infty$ at fixed p_f (heavy quark limit), setting $\epsilon_f = \sqrt{m^2+p_f^2}$:

$$M \approx m - \frac{m}{\gamma}\ln\frac{p_f+\epsilon_f}{m} + \frac{m}{\gamma^2}\left[\ln^2\frac{p_f+\epsilon_f}{m} + \frac{m^2}{\epsilon_f(p_f+\epsilon_f)}\ln\frac{p_f+\epsilon_f}{m}\right]. \tag{B.2}$$

  Energy density (without vacuum subtraction),

$$E \approx -\frac{m^2\gamma}{2\pi} - \frac{m^2}{4\pi} + \frac{p_f\epsilon_f}{2\pi} + \frac{m^2}{2\pi}\ln\frac{p_f+\epsilon_f}{m} - \frac{m^2}{\pi\gamma}\ln^2\frac{p_f+\epsilon_f}{m}.$$

- $p_f \to \infty$ at fixed γ (high density limit):

$$M \approx \frac{m\gamma}{\gamma + \ln(2p_f/m)} - \frac{m^3}{4p_f^2}\frac{\gamma^3}{(\gamma + \ln(2p_f/m))^4}, \tag{B.3}$$

$$E \approx \frac{p_f^2}{2\pi} - \frac{m^2}{2\pi}\frac{\gamma^2}{\gamma + \ln(2p_f/m)} + \frac{m^4}{16\pi p_f^2}\frac{\gamma^4}{(\gamma + \ln(2p_f/m))^4}.$$

As described by Barducci et al. [46], the translationally invariant solution undergoes a first order phase transition at a certain critical chemical potential or density. In the HF solution described above, this manifests itself through the fact that the energy-versus-p_f curve starts out as concave at $p_f = 0$ and becomes convex only above a certain critical Fermi momentum p_f^c. Before drawing conclusions about the stability of the periodic HF solutions in GN_2 and NJL_2, we have to take this fact into account.

Just like at $\gamma = 0$, we make a mixed phase variational ansatz [65]: A fraction λ of space contains all the extra fermions ("droplets"), which therefore have an increased Fermi momentum

$$p_f' = \frac{p_f}{\lambda}.$$

The energy density, subtracting the vacuum contribution, is

$$\Delta E = \lambda \left\{ -\frac{M^2}{4\pi} + \left(\frac{M^2}{2\pi} - \frac{Mm}{\pi}\right)\gamma + \frac{p_f'\epsilon_f'}{2\pi} + \frac{M^2}{2\pi}\ln\frac{p_f' + \epsilon_f'}{m} + \frac{m^2}{4\pi} + \frac{\gamma m^2}{2\pi} \right\} \tag{B.4}$$

with

$$\epsilon_f' = \sqrt{M^2 + (p_f')^2}.$$

Vary with respect to λ,

$$\frac{\partial \Delta E}{\partial \lambda} = 0 \quad \leftrightarrow \quad \Delta E - p_f' \frac{\partial \Delta E}{\partial p_f'} = 0. \tag{B.5}$$

The right hand side can be interpreted as construction of the convex hull of the curve energy density versus fermion density (remember the geometrical meaning of the Legendre transform). The solution p_f' of this equation at $\lambda = 1$ is the critical Fermi momentum. More explicitly, Eq. (B.5) reads

$$(m + M + 2\gamma m(m - M))(m - M) - 2p_f'\epsilon_f' + 2M^2 \ln\frac{p_f' + \epsilon_f'}{m} = 0. \tag{B.6}$$

Vary with respect to M [cf. Eq. (B.1)],

$$(M - m)\gamma + M \ln\frac{p_f' + \epsilon_f'}{m} = 0. \tag{B.7}$$

Eqs. (B.6) and (B.7) determine the mixed phase. To solve them, proceed as follows: Eliminate the ln-term in Eq. (B.6) with the help of Eq. (B.7) and solve the resulting equation for p_f',

$$(p_f')^2 = \frac{-M^2 + \sqrt{M^4 + (m - M)^2(m + M + 2m\gamma)^2}}{2}.$$

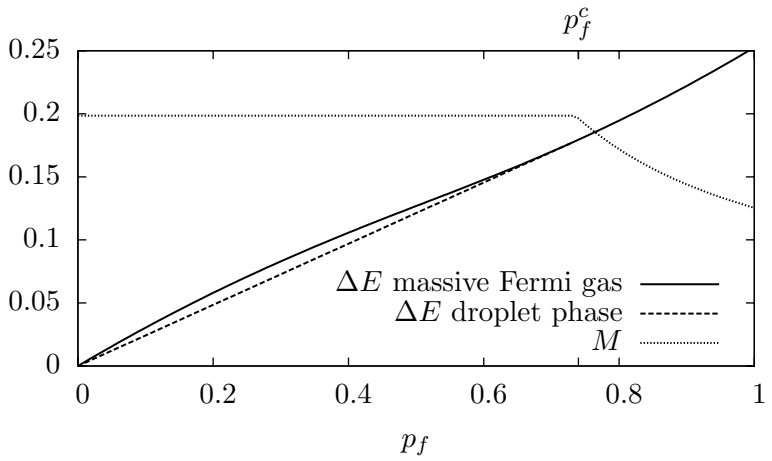

Figure B.1.: Energy density of the massive Fermi gas in 1+1 dimensional models (minus the vacuum energy) versus Fermi momentum p_f for $m = 1$, $\gamma = 0.1$. Below p_f^c this is a concave function which indicates instability against formation of "droplets" containing all extra fermions. The true ground state energy density is obtained as the complex hull which is determined by Eqs. (B.4,B.6,B.7) and plotted with a dashed line. The dotted curve shows the effective mass M of the fermions (constant in the "droplet" region).

Insert this result into Eq. (B.7) and arrive at an equation relating M and γ. This equation always has a non-trivial solution, which has to be determined numerically. The result for the energy difference ΔE is shown in Fig. B.1 for $\gamma = 0.1$. Analytical results can be obtained in limiting cases of interest,

$$\begin{aligned} \frac{M}{m} &\approx \frac{2}{\ln 2}\gamma - \frac{8}{(\ln 2)^2}\gamma^2 + \frac{4[10\ln 2 + (\ln 2)^2 + 2]}{(\ln 2)^4}\gamma^3 \quad \text{for } \gamma \to 0, \\ \frac{M}{m} &\approx m - \frac{3}{2\gamma^2} + \frac{3}{\gamma^3} - \frac{63}{40\gamma^4} \qquad\qquad\qquad\qquad\quad \text{for } \gamma \to \infty. \end{aligned} \tag{B.8}$$

By inserting these expressions into Eqs. (B.8), (B.4), we can determine the behavior of the energy in the mixed phase, as well as the critical point. Find for small γ

$$\begin{aligned} \frac{\Delta E}{m} &\approx \frac{p_f}{\pi}\left\{\frac{1}{\sqrt{2}} + \frac{1}{\sqrt{2}}\gamma - \frac{4+\ln 2}{2\sqrt{2}\ln 2}\gamma^2\right\} \\ \frac{p_f^c}{m} &\approx \frac{(1+\gamma)}{\sqrt{2}} - \frac{(8+4\ln 2+(\ln 2)^2)}{2\sqrt{2}(\ln 2)^2}\gamma^2, \end{aligned} \tag{B.9}$$

and for large γ

$$\begin{aligned} \frac{\Delta E}{m} &\approx \frac{p_f}{\pi}\left\{1 - \frac{3}{8\gamma^2} + \frac{3}{4\gamma^3}\right\} \\ \frac{p_f^c}{m} &\approx \frac{3}{2\gamma} - \frac{3}{2\gamma^2} - \frac{69}{80\gamma^3}. \end{aligned} \tag{B.10}$$

The expressions in curly brackets in Eqs. (B.9) and (B.10) are the critical chemical potentials. This should be compared with the true baryon masses.

C. Translationally invariant solution for 2+1 dimensional models

By assuming a constant mean field — setting $\phi = M$ for GN_2 and $\boldsymbol{\phi}^2 = M^2$ for GN_2 — we can find a self-consistent solution of the HF equations. The spectrum of Hamiltonian H in Eq. (2.6) is that of free fermions with dynamical mass M. The total energy density per flavor E is the sum over single particle energies plus the double-counting correction. Positive energy states are filled up to the Fermi momentum p_f. We get

$$E = \frac{M^2}{2Ng^2} - \int \frac{\mathrm{d}^2p}{(2\pi)^2}\sqrt{\mathbf{p}^2+M^2} + \int_{|\mathbf{p}|<p_f} \frac{\mathrm{d}^2p}{(2\pi)^2}\sqrt{\mathbf{p}^2+M^2}.$$

Using the vacuum gap equation (5.3), the energy is renormalized

$$E = -\frac{M^2 m}{4\pi} + \frac{1}{6\pi}\left(p_f^2+M^2\right)^{3/2},$$

which has to be minimized varying the dynamical mass M, in order to get a self-consistent solution. The minimum condition is

$$\frac{\partial E}{\partial M} = \frac{M}{2\pi}\left(-m+\sqrt{p_f^2+M^2}\right) = 0,$$

solved by $M = 0$ or $M^2 = m^2 - p_f^2$ (if $p_f < m$). The second stationary condition always yields a lower total energy if $p_f < m$. Introducing the baryon density per flavor $\rho = p_f^2/4\pi$ we get

$$E = \begin{cases} -\dfrac{m^3}{12\pi} + \rho\, m & \text{for} \quad \rho \le \frac{m^2}{4\pi} \\ \dfrac{4\sqrt{\pi}}{3}\rho^{3/2} & \text{for} \quad \rho > \frac{m^2}{4\pi}. \end{cases} \tag{C.1}$$

This result is plotted in Fig. C.1. Note that E is continuously differentiable at $\rho = m^2/4\pi$.

Unlike in 2d there is no need to construct a mixed phase by defining spatial regions with broken and unbroken chiral symmetry since the energy (2.9) is already a convex function of the density. However, the chemical potential is $\mu = m$ for all densities below $\rho = m^2/(4\pi)$. This shows that the phase transition at this point is of first order since at $\mu = m$, the density jumps from 0 to $m^2/(4\pi)$ discontinuously, the order parameter from $M = m$ to $M = 0$.

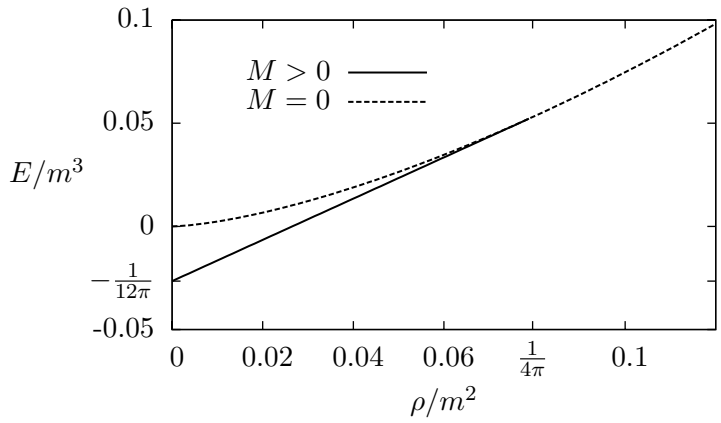

Figure C.1.: Energy density per flavor assuming translational invariance for the scalar potential versus baryon density ρ. The dashed line is the energy of chirally symmetric phase, the solid line is the energy for $M^2 = m^2 - 4\pi\rho$.

D. Elliptic integrals and Jacobi elliptic functions

Since different ways of writing down elliptic integrals and Jacobi elliptic functions are in use, we briefly summarize our conventions. As a rule, we use the Legendre normal form for elliptic integrals. Our notation of the arguments is the same as in Maple.

- Incomplete elliptic integral of the first kind

$$F(z,\kappa) = \int_0^z \mathrm{d}t \frac{1}{\sqrt{1-t^2}\sqrt{1-\kappa^2 t^2}}$$

- Incomplete elliptic integral of the second kind

$$E(z,\kappa) = \int_0^z \mathrm{d}t \frac{\sqrt{1-\kappa^2 t^2}}{\sqrt{1-t^2}}$$

- Incomplete elliptic integral of the third kind

$$\Pi(z,n,\kappa) = \int_0^z \mathrm{d}t \frac{1}{(1-nt^2)\sqrt{1-t^2}\sqrt{1-\kappa^2 t^2}}$$

- Complete elliptic integral of the first kind

$$\mathbf{K} = \mathbf{K}(\kappa) = F(1,\kappa)$$

- Complete elliptic integral of the second kind

$$\mathbf{E} = \mathbf{E}(\kappa) = E(1,\kappa)$$

- Complete elliptic integral of the third kind

$$\mathbf{\Pi}(n,\kappa) = \Pi(1,n,\kappa)$$

- Complementary elliptic modulus $\kappa'^2 = 1-\kappa^2$

$$\mathbf{K}' = \mathbf{K}(\kappa'), \qquad \mathbf{E}' = \mathbf{E}(\kappa')$$

- Jacobi elliptic functions sn, cn, dn and the Jacobi amplitude am

$$F(\mathrm{sn}(u,\kappa),\kappa) = u, \qquad \text{for } -\mathbf{K} < u < \mathbf{K}$$
$$\mathrm{cn}\, u = \sqrt{1-\mathrm{sn}^2\, u}, \qquad \mathrm{dn}\, u = \sqrt{1-\kappa^2\mathrm{sn}^2\, u}, \qquad \sin(\mathrm{am}\, u) = \mathrm{sn}\, u$$

  In Jacobi elliptic functions, we suppress the elliptic modulus κ throughout this paper,

$$\mathrm{sn}\, u = \mathrm{sn}(u,\kappa), \quad \mathrm{cn}\, u = \mathrm{cn}(u,\kappa), \quad \mathrm{dn}\, u = \mathrm{dn}(u,\kappa).$$

  Following the convention implemented in Maple, we have denoted the second argument by κ rather than κ^2.

  Apart from the period $4\mathbf{K}$, the Jacobi elliptic functions can be shown to be periodic in the complex plane with period $4\mathrm{i}\mathbf{K}'$, i.e., they are doubly periodic (=elliptic). This can be used to show identities between elliptic functions. The boundedness theorem of complex analysis guarantees that two elliptic functions of equal periods are identical up to an additive constant once their pole structure is the same. This fact was used to write the ansatz for the scalar condensate in the form (3.20) and to derive the identity (3.40).

- Derivatives

$$\mathrm{am}'\, u = \mathrm{dn}\, u \qquad \mathrm{sn}'\, u = \mathrm{cn}\, u\ \mathrm{dn}\, u$$

- In the limit $\kappa \to 1$

$$\mathbf{K} = \ln\frac{4}{\kappa'} + \mathcal{O}(\kappa'^2)$$
$$\mathrm{sn}\, b \to \tanh b, \qquad \mathrm{cn}\, b \to \mathrm{sech} b, \qquad \mathrm{dn}\, b \to \mathrm{sech} b$$

E. Higher orders in the minimization of the energy density of NJL2

In order to determine corrections to the sine-Gordon kink baryon in NJL_2, we minimize the derivative expansion energy density in Eq. (4.6) with respect to χ and λ. The minimum equations up to order m_π^6 are

$$
\begin{aligned}
\chi_0'' &= \frac{1}{2}\sin 2\chi_0 \\
\lambda_1 &= \frac{1}{4}\left(\cos 2\chi_0 - 1\right) \\
\chi_1'' - \chi_1 \cos 2\chi_0 &= \frac{1}{2}\left(\lambda_1 + \frac{1}{6}\right)\sin 2\chi_0 - \frac{1}{6}\chi_0^{IV}. \\
\lambda_2 &= \frac{1}{24}\left(\cos 2\chi_0 - 1\right) - \frac{1}{2}\chi_1 \sin 2\chi_0 - \frac{1}{6}(\chi_0'')^2 - \frac{1}{4}\lambda_1 - \frac{1}{2}\lambda_1^2 + \frac{1}{12}\lambda_1'' \\
\chi_2'' - \chi_2 \cos 2\chi_0 &= \left(-\chi_1^2 + \frac{1}{2}\lambda_2 + \frac{1}{12}\lambda_1 + \frac{1}{60}\right)\sin 2\chi_0 + \left(\lambda_1\chi_1 + \frac{1}{6}\chi_1\right)\cos 2\chi_0 \\
&\quad - \frac{1}{30}\chi_0^{VI} + \frac{1}{3}\lambda_1\chi_0^{IV} + \frac{1}{3}\lambda_1''\chi_0'' + \frac{2}{3}\lambda_1'\chi_0''' - \frac{1}{6}\chi_1^{IV} \\
\lambda_3 &= -\left(\frac{1}{2}\chi_1^2 - \frac{1}{120}\right)\cos 2\chi_0 - \left(\frac{1}{2}\chi_2 + \frac{1}{12}\chi_1\right)\sin 2\chi_0 \\
&\quad - \lambda_1\lambda_2 - \frac{1}{120} - \frac{1}{10}\chi_0''\chi_0^{IV} - \frac{1}{30}(\chi_0''')^2 - \frac{1}{4}\lambda_2 + \frac{1}{12}\lambda_2'' + \frac{1}{6}\lambda_1^3 \\
&\quad - \frac{1}{3}\chi_0''\chi_1'' - \frac{1}{12}(\lambda_1')^2 - \frac{1}{6}\lambda_1\lambda_1'' + \frac{1}{120}\lambda_1^{IV} - \frac{1}{24}\lambda_1 + \frac{1}{2}\lambda_1(\chi_0'')^2 \\
\chi_3'' - \chi_3 \cos 2\chi_0 &= \left(\frac{1}{6}\chi_2 + \lambda_1\chi_2 + \lambda_2\chi_1 - \frac{2}{3}\chi_1^3 + \frac{1}{30}\chi_1 + \frac{1}{6}\lambda_1\chi_1\right)\cos 2\chi_0 \\
&\quad - \left(2\chi_1\chi_2 - \frac{1}{280} + \frac{1}{6}\chi_1^2 - \frac{1}{12}\lambda_2 - \frac{1}{2}\lambda_3 + \lambda_1\chi_1^2 - \frac{1}{60}\lambda_1\right)\sin 2\chi_0 \\
&\quad - \frac{1}{140}\chi_0^{VIII} - \frac{4}{15}\chi_0''(\chi_0''')^2 - \frac{2}{15}(\chi_0'')^2\chi_0^{IV} + \frac{1}{2}\lambda_1''\chi_0^{IV} + \frac{1}{3}\lambda_1'''\chi_0''' \\
&\quad + \frac{2}{15}\lambda_1\chi_0^{VI} + \frac{2}{5}\lambda_1'\chi_0^{V} + \frac{1}{10}\lambda_1^{IV}\chi_0'' - \frac{1}{6}\chi_2^{IV} + \frac{1}{3}\lambda_2''\chi_0'' + \frac{2}{3}\lambda_1'\chi_1''' \\
&\quad + \frac{2}{3}\lambda_1'\chi_1''' + \frac{1}{3}\lambda_1\chi_1^{IV} + \frac{2}{3}\lambda_2'\chi_0''' + \frac{1}{3}\lambda_1\chi_1^{IV} + \frac{2}{3}\lambda_2'\chi_0''' + \frac{1}{3}\lambda_2\chi_0^{IV} \\
&\quad + \frac{1}{3}\lambda_1''\chi_1'' - \frac{1}{30}\chi_1^{VI} - \lambda_1\lambda_1''\chi_0'' - 2\lambda_1\lambda_1'\chi_0''' - \frac{1}{2}\lambda_1^2\chi_0^{IV} - (\lambda_1')^2\chi_0''.
\end{aligned}
$$

These equations can be solved successively. The leading order result for χ is the sine-Gordon kink solution in Eq. (4.9). Up to order m_π^{12} the coefficients in Eq. (4.7) are

$$\chi_0 = 2\arctan \mathrm{e}^{\xi}$$

$$
\begin{aligned}
\lambda_1 &= -\frac{1}{2}\operatorname{sech}^2\xi \\
\chi_1 &= \frac{1}{8}\sinh\xi\operatorname{sech}^2\xi \\
\lambda_2 &= -\frac{1}{6}\left(\operatorname{sech}^2\xi - \operatorname{sech}^4\xi\right) \\
\chi_2 &= -\frac{1}{1152}\sinh\xi\left(23\operatorname{sech}^2\xi - 122\operatorname{sech}^4\xi\right) \\
\lambda_3 &= -\frac{1}{1440}\left(252\operatorname{sech}^2\xi - 1225\operatorname{sech}^4\xi + 1061\operatorname{sech}^6\xi\right) \\
\chi_3 &= -\frac{1}{691200}\sinh\xi\left(2621\operatorname{sech}^2\xi - 108092\operatorname{sech}^4\xi + 90456\operatorname{sech}^6\xi\right) \\
\lambda_4 &= \frac{1}{604800}\left(-86284\operatorname{sech}\xi^2 + 1693937\operatorname{sech}^4\xi - 4897732\operatorname{sech}^6\xi + 3428239\operatorname{sech}^8\xi\right) \\
\chi_4 &= \frac{1}{3251404800}\sinh\xi\big(-38251715\operatorname{sech}^2\xi + 956627974\operatorname{sech}^4\xi \\
&\quad - 4522865208\operatorname{sech}^6\xi + 4179637264\operatorname{sech}^8\xi\big) \\
\lambda_5 &= -\frac{1}{50803200}\big(6742972\operatorname{sech}^2\xi i - 453795621\operatorname{sech}^4\xi + 3486075693\operatorname{sech}^6\xi \\
&\quad - 7079075471\operatorname{sech}^8\xi + 4115502795\operatorname{sech}^{10}\xi\big) \\
\chi_5 &= -\frac{1}{390168576000}\sinh\xi\big(-7423504897\operatorname{sech}^2\xi - 211364495656\operatorname{sech}^4\xi \\
&\quad + 3218922195888\operatorname{sech}^6\xi - 9461541542720\operatorname{sech}^8\xi + 6979740749440\operatorname{sech}^{10}\xi\big) \\
\lambda_6 &= \frac{1}{33530112000}\big(-3089912332\operatorname{sech}^2\xi + 944194230441\operatorname{sech}^4\xi - 17791295428170\operatorname{sech}^6\xi \\
&\quad + 80145159039319\operatorname{sech}^8\xi - 123840806689072\operatorname{sech}^{10}\xi + 61034281245254\operatorname{sech}^{12}\xi\big) \\
\chi_6 &= \frac{1}{33991486341120000}\sinh\xi\big(-2618519287803409\operatorname{sech}^2\xi + 31800984903656270\operatorname{sech}^4\xi \\
&\quad - 1490342285985619120\operatorname{sech}^6\xi + 10618472289207620320\operatorname{sech}^8\xi \\
&\quad - 21993256972453562240\operatorname{sech}^{10}\xi + 13398988715131727104\operatorname{sech}^{12}\xi\big).
\end{aligned}
$$

We can now insert this result into the derivative expansion of the energy to get the result for the baryon mass in Eq. (4.10).

F. Alternative derivation of the baryon stripe mass

In Appendix E of Ref. [35], Joshua Feinberg presents a simple dimensional argument to derive the mass of the single Callen-Coleman-Gross-Zee kink configuration in massless GN_2. It does not require the summation of single-particle energies, used in this work to calculate the total energy of a mean field configuration. The only information needed is the shape of the self-consistent field and the gap equation. In this appendix we will use the same argument to calculate the total energy of the baryon stripe solution of Section 5.1. This will confirm the result in Eq. (5.4) derived by summing over HF energies.

First, let us repeat Feinberg's argument in 1+1 dimensions and derive the mass of the partially filled kink-antikink baryon in the chiral limit. The result can be compared with Ref. [22] and Section 3.1 with $\gamma = 0$. The mean field σ is given by Eq. (3.3), where the parameter y is fixed by the self-consistency condition Eq. (3.10) in the chiral limit $\gamma = 0$. The mass of this baryon configuration is the total energy (per flavor) minus the vacuum energy

$$M_{\mathrm{B}} = E - E_0,$$

where the energies E and E_0 are given by the sum over HF energies plus the double counting correction (see Eq. (2.9)). Using the spectrum of the HF Hamiltonian, one gets $M_{\mathrm{B}} = 2y/\pi m$ (cp. Eq. (3.11)). This can also be derived using Feinberg's argument. We first observe that M_{B} has to be proportional to the vacuum fermion mass m as the only parameter with the dimension of a mass. Hence,

$$M_{\mathrm{B}} = cm,$$

where the factor c can be calculated by the total derivative with respect to m

$$c = \frac{\mathrm{d}M_{\mathrm{B}}}{\mathrm{d}m}.$$

The baryon mass is now interpreted as a functional of the baryon mean field and a function of the vacuum fermion mass. The derivative with respect to m can be written as

$$\frac{\mathrm{d}M_{\mathrm{B}}}{\mathrm{d}m} = \int \mathrm{d}x \left[\frac{\delta M_{\mathrm{B}}}{\delta\sigma(x)}\frac{\partial\sigma(x)}{\partial m}\right] + \frac{\partial M_{\mathrm{B}}}{\partial m} + \frac{\partial M_{\mathrm{B}}}{\partial g^2}\frac{\partial g^2}{\partial m}.$$

Due to their self-consistency, the vacuum and the kink-antikink baryon extremize M_{B}, so that the first two terms vanish. The remaining term is calculated using the shape of the baryon and the gap equation (2.14). For the first factor, we get

$$\frac{\partial M_{\mathrm{B}}}{\partial g^2} = -\frac{1}{2Ng^4}\int \mathrm{d}x \left(\sigma^2 - m^2\right) = \frac{2my}{Ng^4},$$

where we carried out the integration over the baryon mean field using the result in Ref. [22] (see also Eq. (3.7)). The second factor becomes

$$\frac{\partial g^2}{\partial m} = \frac{Ng^4}{m\pi},$$

so that

$$c = \frac{2y}{\pi}$$

in accordance with the result of the summation over HF energies. With the same line of arguments as above, one can derive the mass of partially filled baryons in the massless NJL_2 model leading to the same result as the conventional calculation found in Ref. [26].

In order to calculate the energy of the "baryon stripe", we observe that the mass per unit length in the x_1-direction parallel to the stripe has the dimension $(\text{mass})^2$. In a slab of width L_1, the energy difference with respect to the vacuum will have the form

$$\Delta \equiv E - E_{(0)} = cL_1 m^2 = cl_1 m,$$

where we wrote the length L_1 in terms of a dimensionless parameter $l_1 = L_1 m$. With the self-consistency of the baryon stripe, we get

$$\frac{\mathrm{d}\Delta}{\mathrm{d}m} = cl_1 = \frac{\partial \Delta}{\partial g^2}\frac{\partial g^2}{\partial m}.$$

With the gap equation (5.3) and the shape of the baryon stripe, we can deduce

$$\frac{\partial \Delta}{\partial g^2} = -\frac{1}{2Ng^4}\int \mathrm{d}^2x \left(\sigma^2 - m^2\right) = \frac{2L_1 my}{Ng^4}$$
$$\frac{\partial g^2}{\partial m} = \frac{Ng^4}{2\pi}.$$

The result for the total energy

$$\Delta = \frac{L_1 y m^2}{\pi}$$

confirms the result in Eq. (5.4).

G. Calculation of traces for the derivative expansion

We use the following useful identities to evaluate the trace over spin and isospin degrees of freedom

$$\{\gamma^\mu,\gamma^\nu\}=2g^{\mu\nu} \qquad \gamma^\mu\gamma^\nu=g^{\mu\nu}-\mathrm{i}\epsilon^{\mu\nu\lambda}g_{\lambda\rho}\gamma^\rho$$
$$(\boldsymbol{a}\cdot\boldsymbol{\tau})(\boldsymbol{b}\cdot\boldsymbol{\tau})=\boldsymbol{a}\cdot\boldsymbol{b}+\mathrm{i}(\boldsymbol{a}\times\boldsymbol{b})\cdot\boldsymbol{\tau} \qquad \epsilon^{mn}(\boldsymbol{a}_m\times\boldsymbol{a}_n)=2\boldsymbol{a}_1\times\boldsymbol{a}_2.$$

The results for the traces in Eq. (6.5) are given up to surface terms. With V defined in Eq. (6.3) we get for the z-terms

$$\begin{aligned}
\operatorname{tr} V^2 &= 4(\nabla\boldsymbol{\phi})^2\\
\operatorname{tr}(\Delta V)V &= -4(\Delta\boldsymbol{\phi})^2\\
\operatorname{tr}(\Delta V)^2 &= 4(\Delta\boldsymbol{\phi}^2)^2+4(\Delta\partial_l\boldsymbol{\phi}\cdot\Delta\partial_l\boldsymbol{\phi})\\
\operatorname{tr} V^3 &= 0\\
\operatorname{tr}(\Delta V)V^2 &= -2\operatorname{tr}(\partial_l V)(\partial_l V)V=\\
&= -32(\boldsymbol{\phi}\cdot\partial_k\boldsymbol{\phi})(\partial_l\partial_k\boldsymbol{\phi}\cdot\partial_l\boldsymbol{\phi})\\
\operatorname{tr} V^4 &= 4\left[(\nabla\boldsymbol{\phi})^4+4(\partial_1\boldsymbol{\phi}\times\partial_2\boldsymbol{\phi})^2\right],
\end{aligned}$$

for the K terms

$$\begin{aligned}
\operatorname{tr}\gamma^0\gamma^k(\partial_k V)V &= \operatorname{tr}\gamma^0\gamma^k V(\partial_k V)V = \operatorname{tr}\gamma^0\gamma^k(\partial_k V)(\Delta V)=0\\
\operatorname{tr}\gamma^0\gamma^k(\partial_k V)V^2 &= 8\mathrm{i}(\Delta\boldsymbol{\phi})\cdot(\partial_1\boldsymbol{\phi}\times\partial_2\boldsymbol{\phi}),
\end{aligned}$$

and for the terms in r_I

$$\begin{aligned}
\operatorname{tr} IV^2 &= -8\boldsymbol{\phi}\cdot(\partial_1\boldsymbol{\phi}\times\partial_2\boldsymbol{\phi})\\
\operatorname{tr} I(\Delta V)V &= \operatorname{tr} IV(\Delta V)=-8(\Delta\boldsymbol{\phi})\cdot(\partial_1\boldsymbol{\phi}\times\partial_2\boldsymbol{\phi})\\
\operatorname{tr} I(\partial_l V)(\partial_l V) &= 4(\Delta\boldsymbol{\phi})\cdot(\partial_1\boldsymbol{\phi}\times\partial_2\boldsymbol{\phi})\\
\operatorname{tr} IV^3 &= 0\\
\operatorname{tr} IV^4 &= -16(\nabla\boldsymbol{\phi})^2\boldsymbol{\phi}\cdot(\partial_1\boldsymbol{\phi}\times\partial_2\boldsymbol{\phi}).
\end{aligned}$$

H. Details of the basis states for numerical diagonalization

This appendix describes in detail the calculation leading to the basis states for numerical diagonalization in NJL_3 in Section 6.2. The main result will be the basis states in Eq. (6.11).

In the vacuum, the radial HF equations equations (6.10) can be decoupled. With $\boldsymbol{\phi} = (0, 0, 1)$ we get

$$\left[\frac{n^2}{r^2} - \frac{1}{r}\partial_r - \partial_r^2\right] g_2 = (E^2 - 1) g_2$$
$$g_1 = \frac{1}{E-1}\left[\frac{n}{r} + \partial_r\right] g_2,$$

and similarly for g_3 and g_4:

$$\left[\frac{(n+1)^2}{r^2} - \frac{1}{r}\partial_r - \partial_r^2\right] g_4 = (E^2 - 1) g_4$$
$$g_3 = \frac{1}{E+1}\left[\frac{n+1}{r} + \partial_r\right] g_4,$$

These are Bessel differential equations solved by

$$\begin{aligned} g_1 &= C_1^{(1)} J_{n-1}(kr) + C_2^{(1)} Y_{n-1}(kr) \\ g_2 = g_3 &= C_1^{(2/3)} J_n(kr) + C_2^{(2/3)} Y_n(kr) \\ g_4 &= C_1^{(4)} J_{n+1}(kr) + C_2^{(4)} Y_{n+1}(kr). \end{aligned}$$

The coefficients can be related using

$$J_{n-1}(kr) = \frac{2n}{kr} J_n(kr) - J_{n+1}(kr),$$

and the same relation for the Y_n's. Thus

$$C_{1/2}^{(1)} = \frac{k}{E-1} C_{1/2}^{(2)} \qquad C_{1/2}^{(3)} = \frac{k}{E+1} C_{1/2}^{(4)}.$$

Since ψ_n has to be continuous at the origin, the radial functions $g_i(r)$ have to vanish at the origin. We therefore have to set $C_2^{(i)} = 0$. Negative energy states are obtained by replacing $E \to -E$ in the above equations. The eigenfunctions then become ($C \equiv C_1^{(2)}$, $D \equiv C_1^{(4)}$)

$$\psi_{n,k,\eta} = \mathrm{e}^{\mathrm{i}n\alpha} \begin{pmatrix} C\frac{k}{\eta E - 1} J_{n-1}(kr)\mathrm{e}^{-\mathrm{i}\alpha} \\ C J_n(kr) \\ D\frac{k}{\eta E + 1} J_n(kr) \\ D J_{n+1}(kr)\mathrm{e}^{+\mathrm{i}\alpha} \end{pmatrix} \qquad \eta \in \{+, -\}, \tag{H.1}$$

with energy eigenvalues $\eta E = \eta\sqrt{k^2+1}$.

We discretize the basis states (H.1) by the boundary condition $J_n(k_{n,j}R) = 0$ on a circle with radius R as described in the text. The discretized basis states can be normalized using the orthogonality relation for Bessel functions on a finite interval[1]

$$\int_0^R \mathrm{d}r\, r J_n\left(\frac{\alpha_{n,i}}{R}r\right) J_n\left(\frac{\alpha_{n,j}}{R}r\right) = \frac{R^2}{2} J_{n+1}^2(\alpha_{n,j})\delta_{ij},$$

and similarly[2]

$$\int_0^R \mathrm{d}r\, r J_{n\pm1}\left(\frac{\alpha_{n,i}}{R}r\right) J_{n\pm1}\left(\frac{\alpha_{n,j}}{R}r\right) = \frac{R^2}{2} J_{n+1}^2(\alpha_{n,j})\delta_{ij}.$$

The states (H.1) still involve the parameters C and D. One of them can be fixed by normalization, the other one stems from an additional degeneracy due to the choice of the four-dimensional reducible representation. States with isospin $\pm 1/2$ are degenerate as $\tau_3/2$ commutes with $H[\boldsymbol{\phi} = (0,0,1)]$ and M_3. Introducing the isospin $s = \pm 1$ as quantum number, the discretized states are given by Eq. (6.11). The normalization conditions are

$$\|\psi_{n,j,k,1}\|^2 = \pi C^2 R^2 J_{n+1}^2(\alpha_{n,j}) \left[\frac{k_{n,j}^2}{(\eta E - 1)^2} + 1\right] \stackrel{!}{=} 1$$

$$\|\psi_{n,j,k,-1}\|^2 = \pi D^2 R^2 J_{n+1}^2(\alpha_{n,j}) \left[\frac{k_{n,j}^2}{(\eta E + 1)^2} + 1\right] \stackrel{!}{=} 1.$$

which leads to Eq. (6.12).

[1] see `http://mathworld.wolfram.com/BesselFunctionoftheFirstKind.html`

[2] derived using `http://functions.wolfram.com/03.01.21.0064.01`

Bibliography

[1] M. Alford, "Dense quark matter in nature", *Prog. Theor. Phys. Suppl.* **153** (2004) 1–14, nucl-th/0312007.

[2] Y. Nambu and G. Jona-Lasinio, "Dynamical model of elementary particles based on an analogy with superconductivity. II", *Phys. Rev.* **124** (1961) 246–254.

[3] Y. Nambu and G. Jona-Lasinio, "Dynamical model of elementary particles based on an analogy with superconductivity. I", *Phys. Rev.* **122** (1961) 345–358.

[4] D. J. Gross and A. Neveu, "Dynamical symmetry breaking in asymptotically free field theories", *Phys. Rev.* **D10** (1974) 3235.

[5] R. F. Dashen, B. Hasslacher, and A. Neveu, "Semiclassical bound states in an asymptotically free theory", *Phys. Rev.* **D12** (1975) 2443.

[6] U. Wolff, "The phase diagram of the infinite N Gross-Neveu model at finite temperature and chemical potential", *Phys. Lett.* **B157** (1985) 303–308.

[7] A. Brzoska and M. Thies, "No first-order phase transition in the Gross-Neveu model?", *Phys. Rev.* **D65** (2002) 125001, hep-th/0112105.

[8] M. Thies, "Analytical solution of the Gross-Neveu model at finite density", *Phys. Rev.* **D69** (2004) 067703, hep-th/0308164.

[9] M. Alford, J. A. Bowers, and K. Rajagopal, "Crystalline color superconductivity", *Phys. Rev. D* **63** (Mar, 2001) 074016.

[10] D. K. Campbell, "Conducting polymers and relativistic field theories", *Synthetic Metals* **125** (2001), no. 1, 117–128.

[11] T. H. R. Skyrme, "A Nonlinear field theory", *Proc. Roy. Soc. Lond.* **A260** (1961) 127–138.

[12] V. Schön and M. Thies, "Emergence of Skyrme crystal in Gross-Neveu and 't Hooft models at finite density", *Phys. Rev.* **D62** (2000) 096002, hep-th/0003195.

[13] B. Rosenstein, B. J. Warr, and S. H. Park, "Four-fermion theory is renormalizable in 2+1 dimensions", *Phys. Rev. Lett.* **62** (Mar, 1989) 1433–1436.

[14] B. Rosenstein, B. J. Warr, and S. H. Park, "Thermodynamics of (2+1) dimensionsal four Fermi models", *Phys. Rev.* **D39** (1989) 3088.

[15] B. Rosenstein, B. Warr, and S. H. Park, "Dynamical symmetry breaking in four Fermi interaction models", *Phys. Rept.* **205** (1991) 59–108. 2p1.

[16] R. Jackiw and V. P. Nair, "Relativistic wave equations for anyons", *Phys. Rev.* **D43** (1991) 1933–1942.

[17] T. W. Appelquist, M. Bowick, D. Karabali, and L. C. R. Wijewardhana, "Spontaneous chiral-symmetry breaking in three-dimensional QED", *Phys. Rev. D* **33** (Jun, 1986) 3704–3713.

[18] V. C. Zhukovsky, K. G. Klimenko, V. V. Khudyakov, and D. Ebert, "Magnetic catalysis of parity breaking in a massive Gross- Neveu model and high-temperature superconductivity", *JETP Lett.* **73** (2001) 121–125, `hep-th/0012256`.

[19] N. D. Mermin and H. Wagner, "Absence of Ferromagnetism or Antiferromagnetism in One- or Two-Dimensional Isotropic Heisenberg Models", *Phys. Rev. Lett.* **17** (Nov, 1966) 1133–1136.

[20] S. R. Coleman, "There are no Goldstone bosons in two-dimensions", *Commun. Math. Phys.* **31** (1973) 259–264.

[21] P. C. Hohenberg, "Existence of Long-Range Order in One and Two Dimensions", *Phys. Rev.* **158** (Jun, 1967) 383–386.

[22] R. Pausch, M. Thies, and V. L. Dolman, "Solving the Gross-Neveu model with relativistic many body methods", *Z. Phys.* **A338** (1991) 441–453.

[23] J. Feinberg and A. Zee, "Fermion bags in the massive Gross-Neveu model", *Phys. Lett.* **B411** (1997) 134–140, `hep-th/9610009`.

[24] M. Thies and K. Ohta, "Continuum light cone quantization of Gross-Neveu models", *Phys. Rev.* **D48** (1993) 5883–5894.

[25] M. Thies and K. Urlichs, "Baryons in massive Gross-Neveu models", *Phys. Rev.* **D71** (2005) 105008, `hep-th/0502210`.

[26] S.-S. Shei, "Semiclassical bound states in a model with chiral symmetry", *Phys. Rev. D* **14** (Jul, 1976) 535–546.

[27] J. Goldstone and F. Wilczek, "Fractional Quantum Numbers on Solitons", *Phys. Rev. Lett.* **47** (1981) 986–989.

[28] M. Carena, S. Chaudhuri, and C. E. M. Wagner, "Induced fermion number in the O(3) nonlinear sigma model", *Phys. Rev.* **D42** (1990) 2120–2126.

[29] T. Jaroszewicz, "Induced fermion current in the sigma model in (2+1)- dimensions", *Phys. Lett.* **B146** (1984) 337.

[30] A. G. Abanov and P. B. Wiegmann, "Geometrical phases and quantum numbers of solitons in nonlinear sigma-models", *JHEP* **10** (2001) 030, `hep-th/0105213`.

[31] G. V. Dunne, J. Lopez-Sarrion, and K. Rao, "Finite temperature induced fermion number in the nonlinear sigma model in (2+1) dimensions", *Phys. Rev.* **D66** (2002) 025004, `hep-th/0204082`.

[32] I. Aitchison, C. Fraser, E. Tudor, and J. Zuk, "Failure of the derivative expansion for studying stability of the baryon as a chiral soliton", *Phys. Lett.* **B165** (1985) 162–166.

[33] M. Thies and K. Urlichs, "From non-degenerate conducting polymers to dense matter in the massive Gross-Neveu model", *Phys. Rev.* **D72** (2005) 105008, `hep-th/0505024`.

[34] F. Cooper, A. Khare, and U. Sukhatme, "Supersymmetry and quantum mechanics", *Phys. Rept.* **251** (1995) 267–385, `hep-th/9405029`.

[35] J. Feinberg, "All about the static fermion bags in the Gross-Neveu model", *Annals Phys.* **309** (2004) 166–231, `hep-th/0305240`.

[36] J. Feinberg and A. Zee, "Generalized supersymmetric quantum mechanics and reflectionless fermion bags in 1+1 dimensions", *M. Olshanetsky (ed.) et. al., Multiple facets of quantization and supersymmetry* (2001) p. 626, `hep-th/0109045`.

[37] M. Thies, "From relativistic quantum fields to condensed matter and back again: Updating the Gross-Neveu phase diagram", *J. Phys.* **A39** (2006) 12707–12734, `hep-th/0601049`.

[38] A. Saxena and A. R. Bishop, "Multipolaron solutions of the Gross-Neveu field theory: Toda potential and doped polymers", *Phys. Rev. A* **44** (Aug, 1991) R2251–R2254.

[39] A. Saxena and W. Cao, "Periodic superstructures in tetrahedrally bonded homopolymers", *Phys. Rev. B* **38** (Oct, 1988) 7664–7673.

[40] B. A. Dubrovin and S. P. Novikov *Sov. Phys. JETP* (1975), no. 40, 1058.

[41] B. Sutherland, "Some Exact Results for One-Dimensional Models of Solids", *Phys. Rev. A* **8** (Nov, 1973) 2514–2516.

[42] E. T. Whittaker and G. N. Watson, *A Course of Modern Analysis.* Cambridge U. Press, 1980.

[43] A. Saxena and J. D. Gunton, "Theory of bipolaron lattices in quasi-one-dimensional conducting polymers", *Phys. Rev. B* **35** (Mar, 1987) 3914–3928.

[44] M. Abramowitz and I. A. Stegun, *Handbook of Mathematical Functions.* Handbook of Mathematical Functions, New York: Dover, 1970, 1970.

[45] P. S. Davids, A. Saxena, and D. L. Smith, "Bipolaron lattice formation at metal-polymer interfaces", *Phys. Rev. B* **53** (Feb, 1996) 4823–4833.

[46] A. Barducci, R. Casalbuoni, M. Modugno, G. Pettini, and R. Gatto, "Thermodynamics of the massive Gross-Neveu model", *Phys. Rev.* **D51** (1995) 3042–3060, `hep-th/9406117`.

[47] M. Thies and K. Urlichs, "Revised phase diagram of the Gross-Neveu model", *Phys. Rev.* **D67** (2003) 125015, `hep-th/0302092`.

[48] G. Baym, *Lectures on quantum mechanics.* Benjamin/ Cummings, Reading, Massachusetts, 1978.

[49] L. Salcedo, S. Levit, and J. Negele, "Mean field solution of QCD_2 in the large-N limit", *Nuclear Physics* **B361** (1991) 585–625.

[50] T. Ohsaku, "Relativistic Model for two-band Superconductivity", `cond-mat/0306472`.

[51] R. MacKenzie, P. K. Panigrahi, and S. Sakhi, "Superconductivity in a planar field theory through the Kosterlitz-Thouless mechanism", *Phys. Rev. B* **48** (Aug, 1993) 3892–3895.

[52] A. N. Kalinkin and V. M. Skorikov, "Phase Transitions in Four-Fermion Models", *Inorganic Materials* **39** (2003), no. 8, 765–779.

[53] W. Bietenholz, A. Gfeller, and U. J. Wiese, "Dimensional reduction of fermions in brane worlds of the Gross-Neveu model", *JHEP* **10** (2003) 018, `hep-th/0309162`.

[54] O. Schnetz, M. Thies, and K. Urlichs, "Phase diagram of the Gross-Neveu model: Exact results and condensed matter precursors", *Ann. Phys.* **314** (2004) 425–447, `hep-th/0402014`.

[55] A. Overhauser, "Charge-density waves and isotropic metals", *Phys. Rev.* **128** (1962) 1437.

[56] B. M. A. G. Piette, B. J. Schroers, and W. J. Zakrzewski, "Dynamics of baby skyrmions", *Nucl. Phys.* **B439** (1995) 205–238, `hep-ph/9410256`.

[57] R. MacKenzie, F. Wilczek, and A. Zee, "Possible Form of Vacuum Deformation by Heavy Particles", *Phys. Rev. Lett.* **53** (Dec, 1984) 2203–2206.

[58] T. Meissner, F. Grümmer, and K. Goeke, "Solitons in the Nambu-Jona-Lasinio Model", *Physics Letters B* **227** (1989) 296.

[59] S. Kahana and G. Ripka, "Baryon density of quarks coupled to a chiral field", *Nucl. Phys.* **A429** (1984) 462–476.

[60] G. V. Dunne, J. Hur, C. Lee, and H. Min, "Calculation of QCD instanton determinant with arbitrary mass", *Phys. Rev.* **D71** (2005) 085019, `hep-th/0502087`.

[61] B.-Y. Park, M. Rho, A. Wirzba, and I. Zahed, "Dense QCD: Overhauser or BCS pairing?", *Phys. Rev. D* **62** (Jul, 2000) 034015.

[62] O. Schnetz, M. Thies, and K. Urlichs, "Full phase diagram of the massive Gross-Neveu model", *Annals of Physics* **321** (November, 2006) 2604–2637, `hep-th/0511206`.

[63] O. Schnetz, M. Thies, and K. Urlichs, "The phase diagram of the massive Gross-Neveu model, revisited", `hep-th/0507120`.

[64] M. Thies *private communication.*

[65] V. Schön and M. Thies, "2D model field theories at finite temperature and density", `hep-th/0008175`.

[66] J. D. Bjorken and S. D. Drell, *Relativistic Quantum Field Theory (German Translation).* Bibliograph.Inst./mannheim 1967, 409 P.(B.i.- hochschultaschenbuecher, Band 101).